AFRL-RQ-WP-TR-2012-0241

DYNAMIC HEAT GENERATION MODELING AND THERMAL MANAGEMENT OF ELECTROMECHANICAL ACTUATORS

Louis Chow, Thomas Wu, Yeong-Ren Lin, Yang Hu, David Woodburn, Ray Zhou, Jared Bindl, Wendell Brokaw, and Tony Camarano

University of Central Florida

JULY 2012
Final Report

Approved for public release; distribution unlimited.

See additional restrictions described on inside pages

STINFO COPY

AIR FORCE RESEARCH LABORATORY
AEROSPACE SYSTEMS DIRECTORATE
WRIGHT-PATTERSON AIR FORCE BASE, OH 45433-7542
AIR FORCE MATERIEL COMMAND
UNITED STATES AIR FORCE

NOTICE AND SIGNATURE PAGE

Using Government drawings, specifications, or other data included in this document for any purpose other than Government procurement does not in any way obligate the U.S. Government. The fact that the Government formulated or supplied the drawings, specifications, or other data does not license the holder or any other person or corporation; or convey any rights or permission to manufacture, use, or sell any patented invention that may relate to them.

This report was cleared for public release by the USAF 88th Air Base Wing (88 ABW) Public Affairs Office (PAO) and is available to the general public, including foreign nationals.

Copies may be obtained from the Defense Technical Information Center (DTIC) (http://www.dtic.mil).

AFRL-RQ-WP-TR-2012-0241 HAS BEEN REVIEWED AND IS APPROVED FOR PUBLICATION IN ACCORDANCE WITH ASSIGNED DISTRIBUTION STATEMENT.

*//Signature//	//Signature//
QUINN LELAND Program Manager Electromechanical Branch	JACK VONDRELL, Chief Electromechanical Branch Power Division

This report is published in the interest of scientific and technical information exchange, and its publication does not constitute the Government's approval or disapproval of its ideas or findings.

*Disseminated copies will show "//Signature//" stamped or typed above the signature blocks.

REPORT DOCUMENTATION PAGE

Form Approved
OMB No. 0704-0188

The public reporting burden for this collection of information is estimated to average 1 hour per response, including the time for reviewing instructions, searching existing data sources, gathering and maintaining the data needed, and completing and reviewing the collection of information. Send comments regarding this burden estimate or any other aspect of this collection of information, including suggestions for reducing this burden, to Department of Defense, Washington Headquarters Services, Directorate for Information Operations and Reports (0704-0188), 1215 Jefferson Davis Highway, Suite 1204, Arlington, VA 22202-4302. Respondents should be aware that notwithstanding any other provision of law, no person shall be subject to any penalty for failing to comply with a collection of information if it does not display a currently valid OMB control number. **PLEASE DO NOT RETURN YOUR FORM TO THE ABOVE ADDRESS**.

1. REPORT DATE *(DD-MM-YY)*	2. REPORT TYPE	3. DATES COVERED *(From - To)*
July 2012	Final	01 January 2009 – 31 May 2012

4. TITLE AND SUBTITLE
DYNAMIC HEAT GENERATION MODELING AND THERMAL MANAGEMENT OF ELECTROMECHANICAL ACTUATORS

5a. CONTRACT NUMBER
FA8650-09-2-2940

5b. GRANT NUMBER

5c. PROGRAM ELEMENT NUMBER
62203F

6. AUTHOR(S)
Louis Chow, Thomas Wu, Yeong-Ren Lin, Yang Hu, David Woodburn, Ray Zhou, Jared Bindl, Wendell Brokaw, and Tony Camarano

5d. PROJECT NUMBER
3145

5e. TASK NUMBER
N/A

5f. WORK UNIT NUMBER
Q0MA

7. PERFORMING ORGANIZATION NAME(S) AND ADDRESS(ES)
University of Central Florida
College of Engineering and Computer Science
4000 Central Florida Boulevard
Orlando, FL 32816-2450

8. PERFORMING ORGANIZATION REPORT NUMBER
UCF-CECS-001

9. SPONSORING/MONITORING AGENCY NAME(S) AND ADDRESS(ES)
Air Force Research Laboratory
Aerospace Systems Directorate
Wright-Patterson Air Force Base, OH 45433-7542
Air Force Materiel Command
United States Air Force

10. SPONSORING/MONITORING AGENCY ACRONYM(S)
AFRL/RQPM

11. SPONSORING/MONITORING AGENCY REPORT NUMBER(S)
AFRL-RQ-WP-TR-2012-0241

12. DISTRIBUTION/AVAILABILITY STATEMENT
Approved for public release; distribution unlimited.

13. SUPPLEMENTARY NOTES
PA Case Number: 88ABW-2012-5137; Clearance Date: 24 Sep 2012. This report contains color.

14. ABSTRACT
The heat loads in an electromechanical actuator (EMA) and an electronic unit (EU) are highly transient and localized in nature; therefore, thermal management systems (TMS) designed for time-averaged, uniform heat loads of an EMA and EU are inadequate. The heat loads of EMAs must be accurately determined and managed if EMAs are to be used as replacements to current hydraulic actuators. This report presents a dynamic heat generation model and a thermal model for a permanent magnet motor and power drive. The input to the model included a flight mission profile and an environmental temperature profile, along with the key parameters unique to the EMA. From the cases studied, it could be concluded that the heat generation profiles are indeed highly dynamic, and the major barrier to heat removal from the motor is external to the motor. Strong forced convection is needed. The model compared well with the detailed finite element analysis. The model was also used to compare its temperature predictions with temperature measurements of the motor and power drive provided by the Air Force Research Laboratory. Though the agreement was good, due to the low heat load associated with the test cases, the model could not be validated conclusively.

15. SUBJECT TERMS
EMA, heat generation, electromechanical actuation, thermal management of electric motors and power drives

16. SECURITY CLASSIFICATION OF:			17. LIMITATION OF ABSTRACT:	18. NUMBER OF PAGES	19a. NAME OF RESPONSIBLE PERSON (Monitor)
a. REPORT	b. ABSTRACT	c. THIS PAGE			Leland Quinn
Unclassified	Unclassified	Unclassified	SAR	126	19b. TELEPHONE NUMBER *(Include Area Code)* N/A

TABLE OF CONTENTS

Table of Contents i
List of Figures iii
List of Tables vii
1. Summary 1
2. Introduction 3
3. Dynamic Heat Generation Modeling of High Performance Electromechanical Actuator 4
3.1 Introduction 4
3.2 Model Layout 4
3.3 Parameter Measurement and FEM Calculation 6
3.3.1 Measurement 7
a. Gearing Ratio, N_{cr} 7
b. Power Train Friction, F_f 7
c. Rod Mass, m 7
d. Rotor Moment of Inertia, I 7
e. Phase Resistance, R_s 7
3.3.2 FEM Calculation 8
3.4 Electromechanical Dynamics 8
3.5 Field-oriented Control 10
3.6 PWM Component 12
3.7 Inputs 12
a. Scaling 12
b. Force-Stroke Equation 13
3.8 Thermal Modeling of the Motor 13
3.8.1 Finite Element Analysis 14
3.8.2 Lumped Node Model 18
3.8.2.1 Examples 23
3.8.3 Lumped Node Model with PCM Module 26
3.8.3.1 Examples 28
3.9 An EMA Example and Results 29
a. Parameters 30
b. Results 33
4. Modeling and Simulation of Power Loss in Driver Unit of Electromechanical Actuator 40
4.1 Introduction 40
4.2 PWM Drive Simulation 40
a. Background 40
b. Simulation Model 41
c. PWM Drive 43
4.3 Structure of the Electronic Unit 46
4.4 Power Loss on the EU 47
4.4.1 Power Loss on IGBTs 47
a. On-state Loss of the IGBTs 49
b. Switching Loss of the IGBTs 50
4.4.2 Power Loss on Unloading Resistor 51
4.4.3 Power Loss on Control Circuits 52

Approved for public release; distribution unlimited.

4.5 Modeling of the Power Loss on the EU ... 53
4.6 Thermal modeling of the EU ... 54
4.7 An EU Example and Results ... 62
5. Conclusion ... 67
6. References ... 68
Appendix A: How to Get Parameters for an EMA Simulation ... 70
A1 WHAT PARAMETERS ARE NEEDED ... 70
A2 WHERE PARAMETERS CAN BE FOUND ... 71
A2.1 What Can Be Found by Measurement ... 71
A2.1.1 No-load speed ... 71
A2.1.2 Stall force ... 71
A2.1.3 Stroke range ... 71
A2.1.4 Gearing ratio ... 71
A2.1.5 Number of poles ... 71
A2.1.6 Power train friction ... 72
A2.1.7 Shaft mass ... 72
A2.1.8 Moment of inertia ... 72
A2.1.9 Phase resistance ... 72
A2.2 What Can Be Found by Modeling ... 72
A3 How to Model a Motor for Parameter Estimation ... 73
A3.1 Design an electric motor to specification ... 73
A3.2 Refine the design ... 77
A3.2.1 Create new motor project ... 77
A3.2.2 Define machine properties ... 78
A3.2.3 Analyze ... 84
A3.3 Model the motor with finite element method (FEM) ... 87
A3.3.1 Export RMxprt Model to Maxwell 2D ... 87
A3.3.2 Make motor whole ... 90
A3.3.3 Add Currents and Polarities ... 91
A3.3.4 Set magnetic polarities ... 97
A3.3.5 Assign vector potential ... 97
A3.3.6 Analyze ... 98
A3.4 Extract the reduced-order parameters ... 104
A3.4.1 Simulate ... 104
A3.4.2 Extract the data ... 108
A4 Conclusion ... 111
List of Acronyms, Abbreviations, and Symbols ... 112

Approved for public release; distribution unlimited.

LIST OF FIGURES

Figure 1 - Model Layout Showing the Connection of the four Major Components: Field-Oriented Control, Pulse-Width Modulation, Electromechanical Dynamics, and the Thermal Component 5
Figure 2 - Direct-Axis Inductance Along the i_d Axis (blue) and the Inductance Value at Zero Current (Green Circle). The Inductance is not mirrored about the Quadrature Axis (going into the page), so its Values for Positive i_d do not match those for Negative i_d 8
Figure 3 - The General Concept of the PWM. A Trailing Edge Carrier Wave (top) is compared to a Normalized Sinusoidal Phase Voltage. When the Normalized Wave is Greater than the Carrier Wave, the Output PWM Voltage is turned on (Bottom). Otherwise, it is off 12
Figure 4 - Actual Force Profile (Blue) and Calculated Force Profile (Green) 13
Figure 5 - 3-D Model of the PMSM Motor Design 14
Figure 6 - Cross-Section of Motor and Rotor 15
Figure 7 - Computation Domain 15
Figure 8 - Step Heat Load of the Motor 16
Figure 9 - Steady State Thermal Simulation Result (Forced Convection) 18
Figure 10 - Transient Temperature Response of the Step Heat Load Shown in Figure 8 18
Figure 11 - Lumped Node Model of EMA (Transient) 20
Figure 12 - Lumped-Node Network Simulation Result 24
Figure 13 - Pulsed Heat Load 24
Figure 14 - Winding Temperature Comparison (FEA and Lumped Node) 25
Figure 15 - Heat Load 25
Figure 16 - Winding and Motor Case Temperatures 26
Figure 17 - Aluminum/PCM Composite 26
Figure 18 - Specific Heat vs. Temperature 27
Figure 19 - Lumped-Node Model Including PCM 27
Figure 20 - h=10W/m^{2}K, PCM (Case 1) 29
Figure 21 - h=100W/m^{2}K, PCM (Case 2) 29
Figure 22 - Static Friction Analysis Showing Stroke (top) and Load Force (Bottom). The Green Lines on the Force Plot Represent the Mean Forces to Pull (-258 N) or Push (425 N) the EMA Rod, Overcoming the Friction of the Drive Train (342 N). The Bias towards Force Required to Push is the Weight of the EMA Rod (84 N) 31
Figure 23 - Direct-Axis Inductance as a Function of Direct Current, i_d, and Quadrature Current, i_q 31
Figure 24 - Quadrature-Axis Inductance as a Function of Direct Current, i_d, and Quadrature Current, i_q 32
Figure 25 - Motor Geometry (Left) and Slot Measurements (Right) 32
Figure 26 - Desired (Blue) and Actual (Green) Stroke Profiles 33
Figure 27 - Input Load Force Profile (Blue) and Motor-Generated Force (Green). The Load Force was a Sustained 450 N 33
Figure 28 - DQ0 Voltages with Pulse Form due to PWM 34
Figure 29 - DQ0 Currents 34

Approved for public release; distribution unlimited.

Figure 30 - Motor Powers Showing the Total Electrical Power at the Terminals of the Motor (First), the Power Loss in the Windings (Second), the Power Stored in the Magnetic Fields (Third), and the Mechanical Power Output on the Rotor (last) 35
Figure 31 - Drive Train Powers Showing the Mechanical Power Input on the Rotor (First), the Load Power (Second), the Frictional Power (Third), the Gravitational Power (Forth), and the Net Kinetic Power (Last) 36
Figure 32 - Temperature Comparison (Above) and Again (Below) Zoomed in. These Plots have Environmental Temperature (blue), experimentally Measured Temperature of Stator (Green), Simulated Temperature of Stator (Red), and the Simulated Temperature of the Windings (Cyan) 37
Figure 33 - Temperature Comparison for a Half-Hour Run Showing Environmental Temperature (Blue), Experimentally Measured Temperature of Stator (Green), Simulated Temperature of Stator (Red), and the Simulated Temperature of the Windings (Cyan). Note that the Simulated Temperatures of the Windings and Stator are About the Same, Indicating the Low Thermal Resistance in the Motor 38
Figure 34 - Temperature Comparison Showing the Disparity between the Experimentally Measured Temperature of the Stator (green) and the Simulated Temperature (red) when Different Values of Control Coefficients are used. In this Case, the Test Data is shown Only for Reference. Obviously, with this Control Tuning, the Temperatures are not expected to Match 38
Figure 35 - Peak Terminal Power. Note that the Peak Power here is Over 50% Higher than Previously in Figure 31 39
Figure 36 - PWM Generation 41
Figure 37 - Simulation System Structure 43
Figure 38 - Mechanical Stroke Following Results Comparison 45
Figure 39 - D-Axis and Q-Axis Voltages Comparison 45
Figure 40 - Electronic Unit of the EMA 46
Figure 41 - Electronic Unit Block Diagram 47
Figure 42 - Two Level Voltage Source Inverter, S1 ~ S6 are Switches, Which are IGBTs in the EMA Application 48
Figure 43 - Collector Current vs. Collector-Emitter voltage. The Curve Becomes Linear When Current is higher than 100A. In that Range, an Equivalent Resistance can be used to calculate the Voltage Drop 49
Figure 44 - Definition of Switching Time of IGBT. The “Input Signal” is the Input to the Gate, and the Device is an N-Channel IGBT 50
Figure 45 - Switching Loss vs. Collector Current. The Total Switching Loss for one Switching Operation is the Sum of the Three Shown in the Figure 51
Figure 46 - Regenerative Energy Storage and Dissipation Circuit 52
Figure 47 - SERVOSTAR S610 Data Sheet 54
Figure 48 - Control Box Configurations 55
Figure 49 - Simulation Results 55
Figure 50 - Thermocouple Locations 56
Figure 51 - Regenerative Power Load History 56
Figure 52 - IGBT Loss Load History 57
Figure 53 - Power Loss & Regenerative Resistor Temperature vs. Time 57
Figure 54 - 3-D Model of Control Unit 58

Approved for public release; distribution unlimited.

Figure 55 - Lumped Node Network 59
Figure 56 - Thermal Load 59
Figure 57 - One Pluse Result 60
Figure 58 - Result with 36W Heat Load 61
Figure 59 - Result with 72W Heat Load 62
Figure 60 - Stroke of the Mission Profile 63
Figure 61 - Load Force of the Mission Profile 63
Figure 62 - Power Loss on IGBTs 64
Figure 63 - Power Loss on IGBTs after Smoothing 64
Figure 64 - Temperature on IGBTs. Hardware Test Data is compared with Simulation Data Based on the Power Loss Model 65
Figure 65 - Temperature on Resistors. We Pick the DC Bus Capacitor to be 0.14F, and DC Bus Voltage Limited to 340V Maximum for the Regenerative Power Loss calculation. It shows that the Unloading Resistor is barely used and the Capacitor is Fully Capable of Absorbing Regenerative Power for this Mission Profile 66

Figure A-1 - Selecting "New" from the "File" Menu 77
Figure A-2 - Creating a New RMxprt Design from the "Project" Menu 77
Figure A-3 - List of Machine Types 78
Figure A-4 - Project Manager Tree 78
Figure A-5 - Properties List 79
Figure A-6 - Model of Stator with Skewed Slots 81
Figure A-7 - End Winding Characteristics (Left) and Slot Filling (Right) 83
Figure A-8 - Diagram of Magnet Arc Offset from Center of Axel 84
Figure A-9 - Selecting "Add Solution Setup…" from "Analysis" 84
Figure A-10 - Solution Setup Ratings 85
Figure A-11 - Selecting "Analyze" from "Setup1" 85
Figure A-12 - Selecting "Solution Data…" from "Results" 86
Figure A-13 - Solution Data Sheet Showing "FEA Input Data" 86
Figure A-14 - Creating a Maxwell Design from the RMxprt Model 87
Figure A-15 - Choosing to Create a 2D Maxwell Design 88
Figure A-16 - Project Manager Tree for Maxwell 2D Design 88
Figure A-17 - Selecting "Solution Type…" from "Maxwell 2D" Menu 89
Figure A-18 - Selecting the User-Defined out Vacuum 90
Figure A-19 - Model Fractions Highlighted in the Properties Box 90
Figure A-20 - Full Model with all Windings and Magnetic Poles Selected 91
Figure A-21 - Separating the Windings and Magnets so that they are no Longer Linked 92
Figure A-22 - Selecting "Design Properties…" from "Maxwell2DDesign1 (Magnetostatic XY)" 93
Figure A-23 - Recommended List of Design Variables 94
Figure A-24 - Defining the Nominal Value of *I* with the Unit A (Ampere) 95
Figure A-25 - An Image from RMxprt of the Winding Layout for the Motor (Left) and an Image from Maxwell 2D of the Color-coded Winding Layout (Right). The Colors Must be added by the User 95
Figure A-26 - Selecting "Current…" from "Assign" from "Excitations" 96
Figure A-27 - Setting the Current Excitation for a Winding 96

Approved for public release; distribution unlimited.

Figure A-28 - Selecting the Polarity of Magnets 97
Figure A-29 - Setting the Selection Option to Edges 97
Figure A-30 - Selecting "Vector Potential…" from "Assign" from "Boundaries" 98
Figure A-31 - Selecting "Add Solution Setup…" from "Analysis" 98
Figure A-32 - Selecting "Matrix…" from "Assign" from "Parameters" 99
Figure A-33 - Selecting all but Return Windings 99
Figure A-34 - Grouping Windings into Phases 100
Figure A-35 - Selecting "Validation Check…" from "Maxwell 2D" Menu 100
Figure A-36 - Selecting "Analyze" from "Setup1" 100
Figure A-37 - Selecting "Solution Data…" from "Results" 101
Figure A-38 - Post-processed Inductances for Phases A, B, and C 101
Figure A-39 - Matlab Command Window Showing the Results of Using dq0 on the ABC Phase Inductances 102
Figure A-40 - Flux Linkages for Phases A, B, and C 103
Figure A-41 - Matlab Command Window Showing the Result of Using dq0 on the ABC Phase Flux Linkages 103
Figure A-42 - Selecting "Parametric…" from "Add" from "Optimetrics" 104
Figure A-43 - Setting up a Sweep Analysis 105
Figure A-44 - Selecting "Analyze" from "Parametric Setup 1" 105
Figure A-45 - Selecting "Data Table" from "Create Magnetostatic Report" from "Results" 106
Figure A-46 - Selecting all Mutual and Self-inductances 106
Figure A-47 - Selecting all Magnetic Flux Linkages 106
Figure A-48 - Transposing the Data Table 107
Figure A-49 - Copying the Data 107
Figure A-50 - Pasting the Data into Excel 108
Figure A-51 - Direct inductance (left) and quadrature inductance (right), both as functions of direct and quadrature currents 110
Figure A-52 - Direct (Left) and Quadrature (Right) Currents Smoothed 110

Approved for public release; distribution unlimited.

LIST OF TABLES

Table 1 - Simulation States 6
Table 2 - EMA Parameters 7
Table 3- Power Losses in Motor Components in a Quarter Section 16
Table 4 - Steady State Simulation Results with ANSYS 17
Table 5- The Analogy of the Equivalent Thermal Circuit 19
Table 6 - The R and C Values of Lumped Node Model of the Motor 21
Table 7 - Network Parameters for Equivalent Thermal Resistances 28
Table 8 - Lumped-Node Cases 28
Table 9 - EMA Parameters 30
Table 10 - EMA Material Properties 32
Table 11 - Lumped Node List 58
Table 12 - Thermal Resistator R and Capciator C Unit 60
Table 13 - Thermal Resistator R and Capciator C Value 60

Approved for public release; distribution unlimited.

1. SUMMARY

In the aviation community, there is a high priority to develop all-electric aircraft. Electro-mechanical actuation (EMA) systems would replace traditional, large, heavy and difficult-to-maintain hydraulic actuation systems. This movement from hydraulic actuation to electrical actuation enhances the flexibility to integrate redundancy and emergency system in future military aircraft. Elimination of the hydraulic fluid removes the possibility of leakage of corrosive hydraulic fluid and the associated fire hazard, as well as environmental concerns. The switch from hydraulic to electrical actuation provides additional benefits in reduced aircraft weight, improved survivability and improved maintainability.

Given the need for predicting dynamically generated heat and power demand, an accurate simulation model is very valuable in designing an EMA system. Advanced analysis techniques such as finite-element method (FEM) and intelligent control systems such as field-oriented control (FOC) are used to better understand the sources of the heat. EMA systems are complex and testing them is a very involved procedure. Such systems are also expensive which discourages testing them to their limits, and many different scenarios are needed to properly test an EMA. Furthermore, there are significant details which cannot be practically measured experimentally. Therefore, it is advantageous to simulate the EMA with only its key parameters. The EMA simulation model presented in this report meets this goal.

We address the two most important components of the EMA – electric motor and power drive. The model takes a flight mission (a desired position profile and a load force profile) and an environmental temperature profile as input and predicts the thermal behavior of the electric motor and the transient power demands of the EMA. It includes a position field-oriented control (FOC), a pulse-width modulation (PWM) component, an electro-mechanical dynamics component, and a thermal component. Model parameters are obtained by experimentation or FEM models. The key parameters, including nonlinear inductance, rotor flux linkage, and thermal resistances and capacitances, are tuned using FEM models of a commercial actuator. The full simulation model is a nonlinear, lumped-element model (NL-LEM). The model corresponds to a linear actuator with a permanent magnet (PM) rotational motor connected to a rotational-to-linear drive train. It was shown that the heat generation profiles are indeed highly dynamic, and control plays a powerful role in how much excess heat is generated and how much the power demand spikes.

For the thermal component, a comprehensive FEM model has been developed to predict the temperature distribution within the electric motor using the heat load generated in a given flight profile. However, the FEM model needs tremendous computational resources. A reduced-order thermal model (lumped-node thermal network) is validated and used instead, which can reduce computational resources considerably. The network can simulate the temperature time histories of the various components in the EMA electric motor during a flight mission.

The thermal lumped-node model is combined with the electromagnetics portion mentioned above to dynamically calculate the temperature within the electric motor. FEM results obtained with or without radiation are compared with the results from the lumped-node model. Radiation

Approved for public release; distribution unlimited.

is important when convection cooling is insufficient and the motor temperature is high. In situations when the heat is excessive and cannot be removed from the motor real-time, we also demonstrate that phase change materials (PCM) is very effective in keeping the motor temperature near the melting point of the PCM until all PCM has melted.

We also study the thermal problem of the control and drive units of EMAs, and build a model to calculate and simulate the power loss and heat generation in the driver board. The driver unit consists of a power inverter, a power dissipating resistor and a control circuit. The power loss of each part is studied. The heat loss in the power inverter comes mainly from the power switches – IGBTs. The on-state loss is proportional to the current of the motor, and the switching loss is determined by the switching frequency as well as currents and voltages. The power loss in the power dissipating resistor is determined by the regenerative power, the capacitor and the control algorithm to stabilize the bus voltage, which varies from different mission profiles and different applications. The power loss on the control circuit is negligible compared with the power loss on IGBTs and the power dissipating resistor, and generates very little heat.

As a brief summary, this report presents a dynamic heat generation model and a thermal model for a PM motor and power drive. The input to the model includes a flight mission profile and an environmental temperature profile, along with the key parameters unique to the EMA. The model compares well with the detailed finite element analysis. The model was also used to compare its temperature predictions with temperature measurements of the motor and power drive provided by the Air Force Research Laboratory. Though the agreement was good, due to the low heat load associated with the test cases, the model could not be validated conclusively.

Approved for public release; distribution unlimited.

2. INTRODUCTION

The development of all-electric aircraft is a high priority in the avionics community [1]. Current aircraft use a combination of hydraulic, pneumatic, and electric systems. However, future airplanes are expected to use a single, electric system, with electromechanical actuators (EMAs) replacing hydraulic pistons. Such a system would reduce the cost to build, operate, and maintain aircraft [2]. It would also make aircraft lighter, more reliable, safer, and more easily reconfigurable, improving the turnaround for new technology [3].

There are two major obstacles in replacing hydraulic actuators with EMAs: heat generation management and power management. Firstly, unlike hydraulic actuators, EMAs do not have the inherent advantage of recirculating fluid to cool their components [4]. Rather, windings in EMAs can overheat rapidly depending on the demands, at which point materials can degrade. Neodymium-iron-boron is one of the most powerful permanent magnets for electric motors, but it begins to demagnetize at relatively low temperatures [5], with an operating range of 120°C to 180°C. Although effective, liquid cooling reinstitutes one of the systems that are being eliminated. Primary flight control actuators are of particular relevance because they are continually engaged during flight, are required to accelerate rapidly, and are often faced with high wind loads. As the complexities of aircraft systems exponentially grow and the demand for lightweight composites increases, thermal concerns are increasingly significant. Heat generation in motor windings can be highly dynamic and localized. Predicting how much heat would be generated by an EMA is critical.

Secondly, EMAs have the advantage of only using power when active, whereas hydraulic systems require that a pump continuously maintain line pressure. This should help to make EMA systems more efficient. However, this advantage brings with it a major complication: the power draw from the electrical supply is also highly dynamic. Compounding this problem are the highly variable demands of all the electrical systems of an entire aircraft drawing power from one source. Predicting how much power will be drawn during operation is critical for sizing system components and choosing the power supply type (e.g. battery-super-capacitor hybrid).

In the next two chapters, we will address the heat generation and power management of the two most important components of the EMA – electric motor and power drive. The model takes a flight mission (a desired position profile and a load force profile) and an environmental temperature profile as input and predicts the thermal behavior of the electric motor and the transient power demands of the EMA.

Approved for public release; distribution unlimited.

3. DYNAMIC HEAT GENERATION MODELING OF HIGH PERFORMANCE ELECTROMECHANICAL ACTUATOR

3.1 INTRODUCTION

Given the need for predicting dynamically generated heat and power demand, an accurate simulation model is tremendously valuable in designing an EMA system. EMA systems are complex and testing them is an involved procedure. Such systems are also expensive which discourages testing them to their limits, and many different scenarios are needed to properly test an EMA. Furthermore, there are significant details which cannot be practically measured experimentally. Therefore, it is advantageous to simulate the EMA with only its key parameters.

The EMA simulation model presented in this chapter meets this goal. It includes a position field-oriented control (FOC), a pulse-width modulation (PWM) component, an electro-mechanical dynamics component, and a thermal component. Model parameters are obtained by experimentation or finite element method (FEM). The full simulation model is a nonlinear, lumped-element model (NL-LEM). The model corresponds to a linear actuator with a permanent magnet (PM) rotational motor connected to a rotational-to-linear drive train (e.g. a ball screw or a roller screw).

The methodology presented here provides a means of predicting heat generation and the overall power demands of an EMA. Such tools will help in reaching the goal of an all-electric aircraft.

Simulation results, including heat generation and power demand, for a commercially available, test EMA are shown in the latter part of this chapter.

3.2 MODEL LAYOUT

The four main components of the NL-LEM are shown in Figure 1.

Approved for public release; distribution unlimited.

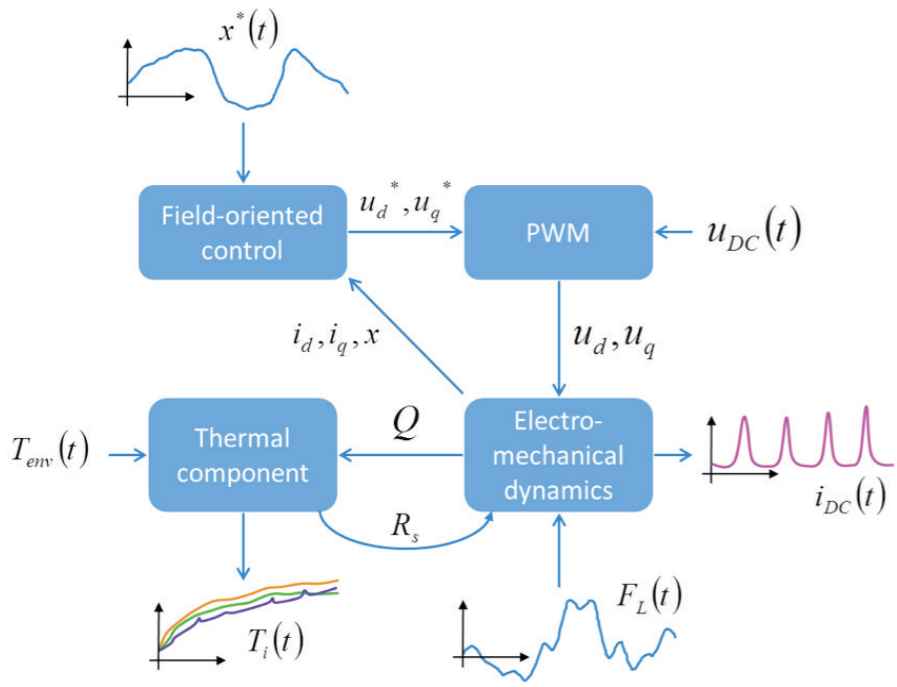

Figure 1 - Model Layout Showing the Connection of the four Major Components: Field-Oriented Control, Pulse-Width Modulation, Electromechanical Dynamics, and the Thermal Component

The model takes the EMA rod's desired motion profile, x^*, as an input to the field-oriented control (FOC). Based on the present state of the direct and quadrature (DQ0) currents, i_d, i_q, and the actual position of the EMA rod, x, the FOC algorithm calculates the reference voltages, u_d^*, u_q^*. The PWM component takes these reference voltages as well as the present state of the DC supply voltage, u_{DC}, and calculates the PWM voltages, u_d, u_q. These are the actual input voltages to the electromechanical dynamics. With these and the present load force, F_L, the electromechanical dynamical equations lead to the calculation of the currents, i_d, i_q, EMA position, x, and dynamically generated heat, Q. An output of the electromechanical component is the DC current to the EMA system, i_{DC}. Together with the DC bus voltage, it represents the power demands of the EMA system at its terminals. The heat generated in the motor is the input to the thermal component. With the present value of the environmental temperature, T_{env}, the thermal equations lead to the nodal temperatures, T_i, and the updated value of resistance, R_s, which is fed back into the electromechanical dynamics. The nodal temperatures represent the thermal behavior of the EMA system. Table 1 summarizes many of these terms.

Approved for public release; distribution unlimited.

Table 1 - Simulation States

Symbol	Name	Units
x	Actual position of EMA rod	mm
x^*	Desired position of EMA rod	mm
θ_{me}	Actual rotor angle scaled by $P/2$	rad
θ_{me}^*	Desired rotor angle scaled by $P/2$	rad
v	Actual velocity of EMA rod	mm/s
v^*	Desired velocity of EMA rod	mm/s
F_L	Load force	N
F_M	Motor-generated force	N
F_g	Gravitational force	N
F_f	Frictional force	N
u_d	Actual direct voltage	V
u_q	Actual quadrature voltage	V
u_d^*	Desired direct voltage	V
u_q^*	Desired quadrature voltage	V
i_d	Actual direct current	A
i_q	Actual quadrature current	A
i_d^*	Desired direct current	A
i_q^*	Desired quadrature current	A
u_{DC}	DC bus voltage	V
i_{DC}	DC bus current	A
Q	Generated heat	W
R_s	Phase resistance	Ω
T_{env}	Environmental temperature	°C
T_i	Nodal temperature	°C

Notice that the desired position, x^*, the load force, F_L, the environmental temperature, T_{env}, and the DC voltage, u_{DC}, all can be variable inputs to the model. An EMA can be run through a motion profile in the presence of a variable load profile while the electrical power demand and the temperatures are calculated.

3.3 Parameter Measurement and FEM Calculation

Table 2 shows a summary of the key EMA parameters. Some of the parameters, such as the number of slots and number of poles, are easily obtained from the actuator's documentation, but others must be measured or carefully calculated. Some of the measurements are performed while the actuator is coupled with a hydraulic press or some other active load.

Approved for public release; distribution unlimited.

Table 2 - EMA Parameters

Symbol	Name	Units
N_{cr}	Gearing ratio	rad/m
S	Number of slots	
P	Number of poles	
$F_{f,\max}$	Maximum power train friction	N
m	Rod mass	kg
I	Rotor moment of inertia	kg·mm^2/rad^2
$R_{s,ref}$	Phase resistance at T_{ref}	Ω
T_{ref}	Reference temperature	°C
α_R	Temperature coefficient of resistance	1/°C
λ_{PM}	PM flux linkage	Wb
$L_d(i_d, i_q)$	Direct inductance	mH
$L_q(i_d, i_q)$	Quadrature inductance	mH

3.3.1 Measurement

a. Gearing Ratio, N_{cr}

The gearing ratio is carefully calculated by counting the teeth on each gear and measuring the linear displacement of the actuator rod for one full revolution of the rotor.

b. Power Train Friction, F_f

The hydraulic actuator is coupled to the unpowered EMA and drives the EMA's rod up and down. The static friction of the EMA's drive train is obtained by using the force and stroke data collected during this test, and the mean forces required to push or pull the EMA rod are calculated. The magnitudes of these forces are unequal due to a bias. This bias exists because of the weight of the rod itself, and the difference between this bias and the push and pull forces is the friction force.

c. Rod Mass, m

The mass of the EMA's entire rod is derived from the friction test. The bias in the force required to move the EMA rod is due to the weight of the rod. This translates to a certain mass.

d. Rotor Moment of Inertia, I

The rotor moment of inertia is obtained by measuring the dimensions of the rotor and the material densities and calculating the moment of inertia.

e. Phase Resistance, R_s

The phase resistance is measured by connecting leads to two of the three phase lines into the motor and measuring the open-circuit line-to-line resistance. This value is then divided by two if the motor is a wye-connected motor.

Approved for public release; distribution unlimited.

3.3.2 FEM Calculation

The material composition and geometry of the motor are used in designing an FEM model in Ansoft's Maxwell 2D. Values of rotor angle, torque angle, and current amplitude are varied as multiple simulation runs are performed.

Many of the motor modeling researchers in the past [6], [7] and even present [8], [9] use constant parameter values in simulations, although some use nonlinear inductances [10], [11], [12]. For this chapter, FEM is used to obtain L_d and L_q as nonlinear functions of i_d and i_q. The derivatives of inductance with respect to current are numerically calculated from these tables. The inductances and their derivatives with respect to DQ0 currents are stored in tables which are then indexed during simulation.

The FEM model is simulated with currents well above the motor's normal operating range in order to capture the behavior during highly transient moments. The torque angle should be varied from 0 to π radians to capture the full character of the inductances. Even if the rotor of an EMA is round, the rotor angle has an effect on the DQ0 reference frame inductances. Therefore, the rotor angle should also be varied over one period of variation in the DQ0 inductances. Such variation occurs mostly at relatively high current values (i.e. at saturation), so this variation is averaged out, but the calculation of inductance at a single rotor angle cannot be assumed to be representative.

Note that the peak inductance values do not necessarily occur at zero current, nor are the inductances mirrored about the quadrature axis. An example of this is in Figure 2. This should clarify the highly variable nature of inductances and the need to use nonlinear modeling instead of assuming constant values.

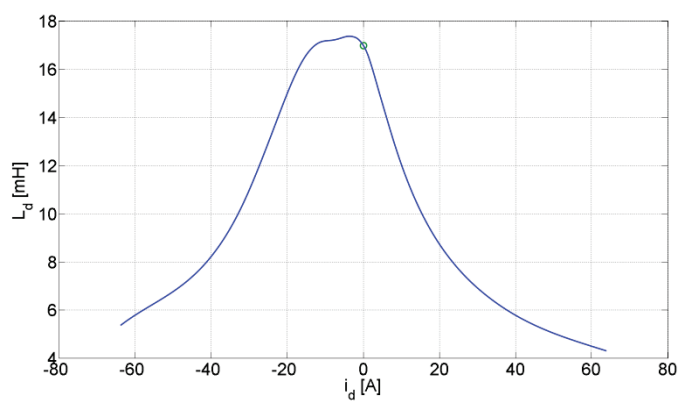

Figure 2 - Direct-Axis Inductance Along the i_d Axis (blue) and the Inductance Value at Zero Current (Green Circle). The Inductance is not mirrored about the Quadrature Axis (going into the page), so its Values for Positive i_d do not match those for Negative i_d

3.4 ELECTROMECHANICAL DYNAMICS

The motor dynamics are modeled by four primary dynamical equations in the DQ0 reference frame [13]. The first two of these equations are

Approved for public release; distribution unlimited.

$$\frac{di_d}{dt} = \frac{L_{qq}G_d - L_{dq}G_q}{L_{dd}L_{qq} - L_{dq}L_{qd}} \tag{1}$$

$$\frac{di_q}{dt} = \frac{L_{dd}G_q - L_{qd}G_d}{L_{dd}L_{qq} - L_{dq}L_{qd}} \tag{2}$$

These come from the voltage Eq. 3 and Eq.4:

$$u_d = R_s i_d + L_{dd}\frac{di_d}{dt} + L_{dq}\frac{di_q}{dt} - L_q i_q \frac{d\theta_{me}}{dt} \tag{3}$$

$$u_q = R_s i_q + L_{qd}\frac{di_d}{dt} + L_{qq}\frac{di_q}{dt} + \left(L_d i_d + \lambda_{PM}\right)\frac{d\theta_{me}}{dt} \tag{4}$$

where

$$L_{dd} = L_d + i_d \frac{dL_d}{di_d} \tag{5}$$

$$L_{dq} = i_d \frac{dL_d}{di_q} \tag{6}$$

$$L_{qd} = i_q \frac{dL_q}{di_d} \tag{7}$$

$$L_{qq} = L_q + i_q \frac{dL_q}{di_q} \tag{8}$$

$$G_d = u_d - R_s i_d + \left(L_q i_q\right)\frac{d\theta_{me}}{dt} \tag{9}$$

$$G_q = u_q - R_s i_q - \left(L_d i_d + \lambda_{PM}\right)\frac{d\theta_{me}}{dt} \tag{10}$$

$$\theta_{me} = \left(xN_{cr}\right)\frac{P}{2} \tag{11}$$

These equations carry the assumption that the variations in inductances over rotor angle can be reasonably averaged out, that the flux linkage from the permanent magnets appears only in the direct axis, and that the motor is balanced.

The voltages are provided by the PWM component; the current rates are calculated using Eq. 1 and Eq. 2; and the currents are found by integration.

In [14], there is a detailed analysis of the motor-generated force equation. Given the assumptions

Approved for public release; distribution unlimited.

made for Eq. 1 – Eq. 11, the motor-generated force equation is

$$F_M = \frac{3P}{4} N_{cr} i_q \left[\lambda_{PM} + \left(L_d - L_q \right) i_d \right] \tag{12}$$

The third dynamical equation is the force-speed equation (Eq. 13) that links the motor-generated force to the acceleration it produces:

$$\frac{dv}{dt} = \frac{1}{J} \left(F_M + F_L + F_g + F_f \right) \tag{13}$$

where J is the combined linear inertia from all moving parts in the EMA. The value J is calculated from the mass of the rod and the angular moment of inertia by

$$J = I \frac{P}{2} N_{cr}{}^2 + m \tag{14}$$

As long as velocity is zero, the frictional force is defined to be equal and opposite to the sum of the other component forces up to a maximum friction value. This keeps the net force and, therefore, velocity at zero. However, when the sum of the other component forces exceeds this maximum friction, the magnitude of the friction holds at this maximum value and its sign always opposes the direction of motion Eq. 15.

$$F_f = \begin{cases} -\left(F_M + F_L + F_g \right) & : \left| F_M + F_L + F_g \right| \le F_{f,\max} \\ -\operatorname{sgn}(v) \cdot F_{f,\max} & : \left| F_M + F_L + F_g \right| > F_{f,\max} \end{cases} \tag{15}$$

Note that air friction is not included because EMAs use position controlled motors which do not reach excessive speeds where air friction is a practical consideration.

Finally, the forth dynamical equation is

$$\frac{dx}{dt} = v \tag{16}$$

This is simply the definition of velocity and is integrated to get position.

3.5 Field-oriented Control

A thorough analysis of dynamic motor heat generation should include motor drive dynamics. This model's field-oriented control (FOC) translates the desired motion profile into simulation drive voltages. The control is an adaptive closed-loop control, which is a type of feedback linearization of the speed and position errors.

In the following derivation, the star superscript is used to indicate desired values. Starting with velocity and position error, a desired linear acceleration, a^*, is developed:

Approved for public release; distribution unlimited.

$$a^* = k_a \frac{\left(v^* - v\right)}{\Delta t_c} + k_v \frac{\left(x^* - x\right)}{\Delta t_c} \tag{17}$$

where Δt_c is the time step of the control loop and k_a and k_v are control coefficients. This equation tends toward changing the present velocity and position to match the desired velocity and position. However, this should happen only at a certain rate and not necessarily all in one time step.

The desired velocity must be redefined based on this newly calculated desired acceleration:

$$v^* = v + a^* \Delta t_c \tag{18}$$

If the load force is predicted by estimating the load force from the previous step and if the frictional and gravitational forces are neglected, then Eq. 13 becomes Eq. 19.

$$\begin{aligned} F_M{}^* = \; & a^* J - \overbrace{F_g - F_f}^{0} - \\ & \underbrace{\left[aJ - \left(i_q \frac{3}{2} N_{cr} \frac{P}{2} \lambda_{PM} \right) - \overbrace{F_g - F_f}^{0} \right]}_{\hat{F}_L} \end{aligned} \tag{19}$$

Solving Eq. 12 for i_q and setting $i_d{}^*$ to zero yields

$$i_q{}^* = \frac{F_M{}^*}{\frac{3}{2} N_{cr} \frac{P}{2} \lambda_{PM}} \tag{20}$$

Substituting Eq.19 into Eq.20 results in Eq.21.

$$i_q{}^* = \frac{\left(a^* - a\right) J}{\frac{3}{2} N_{cr} \frac{P}{2} \lambda_{PM}} + i_q \tag{21}$$

The currents and the current rates are then limited.

Lastly, the desired voltages are calculated:

$$u_d{}^* = R_s i_d{}^* + L_{d0} \frac{di_d{}^*}{dt} - L_{q0} i_q{}^* \frac{d\theta_{me}{}^*}{dt} \tag{22}$$

$$u_q{}^* = R_s i_q{}^* + L_{q0} \frac{di_q{}^*}{dt} + \left(L_{d0} i_d{}^* + \lambda_{PM} \right) \frac{d\theta_{me}{}^*}{dt} \tag{23}$$

where L_{d0} is the direct inductance at zero current, L_{q0} is the quadrature inductance at zero current, and $\theta_{me}{}^*$ is the desired mechanical angle multiplied by the number of pole pairs $P/2$. Its

Approved for public release; distribution unlimited.

relation to desired position is

$$\theta_{me}{}^{*} = \left(x^{*} N_{cr}\right)\frac{P}{2} \tag{24}$$

3.6 PWM Component

The PWM component of the simulation model uses a trailing edge modulation carrier, as demonstrated in Figure 3. The voltages are translated into the ABC reference frame. The PWM algorithm is performed on those voltages. Then, these pulsed voltages are translated back into the DQ0 reference frame.

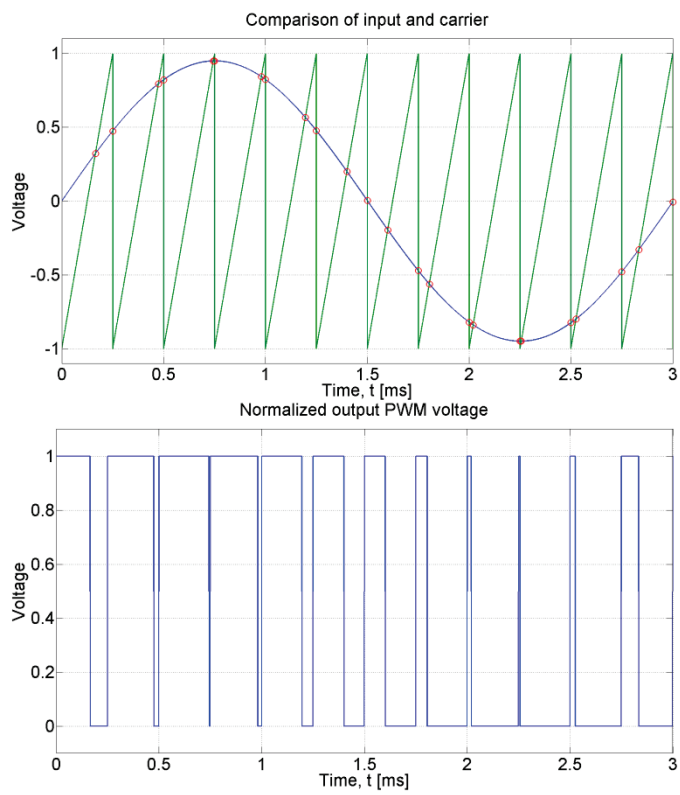

Figure 3 - The General Concept of the PWM. A Trailing Edge Carrier Wave (top) is compared to a Normalized Sinusoidal Phase Voltage. When the Normalized Wave is Greater than the Carrier Wave, the Output PWM Voltage is turned on (Bottom). Otherwise, it is off

3.7 Inputs

a. Scaling

The stroke and load force data are recorded from actual flight profiles. However, these profiles correspond to an actuator with performance characteristics that might not match those of a test actuator. The stroke and force profiles are scaled for a range which is compatible with the test

Approved for public release; distribution unlimited.

actuator. The stroke profile is also adjusted to match the acceleration limits of the actuator by stretching the profile over time.

b. Force-Stroke Equation

In the absence of actual flight profiles, a force-stroke relationship can be useful in simulating the force, given a theoretical stroke profile. This force-stroke equation comes from analyzing actual flight data. The equation is

$$\begin{aligned} \hat{F} = & \left(\rho \cdot C_d + C_{d0}\right) \cdot \\ & \left[\left(x - x_0\right) + C_{x^2}\left(x - x_0\right)^2 + C_{x^3}\left(x - x_0\right)^3\right] s^2 + \\ & F_0 + cv + Ma \\ C_d = & \begin{cases} C_{d1} : x < x_0 \\ C_{d2} : x \geq x_0 \end{cases} \end{aligned} \tag{25}$$

where ρ is the air density which can be derived from the altitude of the aircraft, C_{d1}, C_{d2}, C_{d0}, C_{x^2}, and C_{x^3} are coefficients, s is the aircraft speed, F_0 is the force bias due to the weight of the aileron, c is the net friction coefficient, M is the effective mass of the aileron and EMA, x is the stroke position, x_0 is a stroke bias, v is the first derivative of x, and a is the second derivative of x. The effect of air density depends on whether the flap is down or up ($x < x_0$ or $x \geq x_0$). The effect of aircraft speed is dependent on a Taylor series function of the stroke.

The result of such fitting of the data on hand is shown in Figure 4 where the force is a function of stroke.

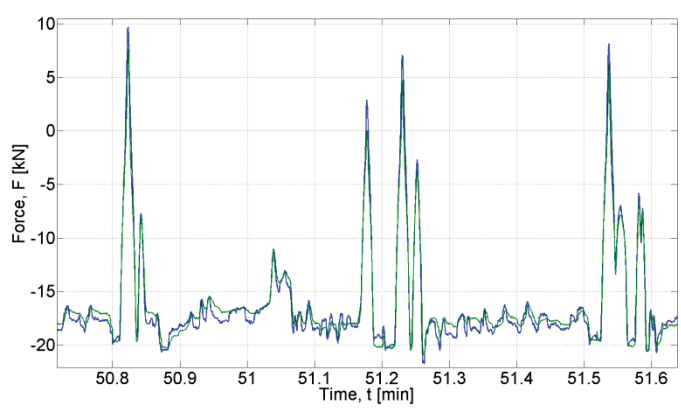

Figure 4 - Actual Force Profile (Blue) and Calculated Force Profile (Green)

3.8 Thermal Modeling of the Motor

High performance electric actuation systems (HPEAS) are being developed for new generation flight control surfaces under the Air Force Research Laboratory's (AFRL) Integrated Vehicle and Energy Technology (INVENT) program. The new distributed electro-mechanical actuation (EMA) systems would replace the traditional, large, heavy and difficult-to-maintain hydraulic

Approved for public release; distribution unlimited.

actuation system. The electric-based actuation is an enabling technology to simplify the whole power generation and distribution system.

The benefits brought from this transition are noticeable. With the traditional hydraulic power system, the pumps always run at 3000 psi, whether the actuators are used or not. All the energy into the hydraulic system becomes heat and the heat dissipated must be dumped into the fuel system and/or discarded to the ambient air. The EMA system provides power on demand. When flying level at near constant speed, the electrical power requirement is small. Only when the aircraft performs turn, pitch, roll and yaw in high acceleration would the actuators need to provide high power to move the flight control surfaces. The new electrical-based actuation systems generate less waste heat than the hydraulic power systems [15].

3.8.1 Finite Element Analysis

Figure 5 is the 3-D model of a typical Permanent Magnet Synchronous Machine (PMSM) servo motor. The motor design features are implemented in a 3-D frame based on the motor structure with a potted epoxy, square case and closed no-venting cover plate. The motor has a 12-slot stator and a 10-pole rotor as shown in Figure 6. This motor is designed to output 10 hp electrical power, with an efficiency of 92%. The total power loss in the motor is 600 W.

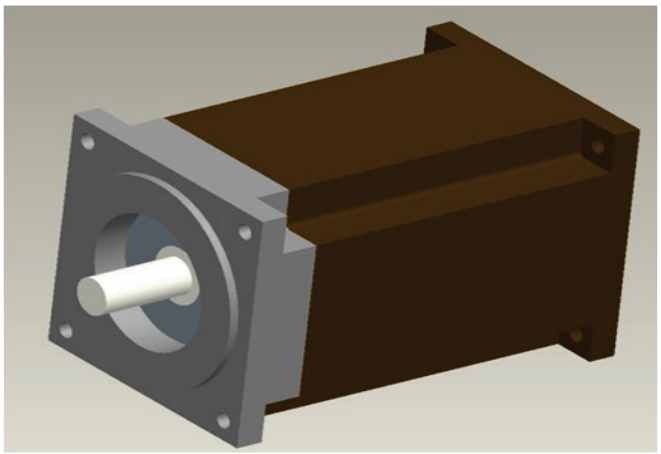

Figure 5 - 3-D Model of the PMSM Motor Design

Approved for public release; distribution unlimited.

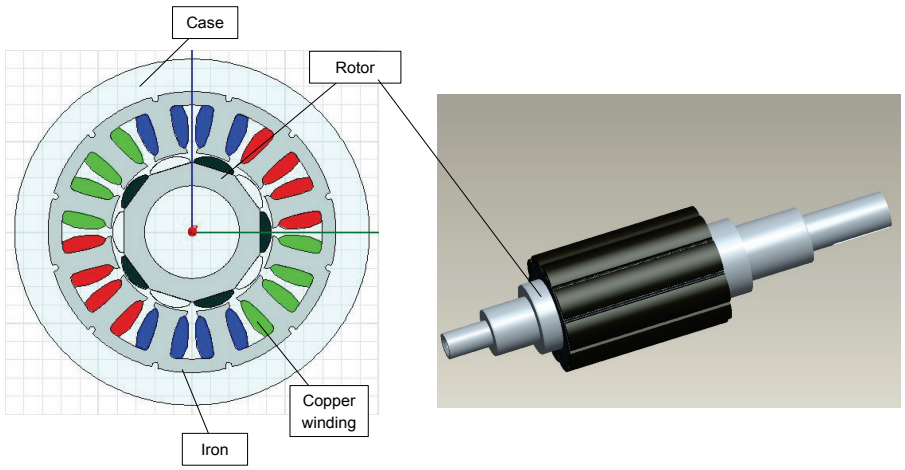

Figure 6 - Cross-Section of Motor and Rotor

Due to the symmetry, the geometry of the model is divided into a quarter section and imported into ANSYS [16] for the FEA simulation. Figure 7 shows the quarter section of the motor where the various components and the air gap are shown. The total thermal load is given in Figure 8. The estimated distribution of the power loss in the motor components is listed in Table 3. We assume all the heat loss occurs at the copper winding and end turns, and neglect the other losses because they are all relatively small. In the computation domain the power loss is 25% of total power loss 600 W or 150 W.

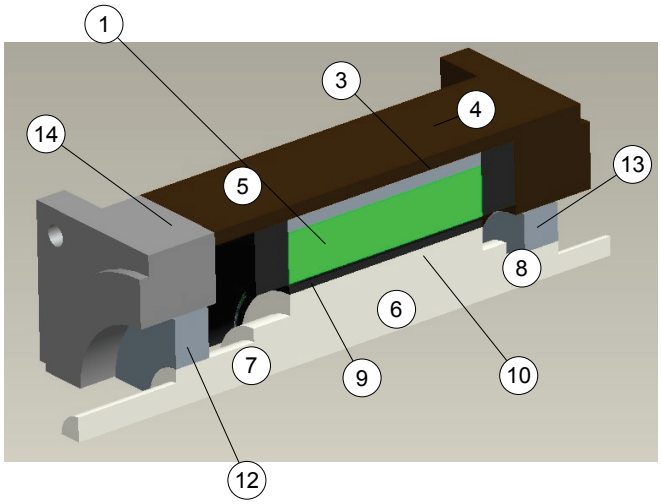

1. copper winding
3. Iron stator
4. case
5. case surface
6. shaft
7. shaft front end
8. shaft back end
9. magnet
10. air gap
12. front bearing
13. rear bearing
14. front cover

Figure 7 - Computation Domain

Approved for public release; distribution unlimited.

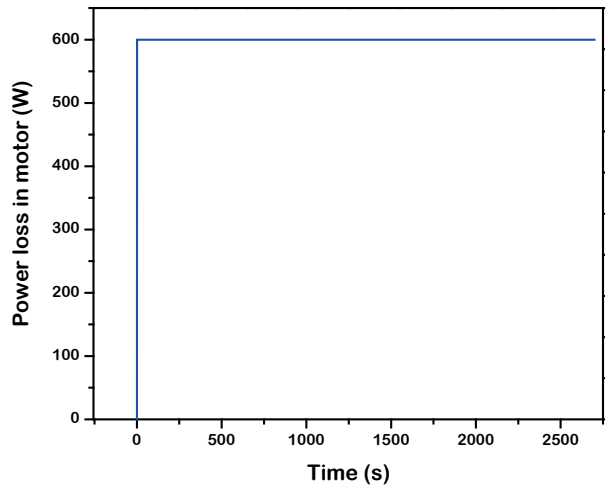

Figure 8 - Step Heat Load of the Motor

Table 3- Power Losses in Motor Components in a Quarter Section

	Power loss (W)	Percentage of total power loss
IC (copper loss)	125.2	83.5%
ICF (front copper end turn loss)	8.1	5.4%
ICB (rear copper end turn loss)	8.1	5.4%
IS (stator loss)	6.0	4.0%
IM (magnet loss)	0.8	0.6%
IW (windage loss)	0.4	0.2%
IBF (front bearing loss)	0.8	0.6%
IBB (rear bearing loss)	0.5	0.6%

ANSYS generally gives temperature information in the whole calculation domain. However, in practice, only several locations are needed to assess the thermal behavior of the motor. We focus on the temperatures of the winding, stator, magnet and bearing. It is noted that for every component, the temperature is not uniform. The temperature range can be characterized by the maximum and minimum temperatures within the particular component. For the copper winding, these two temperatures are quite close because of the high thermal conductivity of copper. While in the stator these two temperatures differ by a few degree Celsius. An external convective heat transfer coefficient of h=100 $W/m^2 \cdot K$ (forced convection), and heat transfer coefficient of h=10 $W/m^2 \cdot K$ (natural convection) are applied to the case of the motor. Table 4 shows the results from the simulation with an ambient temperature of 22°C. The node number in Table 4 corresponds to the part number shown in Figure 7. When radiation (with a surface emissivity ϵ of 0.85 assumed for the motor case) is applied to the model along with forced convection (h=100 $W/m^2 \cdot K$), the results show a lower temperature (~20°C). This means though forced convection is the dominant mode of heat transfer, radiation losses should be included.

Approved for public release; distribution unlimited.

With natural convection (h=10 W/m^2·K), radiation is the dominant mode of heat transfer, but the motor temperature is much too high. Thus it can be concluded at a heat load of 600 W, natural convection is not an acceptable cooling method. Additional discussions on radiation modeling are given later in this chapter.

Table 4 - Steady State Simulation Results with ANSYS

Node name	Material	Node number	Temp. (h=100) in °C	Temp. (h=100) in °C w/ radiation, ϵ =0.85	Temp. (h=10) in °C w/ radiation, ϵ =0.85
Copper winding	Copper	1	162	144	396
Iron stator	Iron	3	161	143	395
Case	Aluminum alloy	4	152	133	385
Case surface		5	150	130	382
Front cover	Aluminum alloy	14	141	124	377
Shaft	Stainless steel	6	149	125	384
Shaft front end	Stainless steel	7	145	124	383
Shaft rear end	Stainless steel	8	148	124	383
Magnet	NdFeB	9	149	125	385
Air gap	Air	10	160	135	395
Front bearing	Steel	12	143	124	381
Rear bearing	Steel	13	147	125	381

For the step heat load shown in Figure 8, the steady-state temperature field and the transient temperature response of the different parts inside the motor are given in Figures 9 and 10. The initial temperature of the motor is uniform at 22°C and ambient temperature is also at 22°C. The heat transfer coefficient is 100 W/m^2·K and radiation is included. The time constants for the temperature rise of the motor components are between 250-500 seconds.

Approved for public release; distribution unlimited.

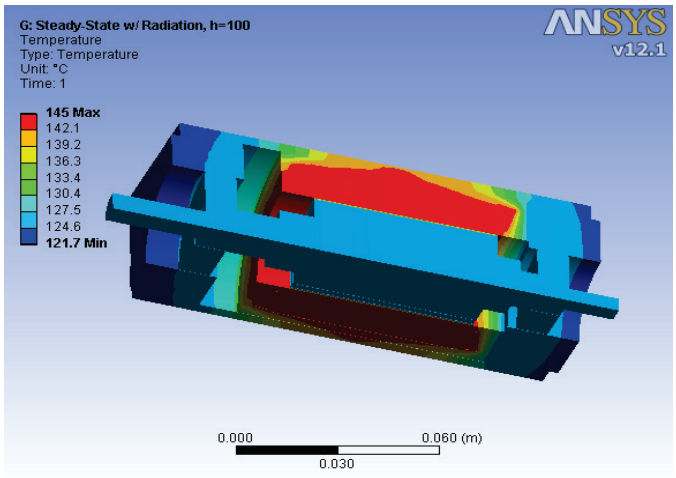

Figure 9 - Steady State Thermal Simulation Result (Forced Convection)

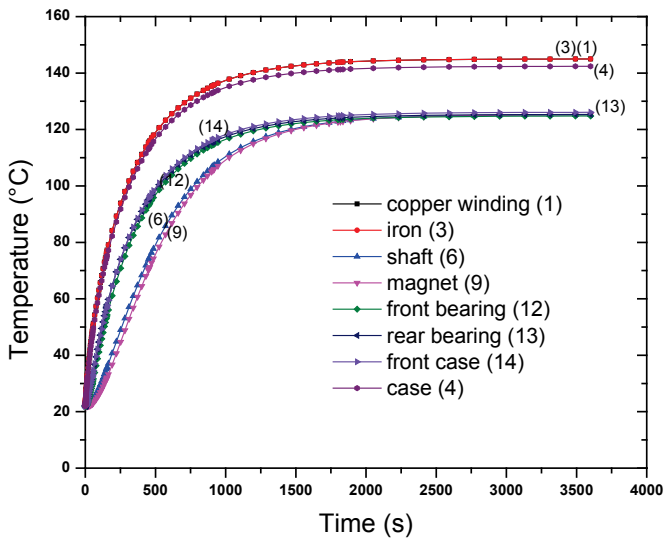

Figure 10 - Transient Temperature Response of the Step Heat Load Shown in Figure 8

3.8.2 Lumped Node Model

A lumped node thermal network to represent the temperature of every solid part of the EMA has been developed. The thermal resistances and capacitances between the nodes can be treated as electrical resistances and capacitances (Table 5). Hence the temperature of every node can be solved as the voltage in this equivalent network. This approach is well developed in the motor design industry [17, 18]. Some commercial software packages have already included the thermal network simulation, i.e. Motor-CAD [19]. Some studies have been made with FEA analysis and experimental testing has shown that such an approach is valid [20].

Approved for public release; distribution unlimited.

In the lumped node network we use a single temperature to represent each component, which generally is the average temperature. This average temperature can be compared with the maximum and minimum temperatures of the components from the FEA simulation. The numbers shown in the Figure 7 are the same as those in the lumped node network.

Table 5- The Analogy of the Equivalent Thermal Circuit

Electrical Circuit			Thermal Circuit		
V	[V]	Voltage	T	[C]	Temperature
I	[A]	Current Flow	Q	[W]	Heat Flow
σ	[1/Ωm]	Electrical Conductivity	k	[W/°Cm]	Thermal Conductivity
R	[Ω]	Resistance	R^{θ}	[°C/W]	Thermal Resistance
C	[F]	Capacitance	C^{θ}	[J/°C]	Thermal Capacitance

$$R^{\theta}{}_{conductive} = \frac{L}{k * A_c}$$

$$R^{\theta}{}_{convective} = \frac{1}{h * A_s} \tag{26}$$

$$C^{\theta} = \rho * V * C_p \tag{27}$$

where

L and A_C are length and cross-section area of the components
V and A_S are volume and surface area of the components
ρ and C_P are density and specific heat of the components

Eq. 26 and Eq. 27 show how to calculate the R and C values for a simple one-dimensional geometry. Accurate estimates for R and C values are not possible for complicated geometries such as an electric motor. A detailed 3-D solid model of a target motor is constructed and imported to FEA software like ANSYS to perform a steady-state and transient simulation. With these results we can estimate and select the values for the thermal resistances and capacitances. The advantage of this method is that we can evaluate the fidelity of the lumped node model with a real motor, add or reduce nodes to increase the model accuracy and efficiency, and estimate the maximum error between the node temperature and maximum temperature in a real motor.

This procedure can also be extended to model the gear-box, motor-driver and drive-train, and even include the aircraft wing surfaces and frames. The thermal network can also be incorporated into a multi-physics model to simulate the electrical, thermal, and mechanical performance of the whole EMA and its supporting structure. Once the proper thermal resistances and capacitances are selected, this simulation engine can be used with various time dependent boundary conditions during the whole mission duration including the air temperature,

Approved for public release; distribution unlimited.

aircraft speed, altitude and sunlight. The computational requirement of such a simulation is negligible compared to the FEA simulation.

The node network is constructed as shown in Figure 11. The electric motor has two thermal paths with other parts of EMA and environment. The first path, also the major one, is through the convection resistances R5, R5a and R5b, and the radiation resistance R5r (which will be discussed later in this chapter). The convection resistances represent the thermal resistances between motor surface and the air around it. Considering that the motor will be installed in a small space inside the wing structure, this convection is likely to be natural convection or weak forced convection. In ANSYS we assume the heat transfer coefficient for the forced convection to be h=100 $W/m^2 \cdot K$, which is a typical value for forced convection in air (Figure 9). The value of R5, R5a and R5b can be easily changed to accommodate the actual flow situation in the motor's final installation and flow conditions. In this model, the epoxy around the copper winding is combined with the copper windings to form node 1, due to the very small temperature difference between them. In some types of motors, such as those with long end turns, the epoxy temperature can be quite different than that of the copper winding. Separating the epoxy and copper winding provides more flexibility to the lumped-node model, and allows the model to be applicable to different motor designs.

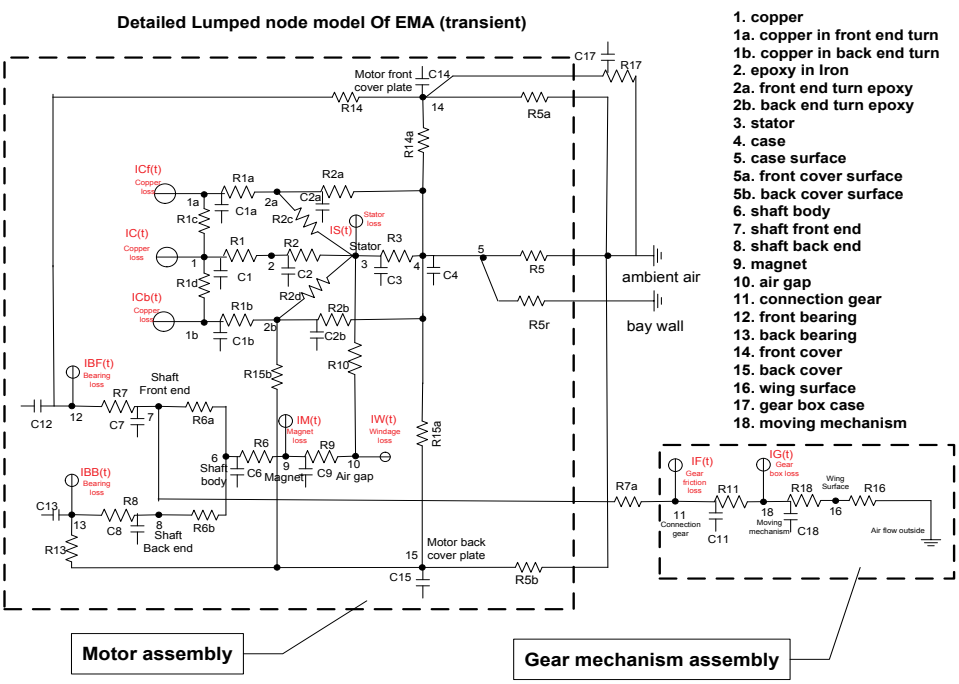

Figure 11 - Lumped Node Model of EMA (Transient)

The second thermal path is the conductive heat transfer from the motor rotor to the gear mechanism. This path, via R7a, is a minor heat flow path because the rotor and bearing loss is relatively small. But there is a possibility that the gear mechanism has higher temperature than the rotor and conduct heat back to motor. There could be additional thermal paths, such as from the motor back plate to the aircraft frame, which are not shown in Figure 11. However, incorporating additional thermal paths into the network and changing the lumped-node model accordingly is straightforward with the method presented in this chapter.

Approved for public release; distribution unlimited.

The following procedure is used to determine the R and C values in the lumped node network of motor assembly shown in Figure 11. The thermal resistances and capacitances are initially estimated using by Eq. 26 and Eq. 27. The R values can be adjusted and updated by comparing with lumped node model results with the steady-state results obtained from ANSYS. Table 4 lists the nodal temperatures from ANSYS steady state simulation for motor with forced convection boundary conditions. After the R values have been determined, the thermal capacitances can be updated by comparing the transient period of the lumped node results with the transient temperature distribution obtained from ANSYS. Table 6 lists the R and C values used in the lumped node model.

Table 6 - The R and C Values of Lumped Node Model of the Motor

R	(K/W)	C	(J/K)
R1	0.0029	C1	77.16
R1a	0.115	C1a	25.94
R1b	0.115	C1b	25.94
R1c	0.896	C2	11.95
R1d	0.896	C2a	44.69
R2	0.0093	C2b	44.69
R2a	0.395	C3	291.21
R2b	0.395	C4	499.39
R2c	1.045	C6	232
R2d	1.045	C7	35.58
R3	0.0305	C8	24.51
R5 (h=100)	0.492	C9	19.43
R5 (h=10)	4.92	C12	140.17
R5a (h=100)	3.199	C13	11.23
R5a (h=10)	31.99	C14	186.65
R5b (h=100)	3.199	C15	186.65
R5b (h=10)	31.99		
R6	0.03556		
R6a	4.054		
R6b	3.22		
R7	1.961		
R8	1.592		
R9	9.21		
R10	19.76		
R13	0.86229		
R14	0.76784		
R14a	0.254		
R15a	0.254		
R15b	0.18		

Approved for public release; distribution unlimited.

After all the resistor and capacitor values of the lumped-node network model of the motor in Figure 11 are known, the same values of the resistors and capacitors can be used to simulate the temperature response of the motor parts with any combination of heat losses and boundary conditions. For this standard resistor-capacitor electrical network, a set of first-order ordinary differential equations can be written as (Eq. 28 - Eq. 44):

$$\frac{T_{1a}-T_1}{R_{1c}}+\frac{T_{1a}-T_{2a}}{R_{1a}}+C_{1a}\frac{dT_{1a}}{dt}=Q_{Cf}(t) \tag{28}$$

$$\frac{T_1-T_2}{R_1}+\frac{T_1-T_{1d}}{R_{1b}}+\frac{T_1-T_{1a}}{R_{1c}}+C_1\frac{dT_1}{dt}=Q_C(t) \tag{29}$$

$$\frac{T_{1b}-T_{2b}}{R_{1b}}+\frac{T_{1b}-T_1}{R_{1d}}+C_{1b}\frac{dT_{1b}}{dt}=Q_{Cb}(t) \tag{30}$$

$$\frac{T_{1a}-T_{2a}}{R_{1a}}+\frac{T_3-T_{2a}}{R_{2c}}+\frac{T_4-T_{2a}}{R_{2a}}-C_{2a}\frac{dT_{2a}}{dt}=0 \tag{31}$$

$$\frac{T_1-T_2}{R_1}+\frac{T_3-T_2}{R_2}-C_2\frac{dT_2}{dt}=0 \tag{32}$$

$$\frac{T_{1b}-T_{2b}}{R_{1b}}+\frac{T_3-T_{2b}}{R_{2d}}+\frac{T_{15}-T_{2b}}{R_{15b}}+\frac{T_4-T_{2b}}{R_{2b}}-C_{2b}\frac{dT_{2b}}{dt}=0 \tag{33}$$

$$\frac{T_3-T_4}{R_3}+\frac{T_3-T_{10}}{R_{10}}+\frac{T_3-T_2}{R_2}+\frac{T_3-T_{2a}}{R_{2c}}+\frac{T_3-T_{2b}}{R_{2d}}+C_3\frac{dT_3}{dt}=Q_S(t) \tag{34}$$

$$\frac{T_{14}-T_4}{R_{14a}}+\frac{T_{15}-T_4}{R_{15a}}+\frac{T_3-T_4}{R_3}+\frac{T_{2a}-T_4}{R_{2a}}+\frac{T_{2b}-T_4}{R_{2b}}+\frac{T_{amb}-T_4}{R_5}+\frac{T_{bay}-T_4}{R_{5r}}=C_4\frac{dT_4}{dt} \tag{35}$$

$$\frac{T_9-T_6}{R_6}+\frac{T_7-T_6}{R_{6a}}+\frac{T_8-T_6}{R_{6b}}-C_6\frac{dT_6}{dt}=0 \tag{36}$$

$$\frac{T_6-T_7}{R_{6a}}+\frac{T_{12}-T_7}{R_7}-C_7\frac{dT_7}{dt}=0 \tag{37}$$

$$\frac{T_6-T_8}{R_{6b}}+\frac{T_{13}-T_8}{R_8}-C_8\frac{dT_8}{dt}=0 \tag{38}$$

$$\frac{T_9-T_6}{R_6}+\frac{T_9-T_{10}}{R_9}+C_9\frac{dT_9}{dt}=Q_M(t) \tag{39}$$

$$\frac{T_{10}-T_3}{R_{10}}+\frac{T_{10}-T_9}{R_9}=Q_W(t) \tag{40}$$

Approved for public release; distribution unlimited.

$$\frac{T_{12}-T_{14}}{R_{14}}+\frac{T_{12}-T_{7}}{R_{7}}+C_{12}\frac{dT_{12}}{dt}=Q_{BF}(t) \tag{41}$$

$$\frac{T_{13}-T_{15}}{R_{13}}+\frac{T_{13}-T_{8}}{R_{8}}+C_{13}\frac{dT_{13}}{dt}=Q_{BB}(t) \tag{42}$$

$$\frac{T_{4}-T_{14}}{R_{14a}}+\frac{T_{12}-T_{14}}{R_{14}}+\frac{T_{amb}-T_{14}}{R_{5a}}-C_{14}\frac{dT_{14}}{dt}=0 \tag{43}$$

$$\frac{T_{13}-T_{15}}{R_{13}}+\frac{T_{2b}-T_{15}}{R_{15b}}+\frac{T_{4}-T_{15}}{R_{15a}}+\frac{T_{amb}-T_{15}}{R_{5b}}-C_{15}\frac{dT_{15}}{dt}=0 \tag{44}$$

where

T_{amb} is ambient temperature,
T_{bay} is bay wall temperature,
Q is heat generation

This equation set can be solved by standard numerical methods. In Table 4, the temperatures with the presence of radiation heat transfer is also considered and listed in the last two columns. It should be noted that in a situation where air cooling is not effective (such as natural convection with a low h), the motor temperature could be very high and radiative heat transfer becomes the dominant mode of heat transfer. As radiation could be important, this feature is included in Eq. 10. The parallel radiation thermal path is modeled by adding a radiative thermal resistance to the lumped node model. The radiative thermal resistance value can be obtained by using the following equations.

$$h_r = \epsilon\sigma(T_1^2 + T_2^2)(T_1 + T_2) \tag{45}$$

$$R_r = \frac{1}{h_r A} \tag{46}$$

where

ϵ is the emissivity
σ is the Stefan-Boltzmann constant
T_1 is motor casing temperature
T_2 is bay wall temperature
A is surface area

Since the motor casing temperature is a temperature to be determined, the inclusion of radiation contribution involves an iterative process in the solution procedure to solve Eq. 28 – Eq. 44.

3.8.2.1 Examples

The simulation results of the lumped node model are compared with the FEA results under the same initial condition and boundary conditions (the step heat load given in Figure 8, Q = 600 W,

Approved for public release; distribution unlimited.

h=100 W/m^2·K). Figure 12 shows the lumped-node model and the FEA produce essentially the same temperature for the copper winding.

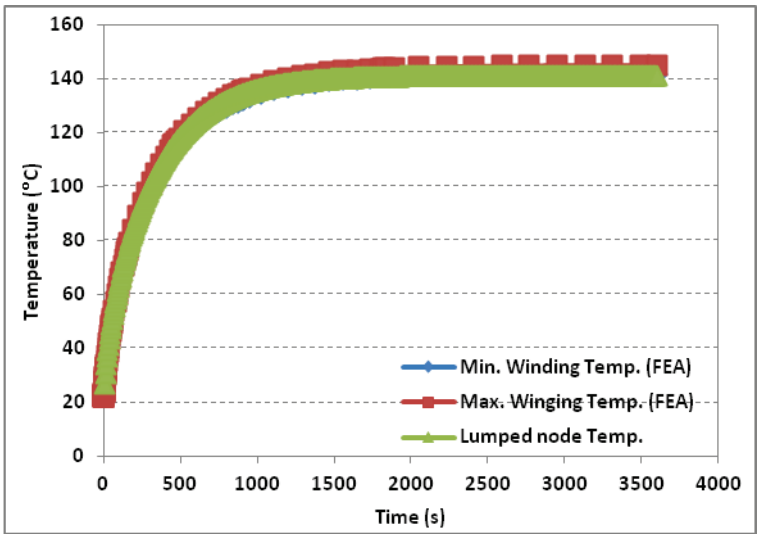

Figure 12 - Lumped-Node Network Simulation Result

This lumped node model is also tested with a pulsed heat load, where the thermal load is a square wave form repeating with time, as shown in Figure 13. Figure 14 shows a comparison between the ANSYS results with the lumped node model for the copper winding temperature. The excellent agreement between ANSYS results and lumped-node model proves that this model is a very effective and attractive alternative to the computational intensive FEA simulation. It is much faster to obtain essentially the same results as the FEA by using the lumped node model (less than a minute for the lumped node model compared to more than 20 hours for the FEA on same computer to simulate 750 seconds of heat load profile).

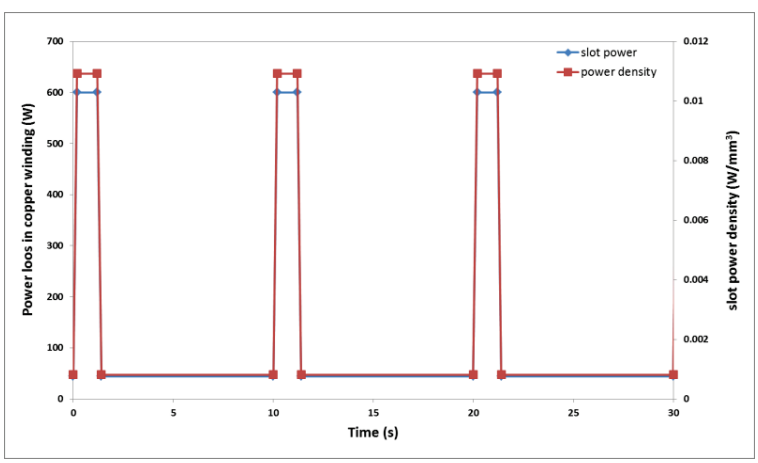

Figure 13 - Pulsed Heat Load

Approved for public release; distribution unlimited.

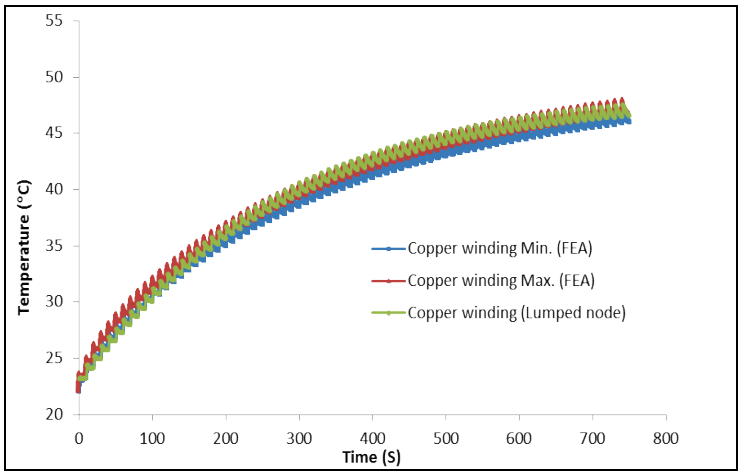

Figure 14 - Winding Temperature Comparison (FEA and Lumped Node)

A second time varying heat load is simulated to show the capability of the lumped node model. Shown in Figure 15 is a highly dynamic heat load typical of those of a 10 hp motor used for powering a flight control surface. The transient temperature of the copper winding and the motor case are given in Figure 16.

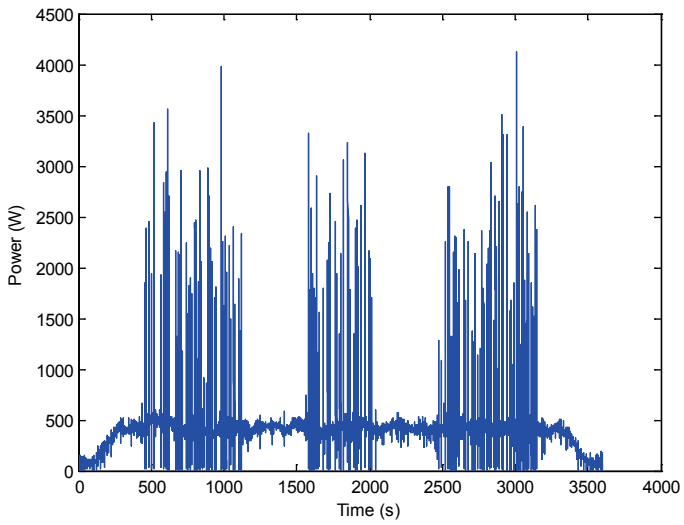

Figure 15 - Heat Load

Approved for public release; distribution unlimited.

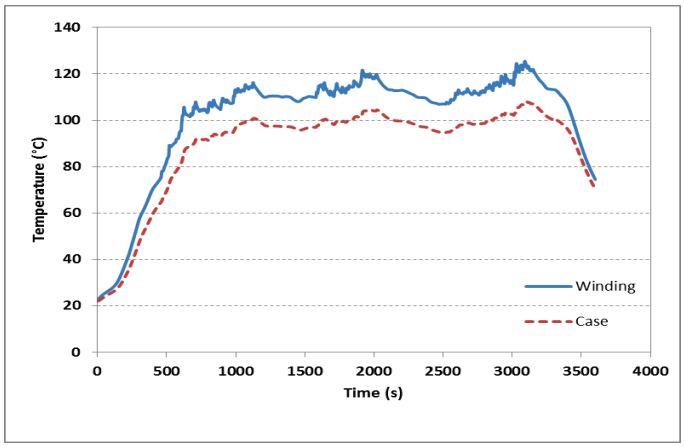

Figure 16 - Winding and Motor Case Temperatures

3.8.3 Lumped Node Model with PCM Module

In situations where the heat load is high and the convection heat transfer is ineffective (such as in an aircraft bay with near stagnant air), the temperature of the motor components can reach an unacceptable level. For example, for a steady heat load of 600 W with h=10 W/m^2·K, the copper winding temperature reaches nearly 400°C (see last column of Table 4). Another situation where excessively high temperature can occur in the copper winding even with forced convection (h=100 W/m^2·K) is when the ambient temperature is high. With an ambient temperature of 100°C instead of 22°C, the copper winding with h=100 W/m^2·K could reach 200°C. A solution to keep the motor temperature at an acceptable level is to use phase change materials (PCM) with a melting temperature below 150°C to store the excess thermal energy. Figure 17 shows the 3-D model of the motor and an aluminum/PCM composite.

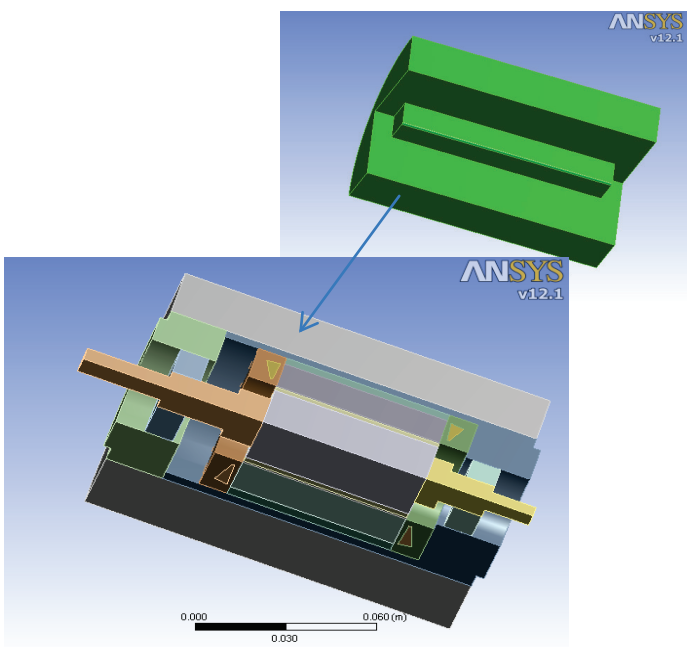

Figure 17 - Aluminum/PCM Composite

Approved for public release; distribution unlimited.

We can embed phase change materials in an aluminum foam structure to form an aluminum/phase change material (PCM) composite. To keep the copper winding below 150°C by storing the excess thermal energy in the PCM, we should choose a PCM with a melting temperature range below 150°C and a high latent heat of fusion. In this chapter, we select Erythritol as the PCM [21]. This PCM has a high latent heat (340 kJ/kg) and suitable phase change temperature range (~120°C). The solid and liquid specific heats are 1.18 kJ/kg and 2.15 kJ/kg, respectively. The PCM is modeled as a material with a temperature-dependent specific heat as shown in Figure 18.

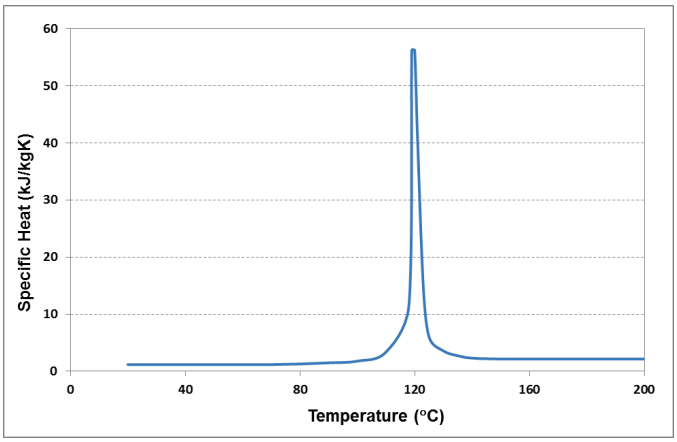

Figure 18 - Specific Heat vs. Temperature

The lumped-node network shown in Figure 19 is based on the motor assembly geometry.

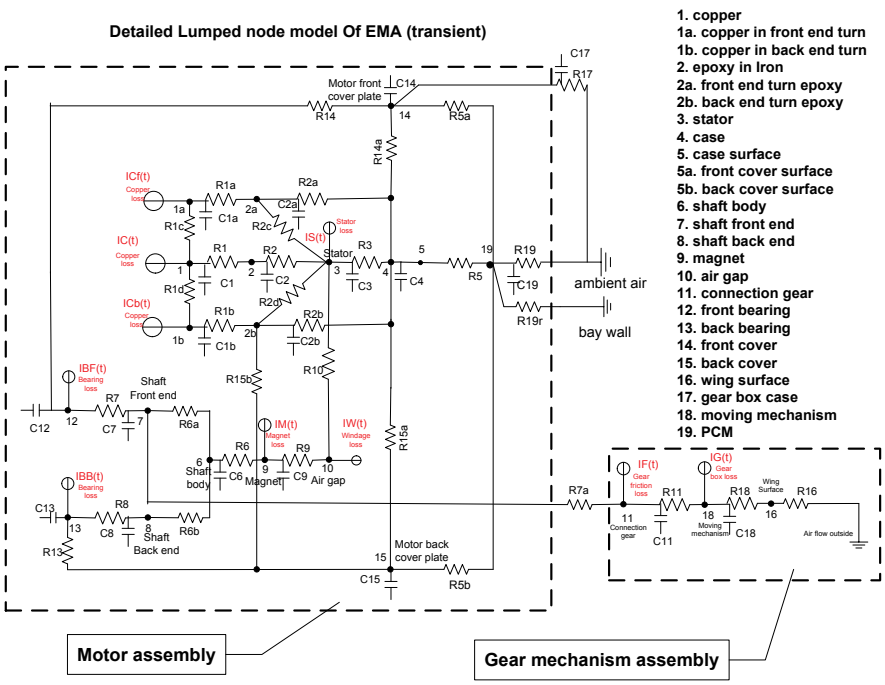

Figure 19 - Lumped-Node Model Including PCM

Approved for public release; distribution unlimited.

The additional R values in this network are listed in Table 7 where R5, R5a and R5b are thermal contact resistances between the case, front cover and back cover to the PCM module. The PCM thermal capacitance is temperature dependent and is obtained by multiplying the specific heat from Figure 18 with the mass of the PCM (see Eq. 47).

Table 7 - Network Parameters for Equivalent Thermal Resistances

R	(K/W)
R5	0.0018
R5a	0.01
R5b	0.01
R19 (h=10)	2.72
R19 (h=100)	0.34

To solve the PCM behavior, Eq. 47 is added into the lumped node model, and Eq. 35, 43 and 44 are replaced by Eq. 35', 43'and 44'.

$$\frac{T_4 - T_{19}}{R_5} + \frac{T_{14} - T_{19}}{R_{5a}} + \frac{T_{15} - T_{19}}{R_{5b}} - \frac{T_{19} - T_{amb}}{R_{19}} - \frac{T_{19} - T_{bay}}{R_{19r}} - C_{19}\frac{dT_{19}}{dt} = 0 \tag{47}$$

$$\frac{T_{14} - T_4}{R_{14a}} + \frac{T_{15} - T_4}{R_{15a}} + \frac{T_3 - T_4}{R_3} + \frac{T_{2a} - T_4}{R_{2a}} + \frac{T_{2b} - T_4}{R_{2b}} + \frac{T_{19} - T_4}{R_5} = C_4\frac{dT_4}{dt} \tag{35'}$$

$$\frac{T_4 - T_{14}}{R_{14a}} + \frac{T_{12} - T_{14}}{R_{14}} + \frac{T_{19} - T_{14}}{R_{5a}} - C_{14}\frac{dT_{14}}{dt} = 0 \tag{43'}$$

$$\frac{T_{13} - T_{15}}{R_{13}} + \frac{T_{2b} - T_{15}}{R_{15b}} + \frac{T_4 - T_{15}}{R_{15a}} + \frac{T_{19} - T_{15}}{R_{5b}} - C_{15}\frac{dT_{15}}{dt} = 0 \tag{44'}$$

3.8.3.1 Examples

Two heat load cases are simulated using the lumped node thermal network model. The cases are listed in Table 8. In both of these cases, the ambient temperature was chosen to be 100°C.

Table 8 - Lumped-Node Cases

Case No.	h ($W/m^2 \cdot K$)	Load Type	Load Power(W)
1	10	step	600
2	100	step	600

Figures 20 and 21 show the simulation results for the copper winding temperature. The results show that PCM module can hold the copper winding temperature under 130°C for as long as 400 s (h=10 $W/m^2 \cdot K$) or 500 s (h=100 $W/m^2 \cdot K$) under the 600 W heat load.

Approved for public release; distribution unlimited.

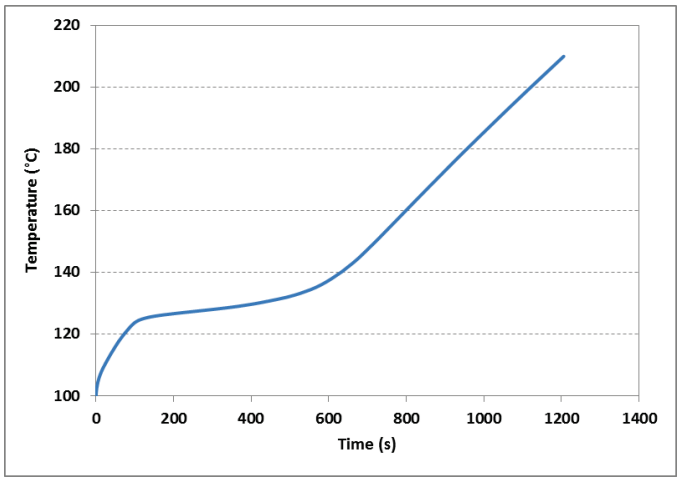

Figure 20 - h=10 W/m^{2}K, PCM (Case 1)

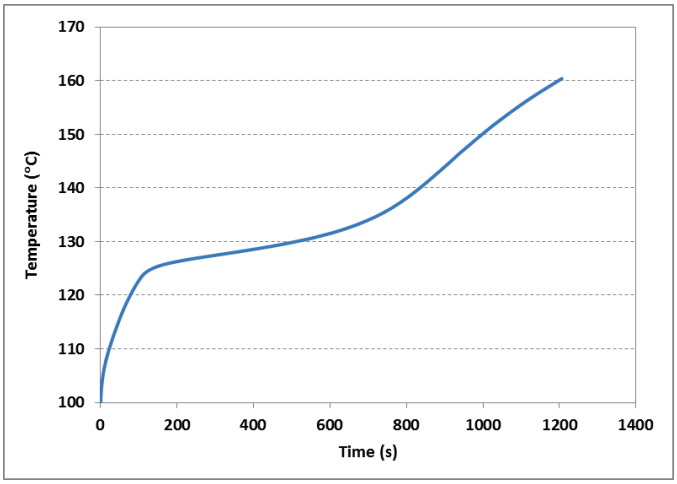

Figure 21 - h=100 W/m^{2}K, PCM (Case 2)

The lumped node thermal network is a feasible approach to simulate the mission-level EMA thermal performance. A new lumped node modeling technique which is based on tuning the R and C values with the FEA results is developed to overcome the difficulty in obtaining accurate R and C values in the motor thermal network. The lumped node model has been successfully applied to step and transient heat loads with cooling by both convection and radiation. For situations where phase change materials may be needed to store the thermal energy to avoid the motor reaching excessively high temperature, a PCM module has been incorporated successfully into the lumped node model as well.

3.9 An EMA Example and Results

A commercially available EMA was measured, modeled, simulated, and experimentally tested. Here are the results.

Approved for public release; distribution unlimited.

a. Parameters

The key parameters for the test EMA are shown in Table 9.

Table 9 - EMA Parameters

Symbol	Name	Value
N_{cr}	Gearing ratio	1963 rad/m
S	Number of slots	12
P	Number of poles	10
F_f	Power train friction	342 N
m	Rod mass	8.5 kg
I	Rotor moment of inertia	113.2 kg·mm^2/rad^2
$R_{s,ref}$	Phase resistance at T_{ref}	1.4 Ω
T_{ref}	Reference temperature	20 °C
α_R	Temperature coefficient of R_s	0.004041 1/°C [22]
λ_{PM}	PM flux linkage	0.149 Wb
$L_{d,peak}$	Peak direct inductance	17.35 mH
$L_{q,peak}$	Peak quadrature inductance	17.27 mH

Figure 22 shows the force-stroke data for the friction analysis.

Approved for public release; distribution unlimited.

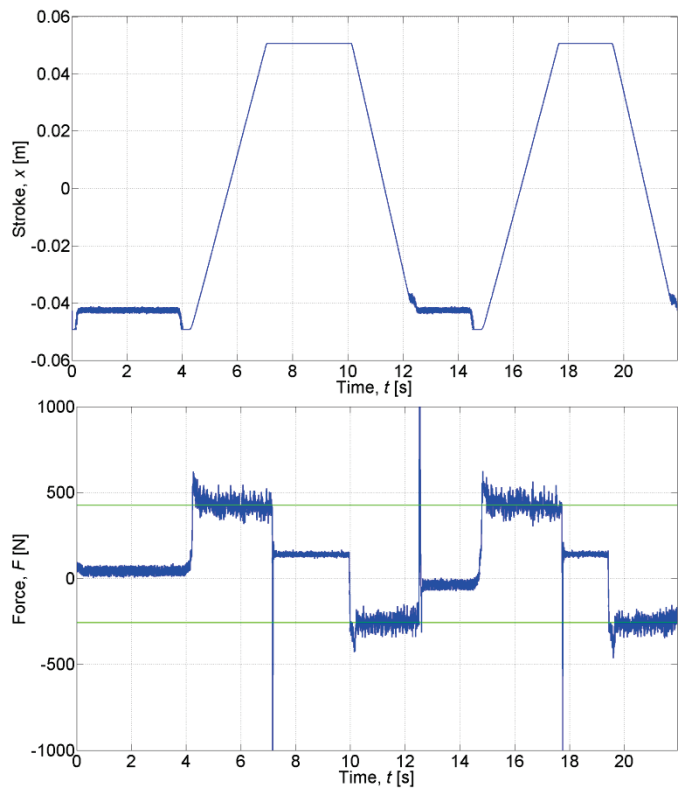

Figure 22 - Static Friction Analysis Showing Stroke (top) and Load Force (Bottom). The Green Lines on the Force Plot Represent the Mean Forces to Pull (-258 N) or Push (425 N) the EMA Rod, Overcoming the Friction of the Drive Train (342 N). The Bias towards Force Required to Push is the Weight of the EMA Rod (84 N)

The direct and quadrature inductances are obtained as shown in Figure 23 and Figure 24. The FEM model is simulated with a range of currents 0 A to 50 A, a range of torque angles 0 to π radians, and a range of rotor angles 0 to π/3 radians. For this motor, a range of π/3 radians captures one full cycle of variation in inductance values due to rotor angle.

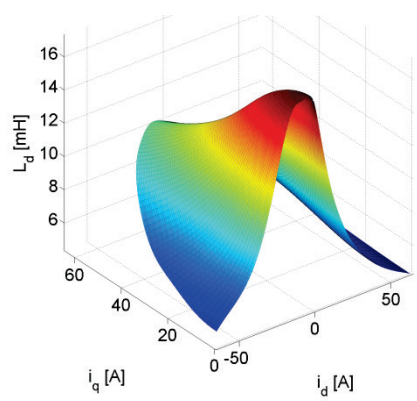

Figure 23 - Direct-Axis Inductance as a Function of Direct Current, i_d, and Quadrature Current, i_q

Approved for public release; distribution unlimited.

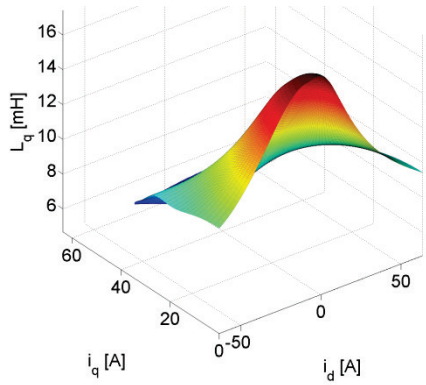

Figure 24 - Quadrature-Axis Inductance as a Function of Direct Current, i_d, and Quadrature Current, i_q

A computer rendering of the motor geometry is shown in Figure 25. This geometry is used for FEM modeling.

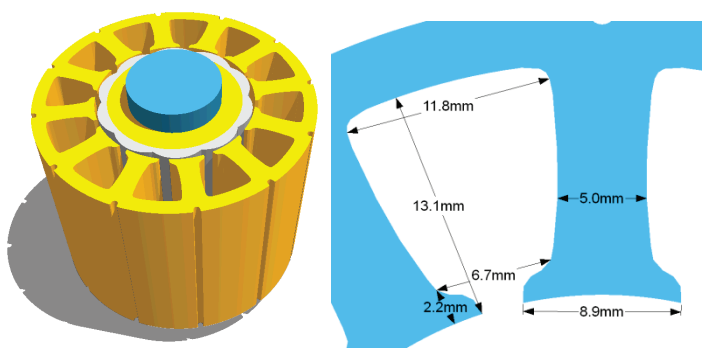

Figure 25 - Motor Geometry (Left) and Slot Measurements (Right)

Table 10 shows some of the material properties of the EMA motor.

Table 10 - EMA Material Properties

Part	Name	C_P	k	ρ
Casing	AL-384	963	96.2	2820
Lamination	Steel 1010	448	51.9	7872
Windings	Copper	385	401	8940
Epoxy	(unknown)	1050	0.85	1200
Axle	Steel	480	15	7750
Magnets	NdFeB-30	5e4	8.95	7400

C_p is the specific heat capacity.
k is the thermal conductivity.
ρ is the density.

Approved for public release; distribution unlimited.

b. Results

The desired stroke profile and the motor's actual stroke profile are shown in Figure 26. The motor followed the desired stroke profile very well.

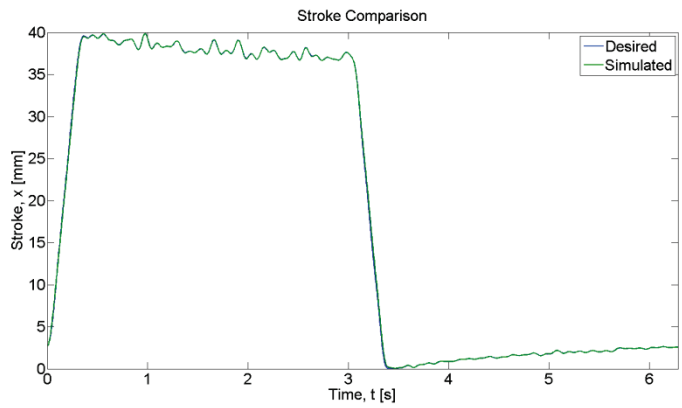

Figure 26 - Desired (Blue) and Actual (Green) Stroke Profiles

The load force profile and the motor-generated force, are shown in Figure 27.

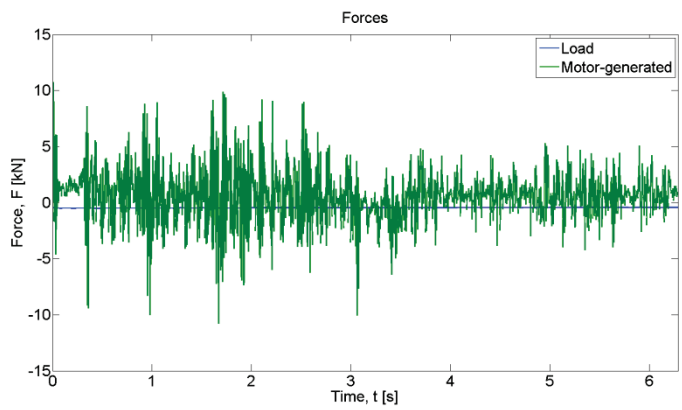

Figure 27 - Input Load Force Profile (Blue) and Motor-Generated Force (Green). The Load Force was a Sustained 450 N

The DQ0 voltages and currents are shown in Figure 28 and Figure 29, respectively.

Approved for public release; distribution unlimited.

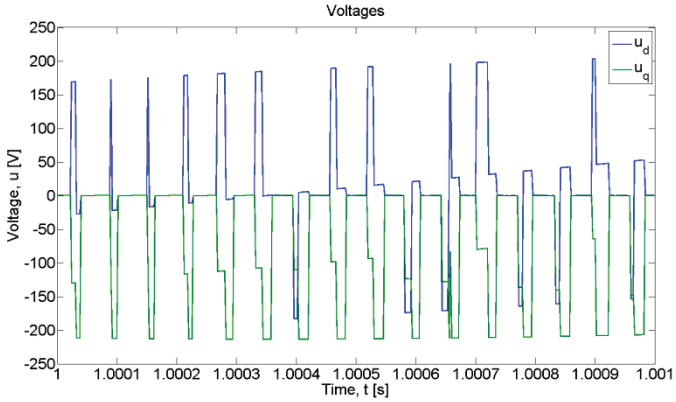

Figure 28 - DQ0 Voltages with Pulse Form due to PWM

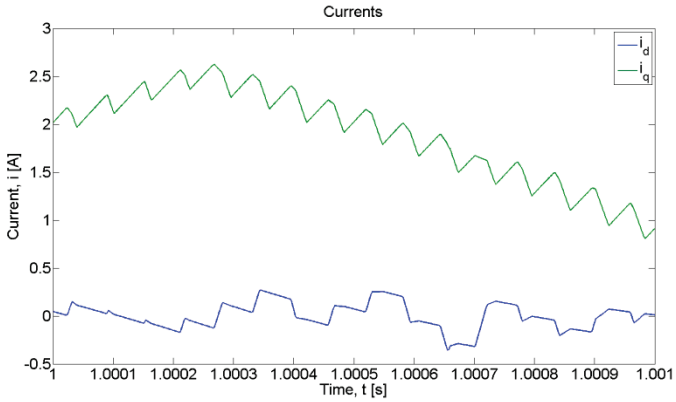

Figure 29 - DQ0 Currents

If the motor is treated as a system, the powers into (positive) and out of (negative) this system are shown in Figure 30.

Approved for public release; distribution unlimited.

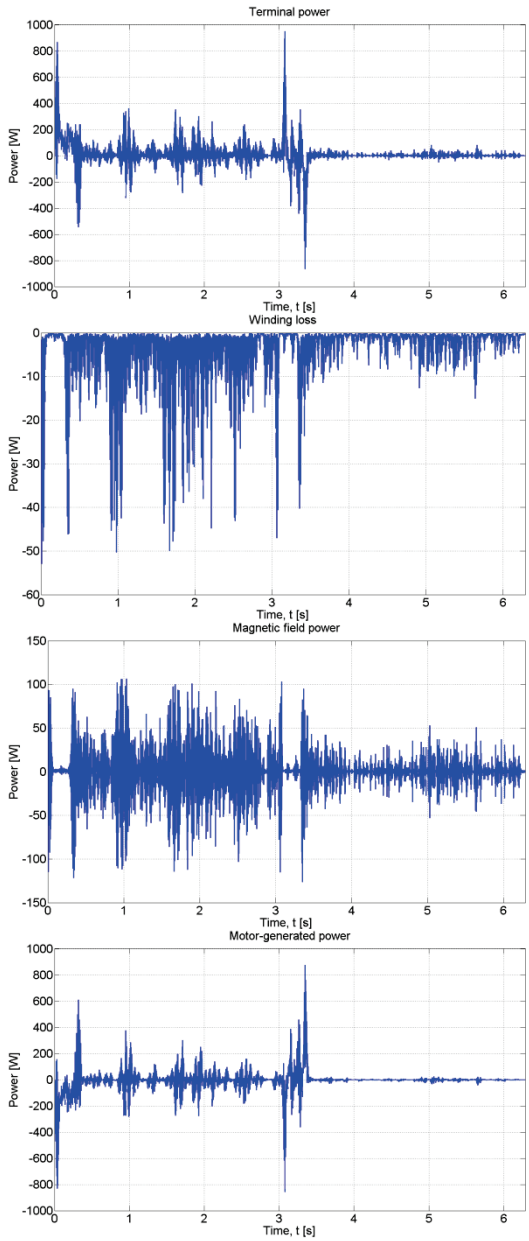

Figure 30 - Motor Powers Showing the Total Electrical Power at the Terminals of the Motor (First), the Power Loss in the Windings (Second), the Power Stored in the Magnetic Fields (Third), and the Mechanical Power Output on the Rotor (last)

The electrical power at the terminals is the power on the DC bus line. Note that sometimes this power is negative, meaning that the motor is actually sending power back to the source. The reason for this is that the wind load is actually driving the flight control surface, pushing against it as it yields to the wind pressure.

If the drive train is treated as a system, the power into and out of this system is shown in Figure 31.

Approved for public release; distribution unlimited.

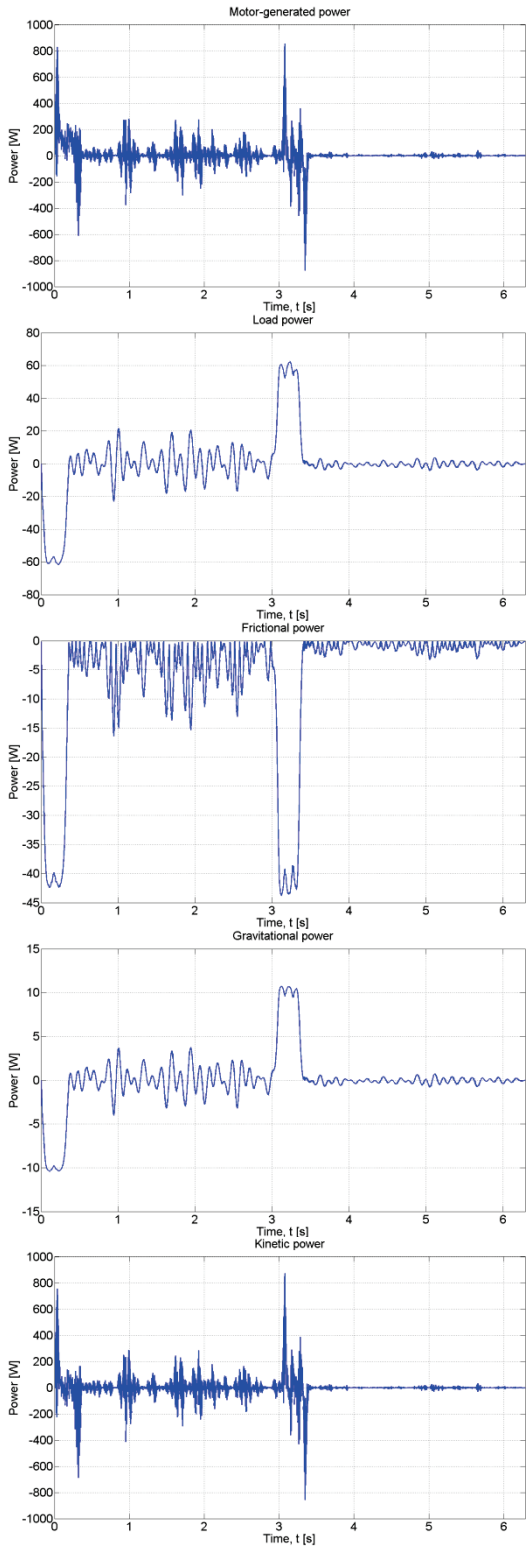

Figure 31 - Drive Train Powers Showing the Mechanical Power Input on the Rotor (First), the Load Power (Second), the Frictional Power (Third), the Gravitational Power (Forth), and the Net Kinetic Power (Last)

Approved for public release; distribution unlimited.

The comparison of the recorded temperatures and the simulated temperature of the stator is shown in Figure 32.

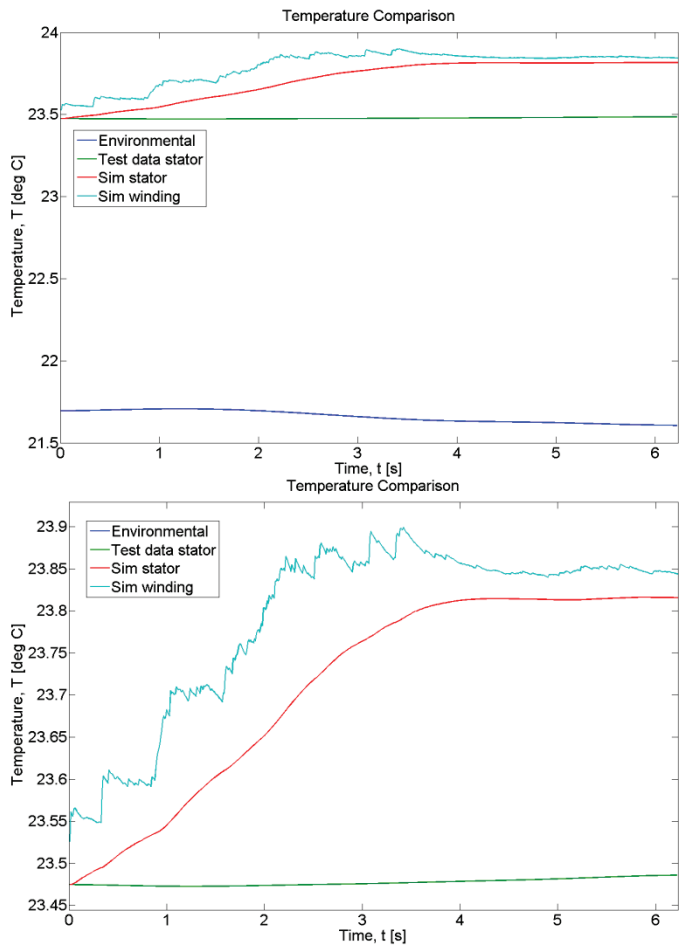

Figure 32 - Temperature Comparison (Above) and Again (Below) Zoomed in. These Plots have Environmental Temperature (blue), experimentally Measured Temperature of Stator (Green), Simulated Temperature of Stator (Red), and the Simulated Temperature of the Windings (Cyan)

The difference here is actually quite small, only about 0.34 °C, much less than the 1 °C sensitivity of the thermocouples used.

The accuracy of the temperature prediction is more readily observed for longer simulation profiles. Another test is shown in Figure 33 lasting a half-hour. The simulation of this test matches the stator temperature very well with a maximum error of 0.17 °C.

Approved for public release; distribution unlimited.

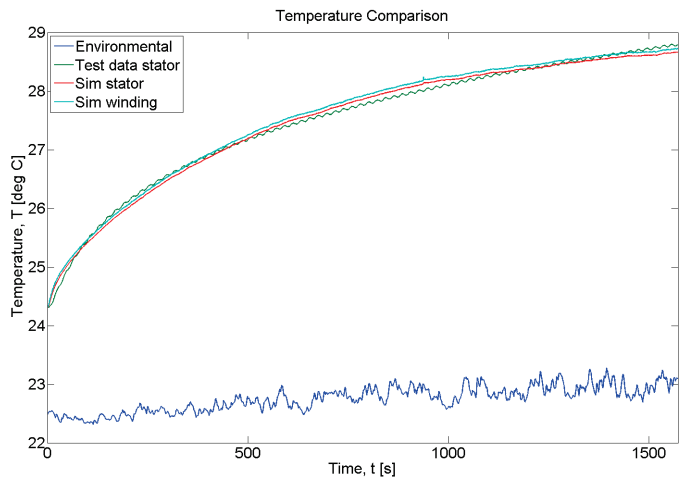

Figure 33 - Temperature Comparison for a Half-Hour Run Showing Environmental Temperature (Blue), Experimentally Measured Temperature of Stator (Green), Simulated Temperature of Stator (Red), and the Simulated Temperature of the Windings (Cyan). Note that the Simulated Temperatures of the Windings and Stator are About the Same, Indicating the Low Thermal Resistance in the Motor

The test shown in Figure 32 is run using k_v and k_a control coefficient values of 0.4 and 0.85, respectively. When these coefficients are instead both set to 1.04, the mean copper loss in the windings increased by a factor of 11.5. The temperature comparison between simulation and test is shown in Figure 34 and the terminal power is shown in Figure 35.

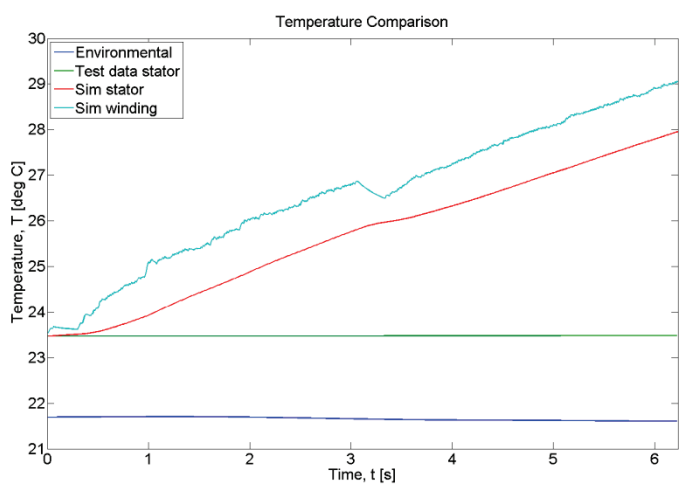

Figure 34 - Temperature Comparison Showing the Disparity between the Experimentally Measured Temperature of the Stator (green) and the Simulated Temperature (red) when Different Values of Control Coefficients are used. In this Case, the Test Data is shown Only for Reference. Obviously, with this Control Tuning, the Temperatures are not expected to Match

Approved for public release; distribution unlimited.

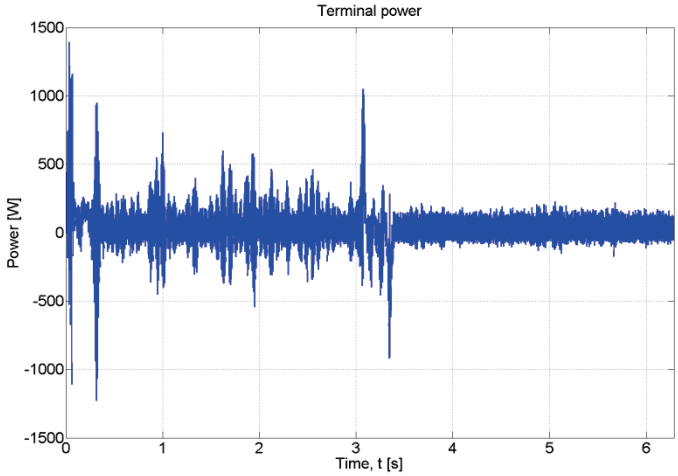

Figure 35 - Peak Terminal Power. Note that the Peak Power here is Over 50% Higher than Previously in Figure 31

This illustrates the significance that control has on excess heat generation. Inadequate control can lead to significantly higher losses.

There is a strong motivation to move towards all-electric aircraft. However, the significant obstacles to full realization of all-electric aircraft are the thermal management of heat loads and power management. In this chapter, it shows the successful implementation of an EMA model with a control algorithm, a PWM component, an electromechanical component with nonlinear parameters, and a thermal component. The model takes a desired position profile, a load force profile, and an environmental temperature profile as inputs and predicts the thermal behavior of the motor and the transient power demands of the EMA. It is shown that control plays a powerful role in how much excess heat is generated and how much the power demand spikes. It is also shown that the temperatures within the motor of the EMA are all within a fairly narrow band. This approach of using finite element method and nonlinear, lumped-element, integrated modeling gives a complete picture of the dynamic behavior of an EMA, thereby helping to make all-electric aircraft a reality.

Approved for public release; distribution unlimited.

4. MODELING AND SIMULATION OF POWER LOSS IN DRIVER UNIT OF ELECTROMECHANICAL ACTUATOR

4.1 INTRODUCTION

Since the operation of the EMA is highly transient and unpredictable due to the unexpected turbulence, the load torque and stroke might change rapidly or need to keep stable for a certain amount of time. The power loss and heat generation is different and more challenging from ordinary motors that operates under normal conditions with torque and speed that does not change dramatically. The highly transient load and stroke profile will result in a highly transient current and voltage in the driver circuit. And there may be a large amount of regenerative power generated from the deceleration process of the EMAs, which may also be converted to heat.

In this chapter, we study the heat problem of the control and drive units of EMAs, and build a model to calculate and simulate the power loss and heat generation in the driver board. The driver unit consists of a power inverter, a power dissipating resistor and a control circuit. The power loss of each part is studied. The heat loss in the power inverter comes mainly from the power switches – IGBTs. The on-state loss is proportional to the current of the motor, and the switching loss is determined by the switching frequency as well as currents and voltages. The power loss in the power dissipating resistor is determined by the regenerative power, the capacitor and the control algorithm to stabilize the bus voltage, which varies from different mission profiles and different applications. All those parameters can be obtained in our simulation code. The power loss on the control circuit is negligible compared with the power loss on IGBTs and the power dissipating resistor, and generates very little heat in the system.

4.2 PWM DRIVE SIMULATION

a. Background

Pulse-width modulation (PWM) is a commonly used technique for controlling power in inertial electrical devices, made practical by modern electronic power switches.

The average value of voltage (and current) fed to the load is controlled by turning the switch between supply and load on and off quickly. The longer the switch is on compared to the off periods, the higher the power supplied to the load.

The main advantage of PWM is its very low power loss in the switching devices. When a switch is off, there is practically no current, and when it is on, there is almost no voltage drop across the switch. Power loss, being the product of voltage and current, is thus in both cases close to zero. PWM also works well with digital controls, which, because of their on/off nature, can easily set the needed duty cycle.

Approved for public release; distribution unlimited.

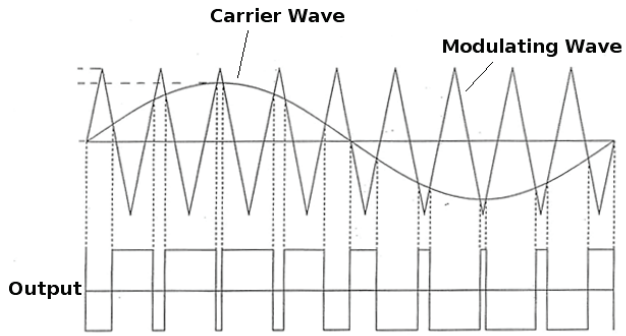

Figure 36 - PWM Generation

The PWM wave generation is shown in Figure 36. Comparing the carrier wave and modulating wave determines the PWM output. In this example, there are two output levels of the PWM wave, high and low. The amplitude of the carrier or sinusoidal wave directly corresponds to the output level: If the carrier wave is higher than the modulating wave, the output level is high; otherwise, the output level is low. Correct configuration of the modulating wave and output voltage can create the output with two voltages which can be used to drive the motor. The same result occurs because the main component in the square wave is still coordinated with the carrier wave. The high- frequency components that made it square would be automatically filtered by the inductance and would not contribute to the power input to the motor. This attribute allows us to use the PWM wave to drive the motor.

b. Simulation Model

The model used for simulation consists of a PMSM motor and a controller previously developed for this project. Two inputs are given: a time-history profile (a sequence of data points versus time) of desired positions (stroke reference profile) and another time-history profile of load forces (force profile). Both of these profiles can be translated to the perspective of the motor through the conversion factor of the drive train ratio. This enables us to generate a rotor-angle profile and a load-torque profile. Then, for each time step, the appropriate applied voltages to make the motor follow the stroke profile in the presence of the load torque profile are calculated by the control algorithm. These voltages are then applied to the motor, at which point the simulation enters a convergence loop to determine the correct currents and motor-generated torques in the presence of such applied voltages. With the motor-generated torque determined, the new rotor position can be calculated for that time step. Thus, the motion of the motor is simulated. Now, for each time step, once the currents are calculated, the power loss in the windings can also be found. These copper power losses then become the heat sources for the thermal algorithm, where temperatures for various points (nodes) in the motor are calculated. The outputs from the simulation are the actual stroke profile of the motor (as opposed to what was desired: the reference profile), the electrical power flowing in and out (regenerative) of the motor, and the temperature profiles for the various nodes.

The Dynamic equations of the motor:

Approved for public release; distribution unlimited.

$$\frac{di_d}{dt} = (1/L_d)(-R_s i_d + \omega_{me} L_q i_q + u_{dPWM}) \tag{48}$$

$$\frac{di_q}{dt} = (1/L_q)(-R_s i_q - \omega_{me} L_d i_d - \omega_{me}\lambda_p + u_{qPWM}) \tag{49}$$

$$\frac{d\omega_m}{dt} = (1/J)(\tau_M - \tau_L) \tag{50}$$

$$\frac{d\theta_m}{dt} = \omega_m \tag{51}$$

where u_d is input direct voltage, u_q is input quadrature voltage, i_d is direct current, i_q is quadrature current, R_s is phase resistance, L_d is direct inductance, L_q is quadrature inductance, ω_{me} is the mechanical frequency multiplied by the number of pole pairs $p/2$, λ_{PM} is the flux linkage from the permanent magnet, J is the rotor's moment of inertia, τ_M is the EM torque, and τ_L is the load torque, θ_m is the rotor's position, ω_m is the mechanical frequency.

The controller follows the voltage control equation:

$$i_q^* = i_q + k_i \frac{e_{\theta_m}}{\Delta t} + \frac{i_q}{\tau_M}\left[I\left(k_p \frac{e_{\omega_m}}{\Delta t} \right) - \alpha_m + c\left(k_p e_{\omega_m} \right) \right] \tag{52}$$

$$u_d^* = R_s i_d^* + L_d^* \frac{di_d^*}{dt} - \omega_{me}^* L_q^* i_q^* \tag{53}$$

$$u_q^* = R_s i_q^* + L_q^* \frac{di_q^*}{dt} + \omega_{me}^* L_d^* i_d^* + \omega_{me}^* \lambda_{PM} \tag{54}$$

where the variables with stars are the calculated values of next time step.

Besides the controller and the motor, a PWM block is introduced. The input to this PWM block is the control voltage, u_d and u_q. The output is the PWM control voltage. This module adjusts the control signal, generates a PWM wave, and sends it to the motor model. The whole system's structure is shown in Figure 37.

Approved for public release; distribution unlimited.

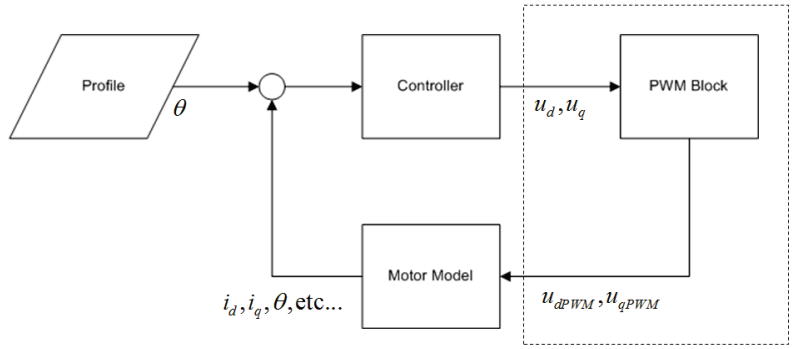

Figure 37 - Simulation System Structure

c. PWM Drive

The PWM drive module is added to our simulation to realize PWM function. The input is the control signal, u_d and u_q.

Before modulation, the input signal needs to be converted by the Park Transformation. This is a mathematical conversion that changes the quantities between stator-referenced domain (abc frame) into rotor-referenced domain (dq0 frame). In a simulation, we use a dq0 frame because it simplifies the computation. However, modulation of the voltages should be done in an abc frame because that is the quantities with physical significance and can be detected and used in real applications.

The basic equation of Park Transformation is:

$$\underline{S}_{dq0} = \underline{\underline{K}}\,\underline{S}_{abc} \tag{55}$$

$$\underline{S}_{abc} = \underline{\underline{K}}^{-1}\,\underline{S}_{dq0} \tag{56}$$

$$\underline{\underline{K}} = \frac{2}{3}\begin{bmatrix} \cos(\theta_{me}) & \cos(\theta_{me}-120°) & \cos(\theta_{me}+120°) \\ -\sin(\theta_{me}) & -\sin(\theta_{me}-120°) & -\sin(\theta_{me}+120°) \\ 1/2 & 1/2 & 1/2 \end{bmatrix} \tag{57}$$

$$\underline{\underline{K}}^{-1} = \begin{bmatrix} \cos(\theta_{me}) & -\sin(\theta_{me}) & 1 \\ \cos(\theta_{me}-120°) & -\sin(\theta_{me}-120°) & 1 \\ \cos(\theta_{me}+120°) & -\sin(\theta_{me}+120°) & 1 \end{bmatrix} \tag{58}$$

$$\theta_{me} = \frac{p}{2}\theta_m \tag{59}$$

where θ_m is rotor mechanical angle

In the PWM drive module, the quantities to be transformed are u_d and u_q. So the Park Transformation can be written as:

Approved for public release; distribution unlimited.

$$\underline{u}_{abc} = \underline{\underline{K}}^{-1} \underline{u}_{dq0} \tag{60}$$

$$\begin{bmatrix} u_a \\ u_b \\ u_c \end{bmatrix} = \begin{bmatrix} \cos\theta_{me} & -\sin\theta_{me} & 1 \\ \cos(\theta_{me} - 120°) & -\sin(\theta_{me} - 120°) & 1 \\ \cos(\theta_{me} + 120°) & -\sin(\theta_{me} + 120°) & 1 \end{bmatrix} \begin{bmatrix} u_d \\ u_q \\ u_0 \end{bmatrix} \tag{61}$$

$$u_a = u_d \cos\theta_{me} - u_q \sin\theta_{me} + u_0 \tag{62}$$

$$u_b = \cos(\theta_{me} - 120°) u_d - \sin(\theta_{me} - 120°) u_q + u_0 \tag{63}$$

$$u_c = \cos(\theta_{me} + 120°) u_d - \sin(\theta_{me} + 120°) u_q + u_0 \tag{64}$$

$$\underline{u}_{dq0} = \underline{\underline{K}} \underline{u}_{abc} \tag{65}$$

$$\begin{bmatrix} u_d \\ u_q \\ u_0 \end{bmatrix} = \frac{2}{3} \begin{bmatrix} \cos\theta_{me} & \cos(\theta_{me} - 120°) & \cos(\theta_{me} + 120°) \\ -\sin\theta_{me} & -\sin(\theta_{me} - 120°) & -\sin(\theta_{me} + 120°) \\ 1/2 & 1/2 & 1/2 \end{bmatrix} \begin{bmatrix} u_a \\ u_b \\ u_c \end{bmatrix} \tag{66}$$

$$u_d = \frac{2}{3}\left(u_a \cos\theta_{me} + u_b \cos(\theta_{me} - 120°) + u_c \cos(\theta_{me} + 120°)\right) \tag{67}$$

$$u_q = -\frac{2}{3}\left(u_a \sin\theta_{me} + u_b \sin(\theta_{me} - 120°) + u_c \sin(\theta_{me} + 120°)\right) \tag{68}$$

$$u_0 = \frac{1}{3}\left(u_a + u_b + u_c\right) \tag{69}$$

PWM is done by comparing the carrier wave with the control signal. The carrier waves are often high-frequency period signals. The carrier wave frequency carrier wave should be higher than the highest frequency component that we want to keep in the control signal. That is because, after modulation, the components with frequency higher than the carrier wave will be lost.

The time step is an important parameter in the simulation. After PWM is introduced into our simulation, the time step should be smaller because of the high-frequency carrier wave's introduction. This will significantly increase the simulation time. Some strategy is used to reduce the computation time. The simulation uses small time steps when doing computation with PWM but for other parts a lower resolution is used.

The PWM-driven simulation results show that our motor and controller model can function properly with PWM driving the motor. Some simulation results and comparison with simulation results without PWM are shown in Figure 38 and Figure 39:

Approved for public release; distribution unlimited.

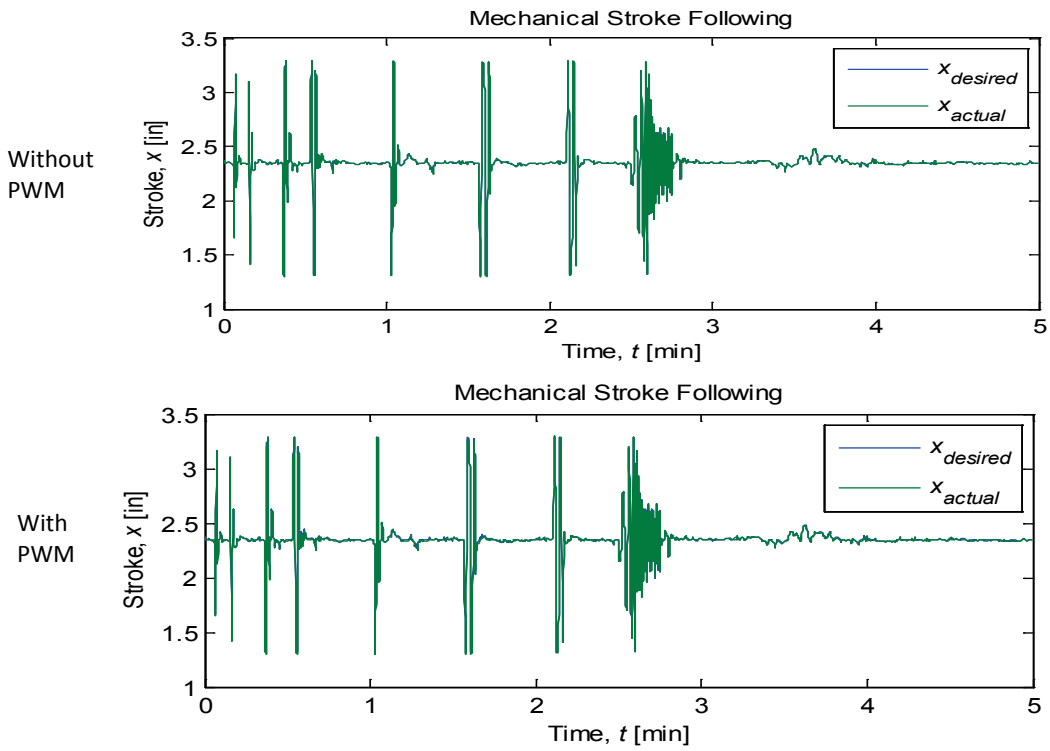

Figure 38 - Mechanical Stroke Following Results Comparison

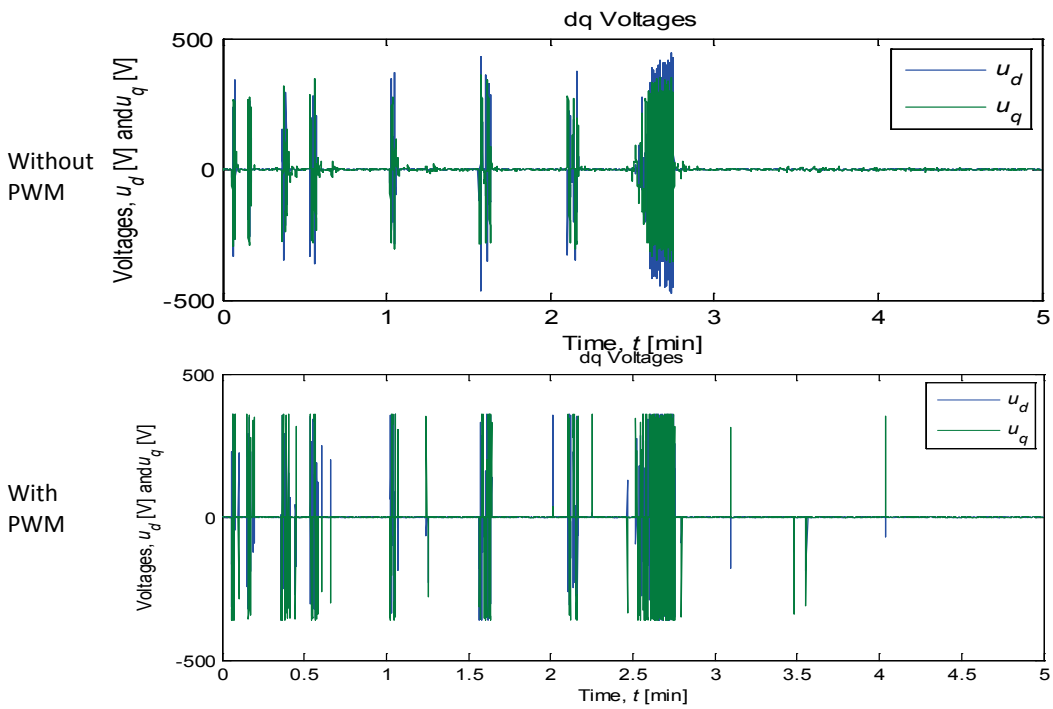

Figure 39 - D-Axis and Q-Axis Voltages Comparison

Approved for public release; distribution unlimited.

4.3 Structure of the Electronic Unit

The electronic unit is a circuit board combining the control and drive modules for the EMA. It is based on a Danaher control unit (SERVOSTAR S610). The control module has a microprocessor and its peripheral circuits. The drive module is an IGBT package. There is a resistor called an unloading resistor. Its function is to dissipate the excessive regenerative energy produced. There is a capacitor on the DC bus to store the regenerative power. The amount of energy that the capacitor could store is limited by the DC bus voltage range. When the DC bus voltage reaches its upper limit, the capacitor cannot be charged, and the excessive regenerative energy will be dissipated on the resistor. The circuit board is shown in Figure 2. The red square indicates where the IGBTs and the resistor are. The IGBT package is under the heat spreader marked by "EP". The green resistor is the one for dissipating regenerative power. On the left is the heat sink which covers the red square area. It is removed to reveal the IGBT package and the unloading resistor.

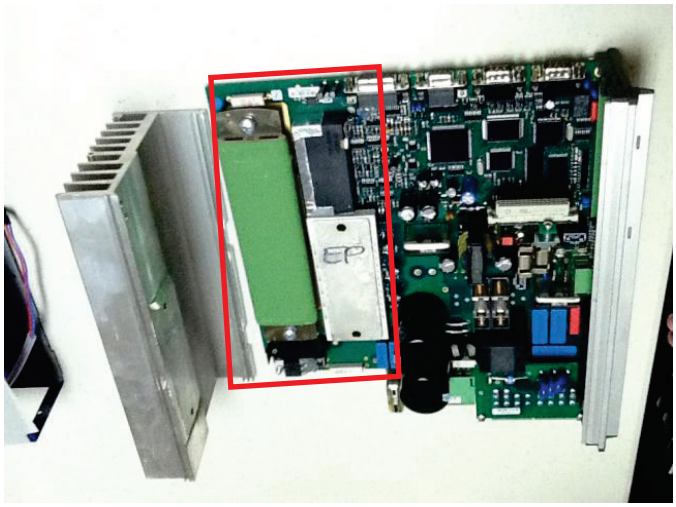

Figure 40 - Electronic Unit of the EMA

The board can be divided into three main components: controller circuit, the IGBT package and unloading resistor. The diagram that shows the function and relationship of each component is in Figure 41. The bold wires indicate the power flow through and the current can be large. The thin wires means those electrical quantities are just signals and do not carry large current.

Approved for public release; distribution unlimited.

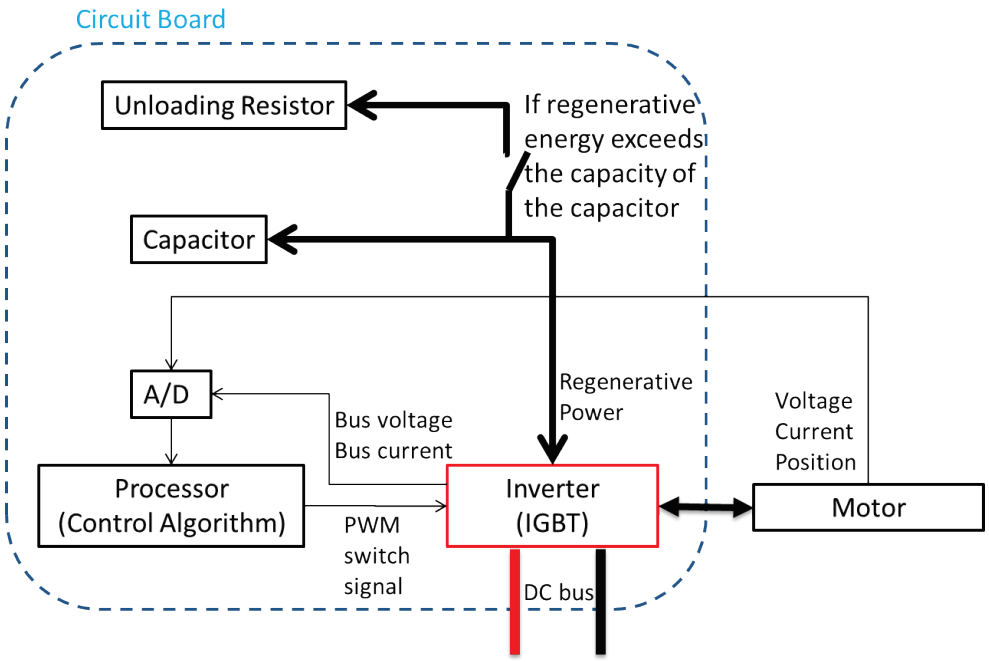

Figure 41 - Electronic Unit Block Diagram

4.4 Power Loss on the EU

Since we are concerned about power loss that will cause heating problems and do not focus on efficiency, only the absolute amount of power loss is meaningful to our study.

As shown in Figure 41, large power only goes through the IGBTs, the unloading resistor and the capacitor. The controller module only deals with signals and does not carry large currents. The power level of that part is much smaller than the other two parts on the board.

4.4.1 Power Loss on IGBTs

IGBTs are switching components that control the input voltage to the motor. In this EMA, a full bridge IGBT power module is used as an inverter to drive the motor. There are six IGBTs packaged in the module. It connects to the DC source which provides the power, and provides PWM voltage to the motor. The switches are controlled by the controller, and operate at approximately 1 kHz.

In an aircraft power system, a DC power supply is available to the EMA system. In order to drive the motor, we need to use the inverter to generate AC power. An inverter is also essential to implement PWM control. A typical full bridge inverter diagram is shown in Figure 42. Six IGBTs are used to build the inverter.

Approved for public release; distribution unlimited.

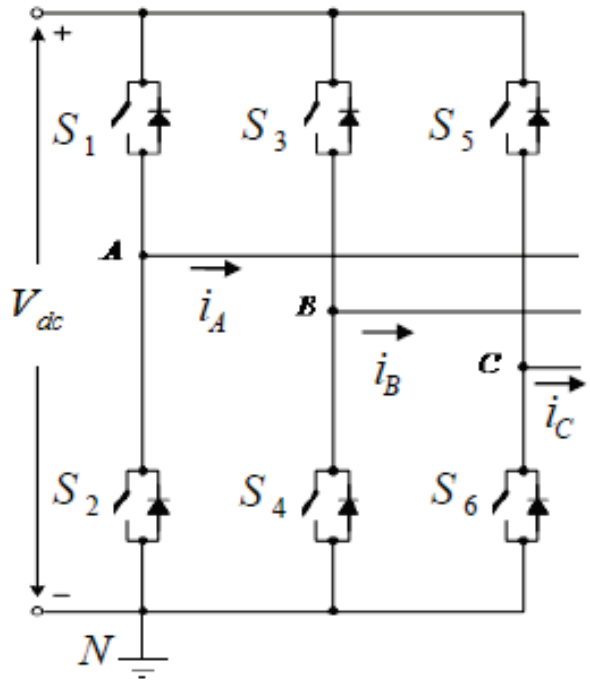

Figure 42 - Two Level Voltage Source Inverter, S1 ~ S6 are Switches, Which are IGBTs in the EMA Application

The IGBTs are controlled by the gate signals, and function as switches. The controller determines when the IGBTs should be turned ON or OFF. The control of the motor is accomplished by switching IGBTs. The motor stator current will go through the IGBTs that are ON, and the motor terminal voltage will be applied on the IGBTs that are OFF. The voltage and current can be large if the power consumed by the motor is high.

Since the IGBTs deal with large current and voltage, the power loss on them are very important in the system. The power loss on IGBTs comes from two sources: on-state loss and switching loss.

On-state loss is caused by the current flowing through the non-perfect device's on-state resistance. While the device is turned "ON" and current flows through the device, there will be a voltage drop and the on-state resistance could be used to characterize this power loss.

Switching loss the loss happens when the IGBT is turning on and off. The transition between ON and OFF states is not instant, during the rise and fall of the current and voltage the product of them will generate some power loss.

For a given IGBT, the on-state loss is related to the current and voltage on the IGBTs, which depends on the control scheme and the load of the motor. The switching loss is determined by the switching frequency.

Approved for public release; distribution unlimited.

a. On-state Loss of the IGBTs

The IGBTs function as switches in the circuit. When the switch is turned "ON", it should perform like an ideal switch, and have zero resistance. However, for IGBTs, especially those with high power ratings, the voltage drop is not negligible even when they are turned ON.

Since the current is relatively large when the switch is ON, with a voltage drop, the power loss

$$p_{ON} = v_{ON} i \tag{70}$$

where v_{ON} is the on-state voltage drop across the device, and i is the current flowing through the collector (for IGBTs)/drain (for MOSFETs) terminal.

Then the power loss can be expressed as follows, with R_{ON} being the on-state resistance:

$$p_{ON} = i^2 R_{ON} \tag{71}$$

Figure 43 is an example showing the current versus voltage of an IGBT. The data is from the datasheet of a 600V/300A IGBT module.

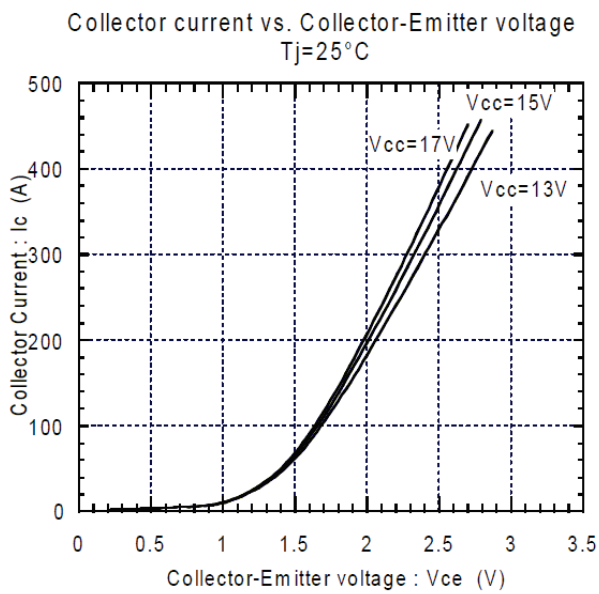

Figure 43 - Collector Current vs. Collector-Emitter voltage. The Curve Becomes Linear When Current is higher than 100A. In that Range, an Equivalent Resistance can be used to calculate the Voltage Drop

As shown in the figure, the current versus voltage is almost linear when current is higher than 100A. An equivalent resistance can be used to calculate the on-state loss if we know the stator current.

Approved for public release; distribution unlimited.

Because the stator current is dependent on the mission profile, the on-state loss is also determined by the mission profile. Different load and stroke curves may result in very different on-state losses on the IGBTs.

b. Switching Loss of the IGBTs

When the device is turned ON or OFF, the current cannot change instantaneously, there is a switching time for it to rise/fall. During that period of time, both current and voltage are not zero or negligible. The power loss, which is the product of current and voltage, needs to be considered. The switching process is shown in Figure 44.

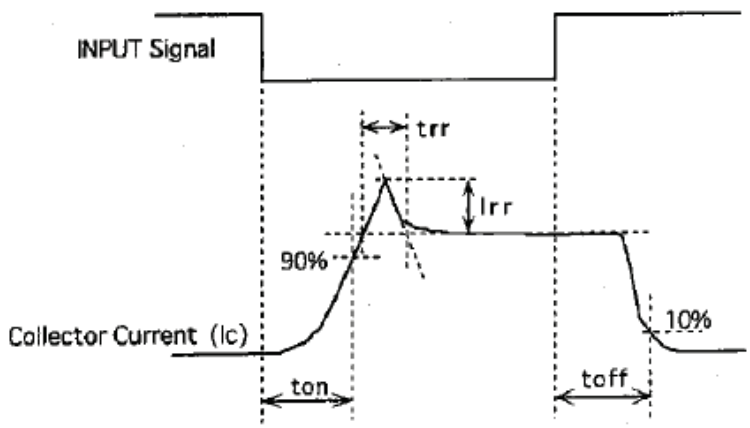

Figure 44 - Definition of Switching Time of IGBT. The "Input Signal" is the Input to the Gate, and the Device is an N-Channel IGBT

Switching loss occurs at every switching of the device. It includes on, off, and reverse recovery losses. For a given device, the power loss during each switch operation could be modeled by the equations given in [23].

$$E_{sw} = A_{sw} i(t)^{B_{sw}} \tag{72}$$

where E_{sw} is the switching energy loss for one switching operation, $i(t)$ is the load current, A_{sw} and B_{sw} are curve fitting constants for the device. The equation can be used for turn-on, turn-off losses as well as reverse recovery losses.

Assuming load current is constant, then E_{sw} is constant for a specific device, and the switching loss could be expressed as:

$$P_{sw} = (E_{on} + E_{off} + E_{rr}) \cdot f \tag{73}$$

where f is the switching frequency. E_{on} is turn-on loss, E_{off} is turn-off loss and E_{rr} is reverse recovery loss. It shows that the switching loss is proportional to switching frequency. A curve showing switching energy loss versus current is usually provided in the datasheet of the device. An example of switching loss curve is shown in Figure 45.

Approved for public release; distribution unlimited.

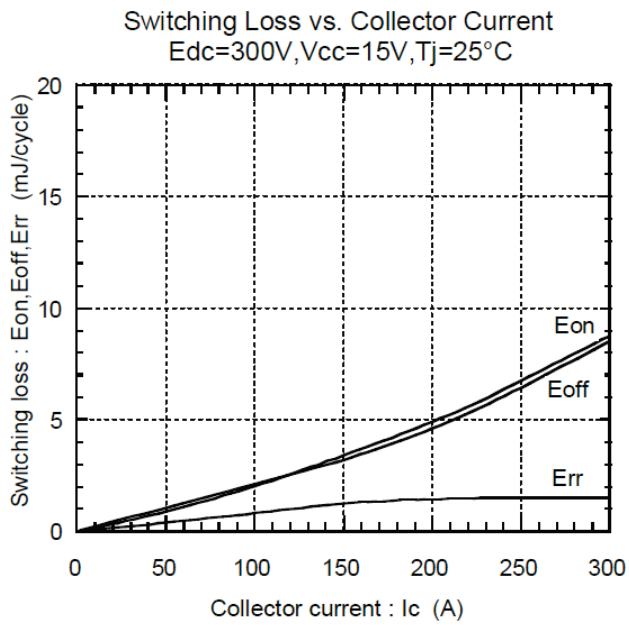

Figure 45 - Switching Loss vs. Collector Current. The Total Switching Loss for one Switching Operation is the Sum of the Three Shown in the Figure

We can estimate the switching loss using the curve. For example, if the load current is 100A, and switching frequency is 1000Hz, then the switching loss for one IGBT is 5 watts. The total loss in the inverter is about 30 watts.

4.4.2 Power Loss on Unloading Resistor

When the motor decelerates, it operates like a generator, and the kinetic energy is transformed to electricity. This regenerative energy will flow back to the EU, and need to be stored or dissipated.

To deal with the regenerative power, a typical circuit shown in Figure 46 is often used. When regenerative power is produced, current will flow back from inverter and charge the capacitor. The switch SW1 (a MOSFET or IGBT) is off. If the capacitor can handle the amount of energy, there will be no power dissipation, and the regenerative energy will be sent to the motor when the inverter draws power from DC bus to the motor.

Approved for public release; distribution unlimited.

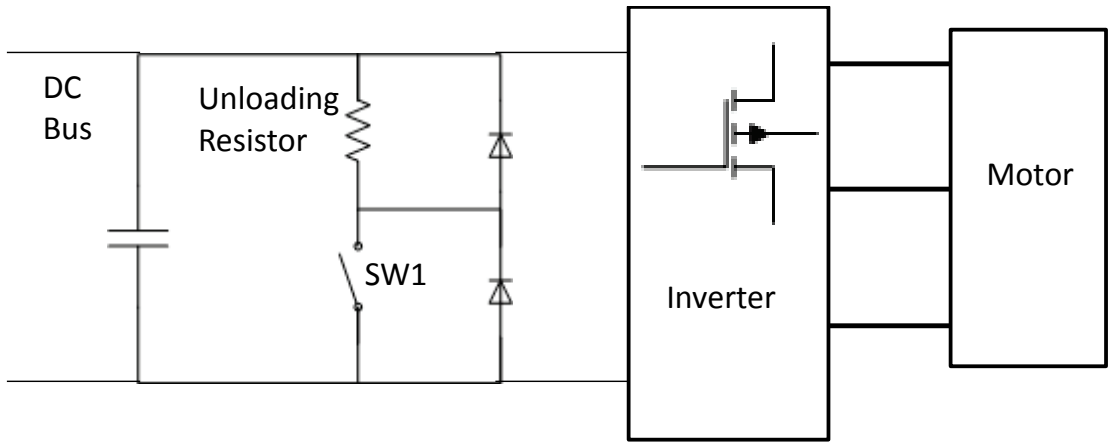

Figure 46 - Regenerative Energy Storage and Dissipation Circuit

The capacitor absorbs the regenerative energy by being charged by regenerative current. While the capacitor is being charged, the DC bus voltage will increase due to the capacitor's voltage equation:

$$V_C(t) = V_{C0} + \int_{t0}^{t} \frac{1}{C} i_C(t)dt \tag{74}$$

where V_{C0} is the DC bus initial voltage, i_C is the charging current, and V_C is capacitor voltage. Since the DC bus voltage has its maximum allowed value, the capacitor's ability to store the regenerative energy is limited. If the regenerative energy exceeds the capacitor's limit, SW1 will turn on and excessive power will be dissipated on the unloading resistor, producing power loss and heat.

The regenerative power can be obtained by calculating the total power input to the motor. From the EMA simulation data or experiment data, we have the voltage and current values of the motor. The instantaneous power consumed by the motor could be calculated:

$$P_{Motor}(t) = \frac{3}{2}[i_d(t)u_d(t) + i_q(t)u_q(t)] \tag{75}$$

where i_d and u_d are direct current and voltage, i_q and u_q are quadrature current and voltage. When the power input is negative, that amount of regenerative power is generated. It is highly dependent on the mission profile. However the amount of regenerative power that is dissipated and lost in the resistor is highly dependent on how the circuit is designed and how much energy can be stored in the capacitor (e.g., the value of the capacitance and the DC bus voltage's upper limit $V_{\max}$).

4.4.3 Power Loss on Control Circuits

The control circuits process the feedback signals and generate gate control signals to control the inverter. The main part is a microcontroller and its auxiliary circuits and power supply. All those

Approved for public release; distribution unlimited.

components work in a low voltage level. The power supply to the microcontroller is 3.3V or 5V, and the typical power consumption is about 1 to 2 W depending on the load of computation [24].

The working current of those components are at milliamperes, and the total power consumption of the circuit is almost negligible compared to the power loss on IGBTs and the unloading resistor. Therefore when modeling the power loss on the control and drive board, the control circuit part will not be considered.

4.5 Modeling of the Power Loss on the EU

After the analysis of the contributing power losses on the EU, a model can be built to calculate the total power loss. This total loss will include the losses from both contributors: the IGBTs and the unloading resistor.

The power loss on IGBTs is calculated using the stator current, which can be obtained from motor simulation model [25], or from measurements. Eq. 70 and Eq. 72 are used to calculate the power loss. Parameters such as R_{ON}, E_{on}, E_{off} and E_{rr} can be obtained from datasheet of the device. If such data is not available, we can use the values of a device with the same power rating as an approximation.

The regenerative power is calculated using terminal voltages and currents of the stator, either from simulation data or measurements. Follow Eq. 74 we can calculate the instantaneous power consumed by the motor, and when it's negative power, there is regenerative power flows through the motor back to the DC bus.

The DC bus capacitor voltage is monitored. When the capacitor is being charged by regenerative current, its voltage follows Eq. 73. When the inverter draws power from the DC bus, the capacitor is discharged first before drawing power from the rectifier and the power system. It follows the same equations above, only the sign of the current will be negative. When the voltage on the capacitor drops to the initial DC bus voltage, the EMA will be powered by the rectifier, and the capacitor voltage will be locked at the rectifier's output voltage. To sum up, the capacitor voltage can be written as:

$$\begin{cases} V_C(t) = V_{C0} + \int_{t0}^{t} \frac{1}{C} i_C(t)dt & \text{if } V_{C0} < V_C < V_{\max} \\ V_C(t) = V_{C0} & \text{if } i_C < 0 \text{ and } V_C \le V_{C0} \\ V_C(t) = V_{\max} & \text{if } i_C > 0 \text{ and } V_C \ge V_{\max} \end{cases} \tag{76}$$

When the voltage on the capacitor reaches the voltage limit (the third situation in the above equation), regenerative current will go through the unloading resistor and there will be power loss from regenerative power. The power loss on the unloading resistor will be

$$P_{UR} = i^2 R_{UR} \tag{77}$$

where i is the regenerative current and R_{UR} is the unloading resistance.

Approved for public release; distribution unlimited.

4.6 THERMAL MODELING OF THE EU

A Finite Element Analysis (FEA) based lumped node network and its simulation of a mission profile. This model is based on a detailed FEA model to locate the hot spots, to determine the network parameters and to verify its effectiveness. The model can also deal with the nonlinear behavior of the EU introduced temperature-dependent magnetic properties. This model can be incorporated into lumped node magnetic and electric model to develop a full multi-physics, multi-scale simulation engine. This engine can accurately analyze the complete EU in a systematic scale and whole-mission duration.

To develop a lumped node thermal network to represent the temperature of every solid part of the EU. The thermal resistances and capacitances between the nodes can be treated as electrical resistances and capacitances. Hence the temperature of every node can be solved as the voltage in this equivalent network.

A thermal model was present to show the heat load of the EU. The model detail is based on Danaher control unit (SERVOSTAR S610). Figure 41 shows the control unit. There are six IGBTs under the heat spreader marked by "EP". The green rectangular show on Figure 41 is the regenerative resistor. Figure 47 is the data sheet provided by manufacture.

Model	S610
Output Continuous Current Per Phase (RMS/phase)	10
Output Peak Current Per Phase (5 sec)	20
Rated Input Power (KVA) @ 480 VAC	8.1
Internal Power Dissipation Watts	90
AC Input Line Voltage (3 phase)	208-480 VAC
Continuous Regen Power	
Internal Watts	200
External Watts	1500

Figure 47 - SERVOSTAR S610 Data Sheet

The model is generated in FLOTHERM in order to simulate the actual situation of different materials, changing cross-sections, and heat loads. In the thermal model, heat is mostly generated by the IGBTs, and the model only needs to simulate heat flow from IGBTs, not from

Approved for public release; distribution unlimited.

the rest of the board. Heat generated at the IGBTs is conducted to the heat sink through the heat spreader (EP). A fan provides forced air convection to remove heat from the heat sink. According to manufacturer data sheet, the control board internal power dissipation is 90 W at 480 VAC power input. The following assumptions are made. (1) The board is running at half power input with 240 VAC and 45 W power dissipation; (2) 80 percent of power goes to six IGBTs; (3) a Sanyo Denki 60 x 15 mm, 12 V axial fan provides forced air through the heat sink. Figure 48 shows the configuration of simulation of control unit, and the air flow speed inside of control unit (the top cover was removed to show inside of the control board).

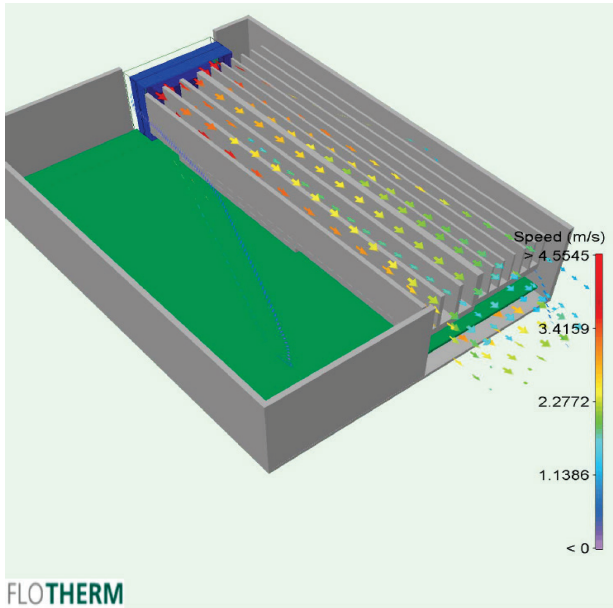

Figure 48 - Control Box Configurations

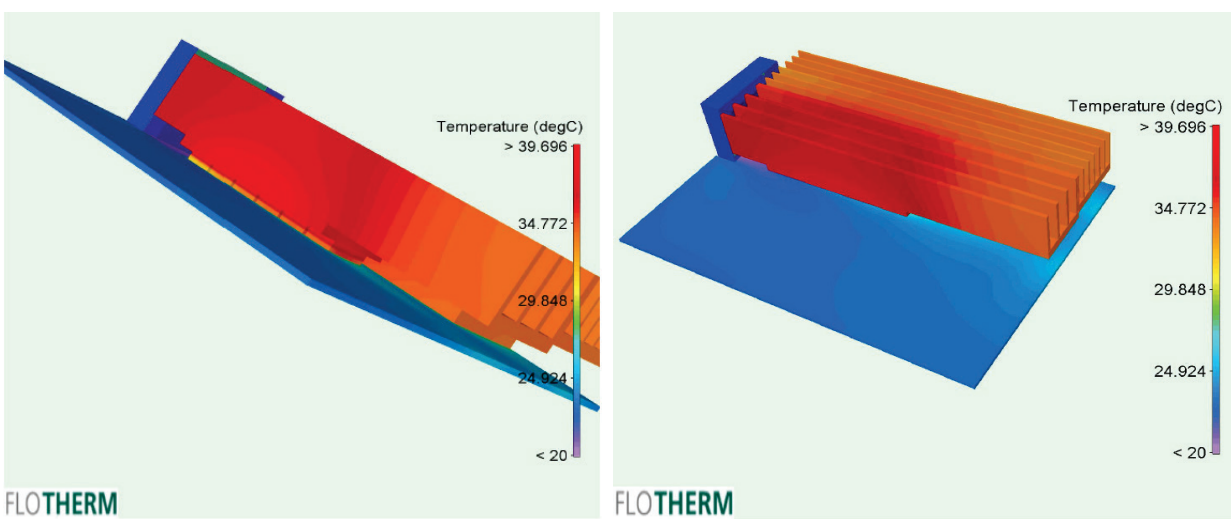

Figure 49 - Simulation Results

Shown in Figure 49, the IGBT temperature is about 40°C. A commercially available fan is adequate to manage the heat generated by the control board.

Approved for public release; distribution unlimited.

In order to monitor the temperature on heat sink, the "modified" simulation has been carried out. There are four temperature monitor points located on the heat sink as shown on Figure 50.

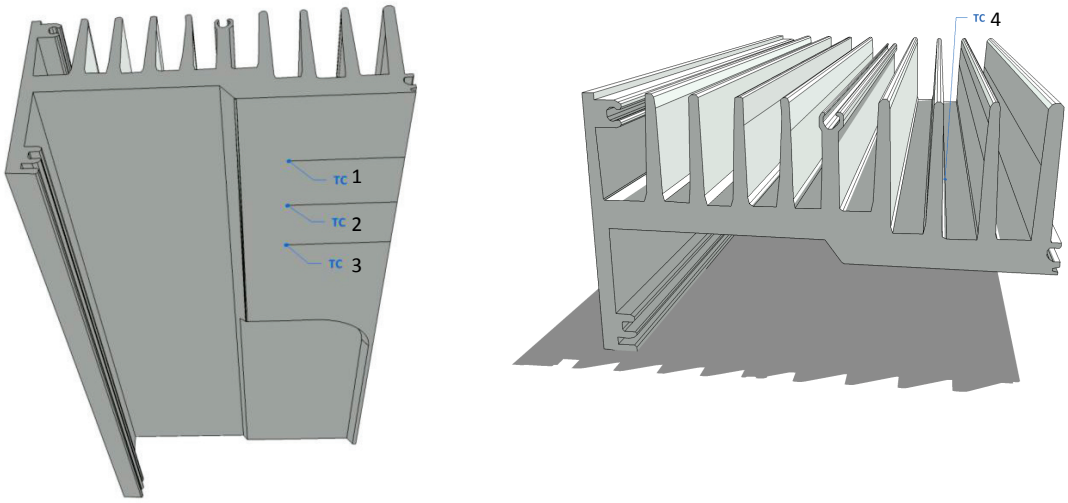

Figure 50 - Thermocouple Locations

AFRL provided the heat load data that form the IGBTs and the regenerative power. These are very high frequency data for 600 seconds (0.00282s/data). To avoid having to use an extremely small time step for heat transfer calculations, the data is averaged by integrating over every 5.6 seconds. Since the time scale for heat transfer is large, this approach is acceptable and saves computation time.

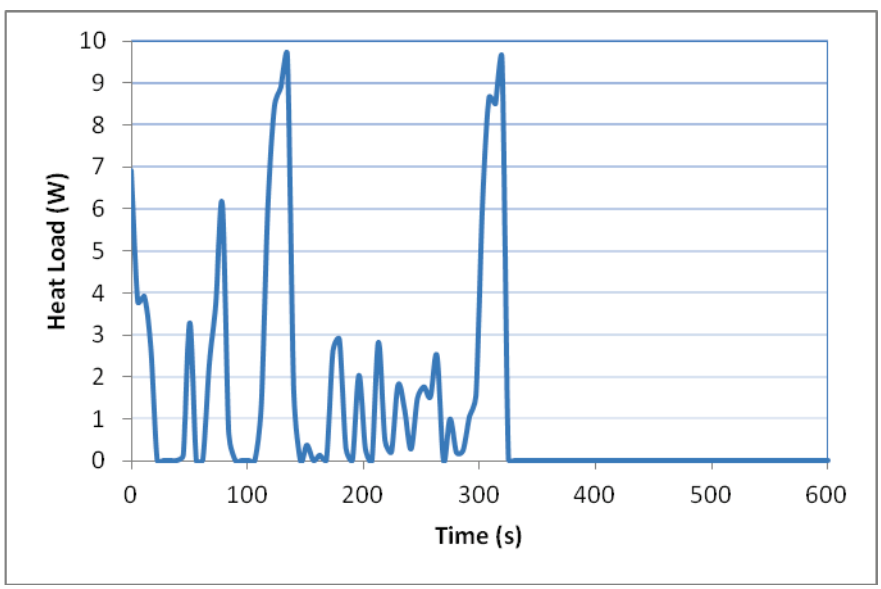

Figure 51 - Regenerative Power Load History

Approved for public release; distribution unlimited.

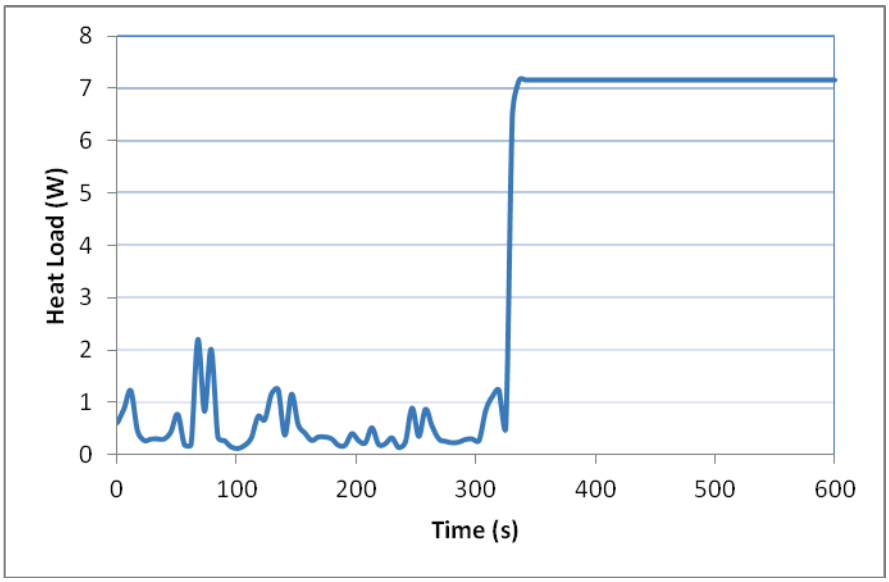

Figure 52 - IGBT Loss Load History

Figure 51 shows the time step of regenerative power load history. Figure 52 shows the time step of IGBT loss load history. Figure 53 shows the Danaher control board simulation results.

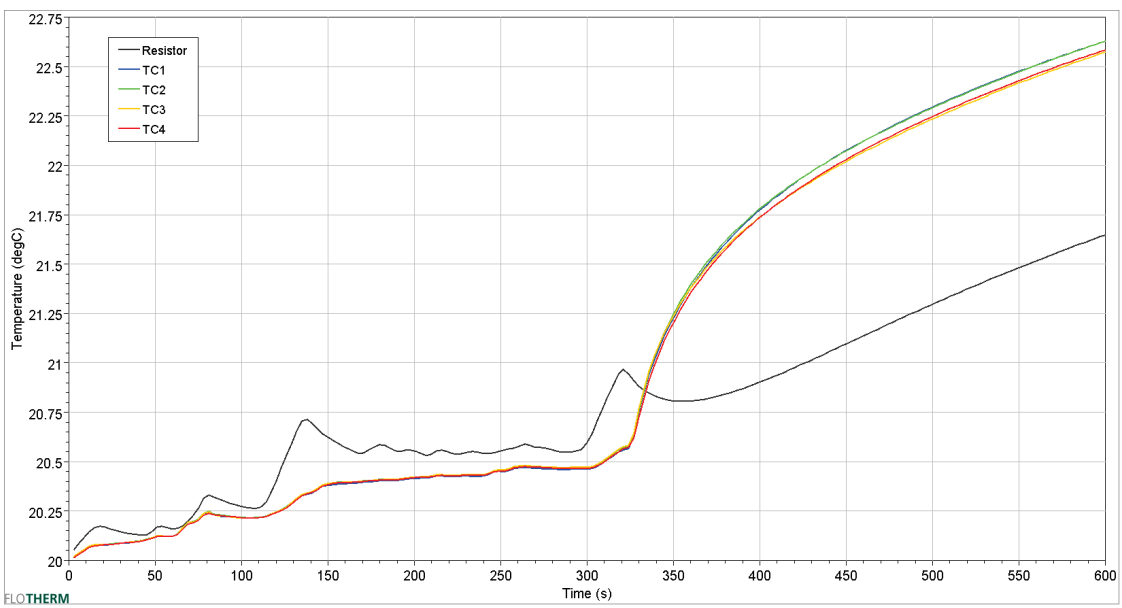

Figure 53 - Power Loss & Regenerative Resistor Temperature vs. Time

The simulation was carried out for the entire 600 seconds of data provided by AFRL. The temperature rise is very modest because of the low level of heat from the IGBTs and the low regenerative power (less than 10 W at all time).

Approved for public release; distribution unlimited.

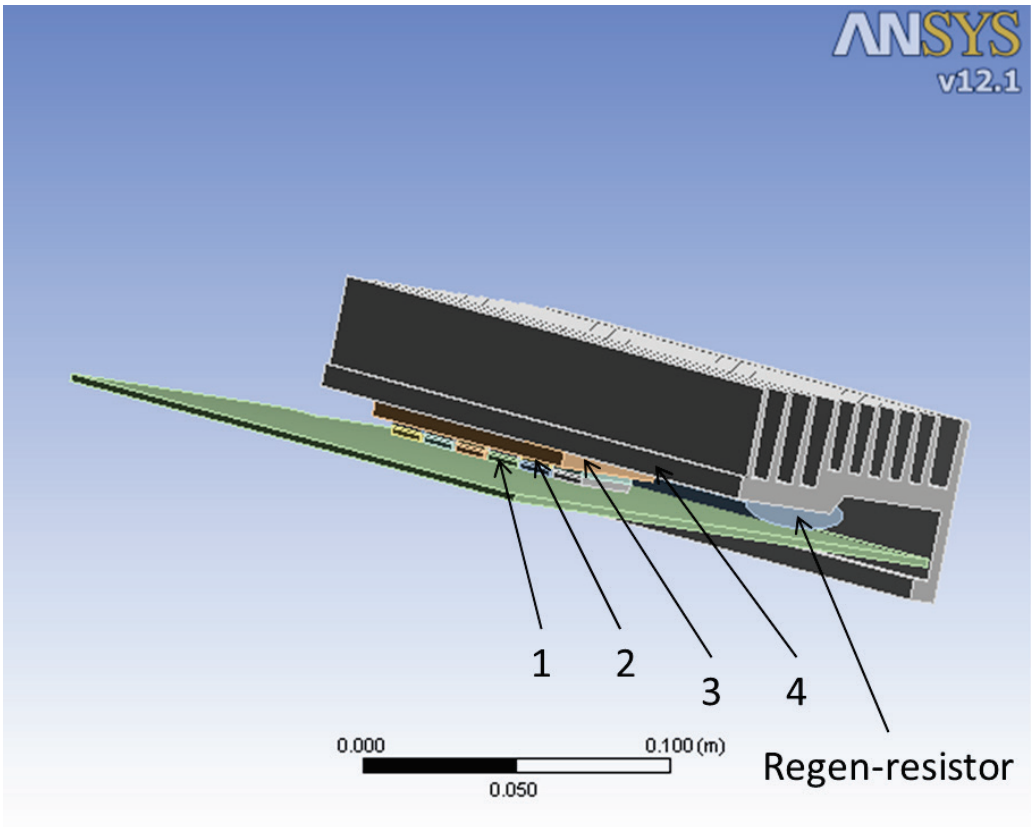

Figure 54 - 3-D Model of Control Unit

Figure 54 is a 3-D model of the Danaher control unit. The distribution of the lumped node is listed in Table 11, and the lumped node network is showed in Figure 55.

Table 11 - Lumped Node List

Node name	Material	Node number
IGBT core	Silicon	1
IGBT base	Aluminum alloy	2
Heat spreader	Aluminum alloy	3
Heat sink	Aluminum alloy	4

Approved for public release; distribution unlimited.

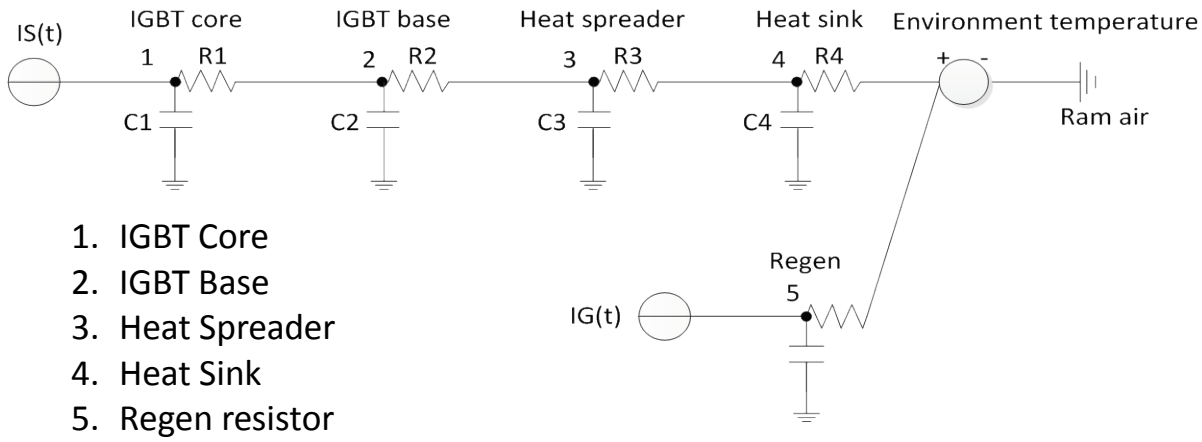

Figure 55 - Lumped Node Network

A total thermal load give in Figure 56 with a heat distribution 36 W/m^2 is assumed. Figure 57 show the transient temperature response inside the EU.

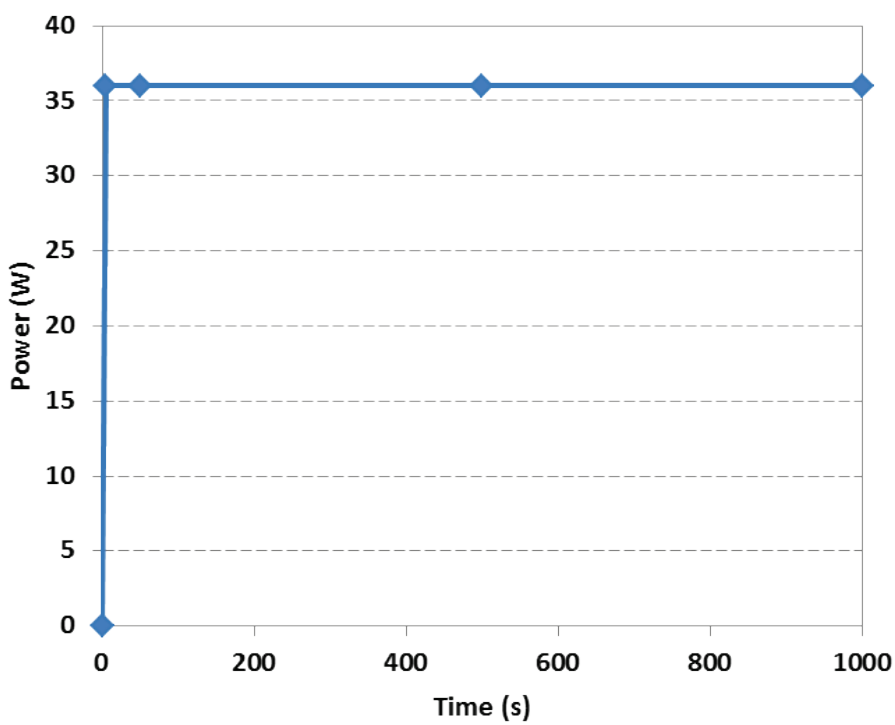

Figure 56 - Thermal Load

Approved for public release; distribution unlimited.

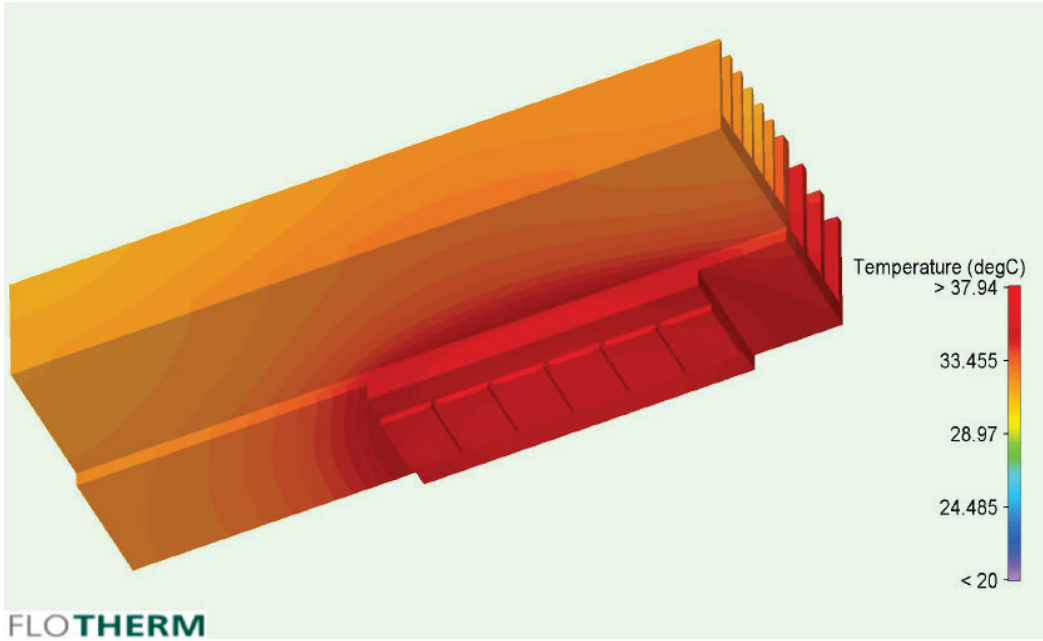

Figure 57 - One Pluse Result

The EU is assumed to have only one thermal path with the other parts and environment. The thermal resistnace, R4, represents the convenction thermal resistance between heat sink and the air around it. Table 12 shows that the thermal resistator value R and capciator value C can be calculated from steady state simulation. Table 13 shows that the value of thermal resistor and capaciator.

Table 12 - Thermal Resistator R and Capciator C Unit

Thermal Inputs	Explanation	Units	Source
R_{th}	thermal resistance	$^oC/W$	FEM
C_{th}	thermal capacitance	$J/^oC$	FEM
T_{evn}	Environment temperature	^oC	Given
I_S	IGBT core loss	W	Electrical Simulation

Table 13 - Thermal Resistator R and Capciator C Value

Model parameters			
R	Unit ($^oC/W$)	C	Unit ($J/^oC$)
R1	0.032	C1	1.36
R2	0.039	C2	10.36
R3	0.043	C3	48.13
R4	0.392	C4	860
R5	0.392	C5	860

Approved for public release; distribution unlimited.

After all the resistor and capacitor values of the lumped-node network model of the EU are know, the value of the resistors and capaciators can be used to simluate the temperature response of the EU. A set of equations can be written as following:

$$\frac{T_1 - T_2}{R_1} + C_1 \frac{dT_1}{dt} = Q_S(t) \tag{78}$$

$$\frac{T_1 - T_2}{R_1} - C_2 \frac{dT_2}{dt} - \frac{T_2 - T_3}{R_2} = 0 \tag{79}$$

$$\frac{T_2 - T_3}{R_2} - C_3 \frac{dT_3}{dt} - \frac{T_3 - T_4}{R_3} = 0 \tag{80}$$

$$\frac{T_3 - T_4}{R_3} - C_4 \frac{dT_4}{dt} - \frac{T_{evn} - T_4}{R_4} = 0 \tag{81}$$

$$\frac{T_5 - T_{evn}}{R_5} + C_5 \frac{dT_5}{dt} = Q_R(t) \tag{82}$$

Those equations set can be solved by standard numerical methods. In Figure 58 and Figure 59 are showing the simulation result in the lumped node model that compares with FEA result under the same initial condition and boundary conditions.

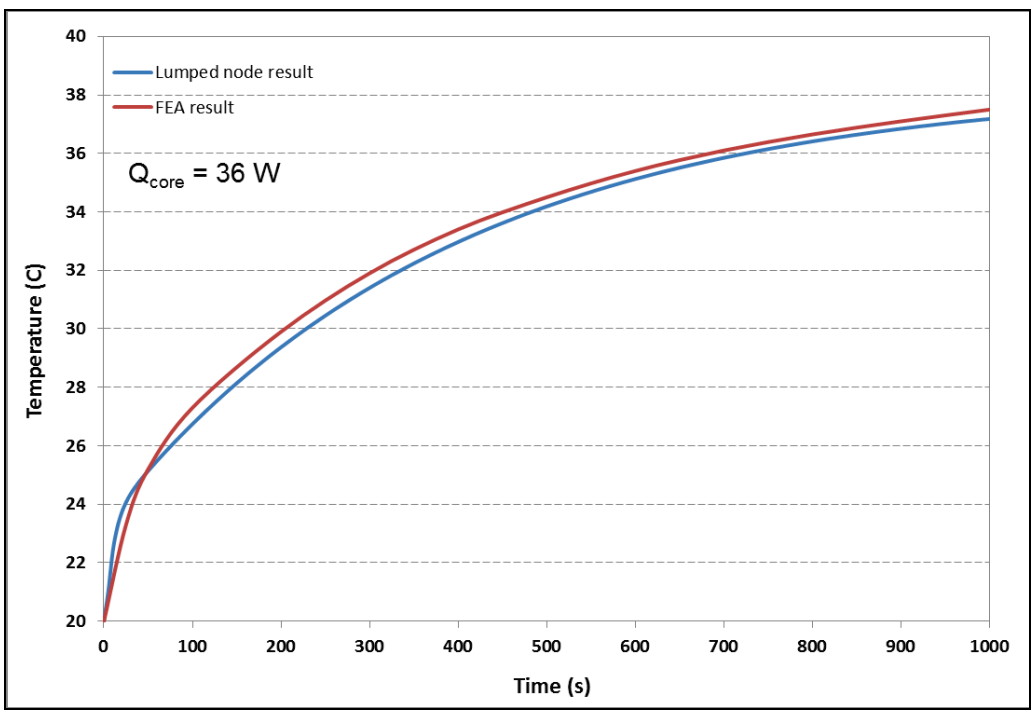

Figure 58 - Result with 36W Heat Load

Approved for public release; distribution unlimited.

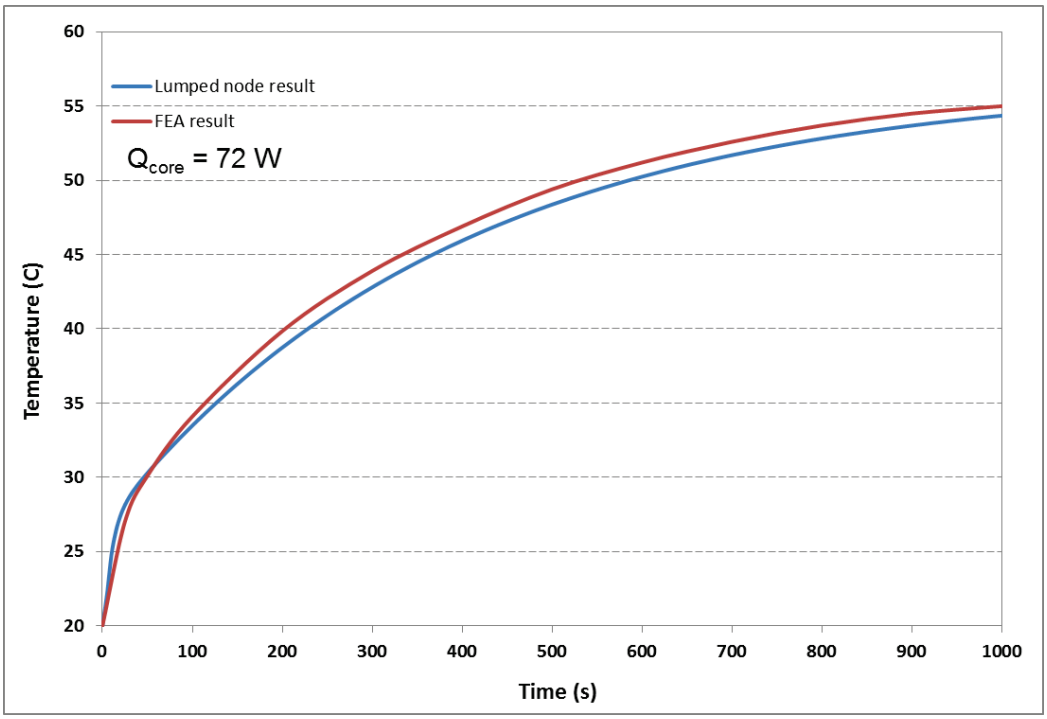

Figure 59 - Result with 72W Heat Load

The result show excellent transient response for the step heat load given in Figure 57. The agreement between FEA results and lumped-node model proves that this model is an effective alternative to computational intensive FEA results.

4.7 AN EU EXAMPLE AND RESULTS

The simulation model is built in MATLAB. It takes the electrical data and outputs the total power loss on the EU. The simulation takes a 325 seconds long mission profile. The stroke and load force profiles of the mission are is shown in Figures 60 and 61. This mission profile is highly dynamic.

Approved for public release; distribution unlimited.

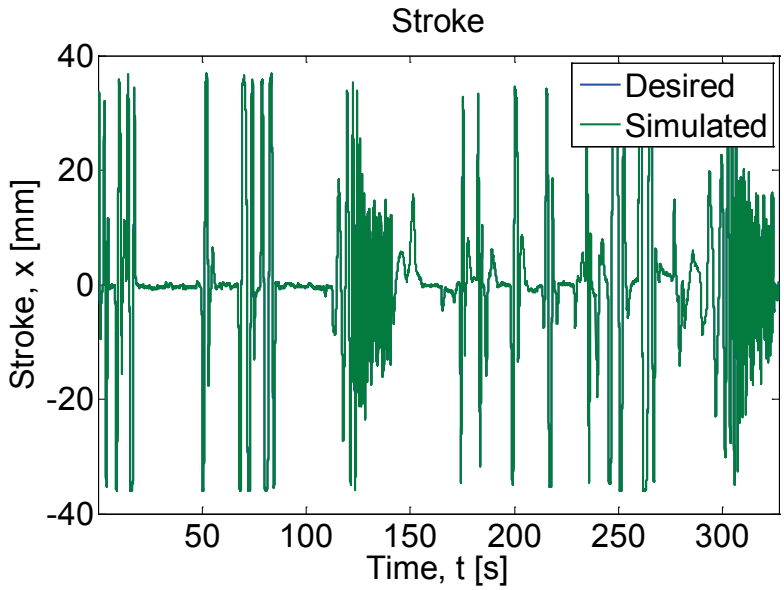

Figure 60 - Stroke of the Mission Profile

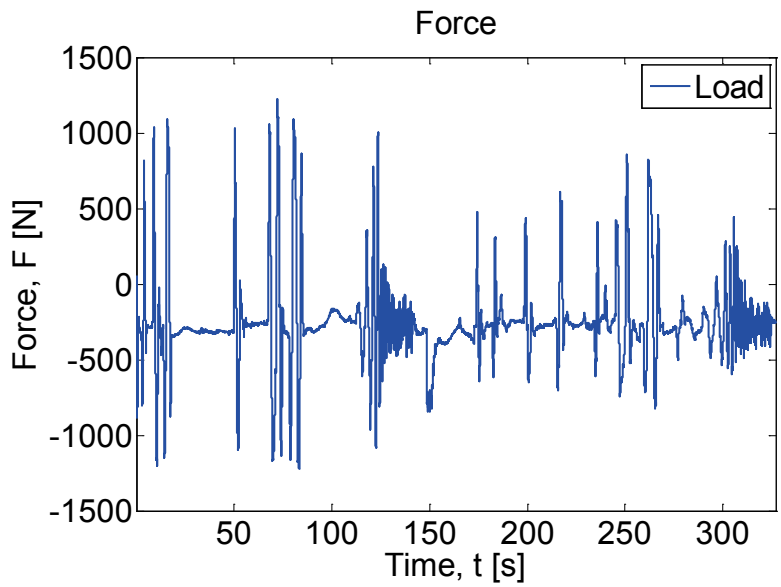

Figure 61 - Load Force of the Mission Profile

The power loss in the EU is calculated and plotted in Figures 62 and 63. Because the profile is highly transient, the plot consists of lots of high spikes, which makes it hard to see the details of the power loss. Further processing is done to the data to get an average over every second, so that the magnitude of power loss can be better viewed. Figure 62 is the power loss on the IGBTs. Figure 63 is a smoothed version of Figure 62. For the regenerative power loss, we pick the DC bus capacitor to be 0.14F, and DC bus voltage limited to have a 340 V maximum. Under this setting, the capacitor is fully capable of buffering the regenerative power, and no power is dissipated on the unloading resistor in this simulation.

Approved for public release; distribution unlimited.

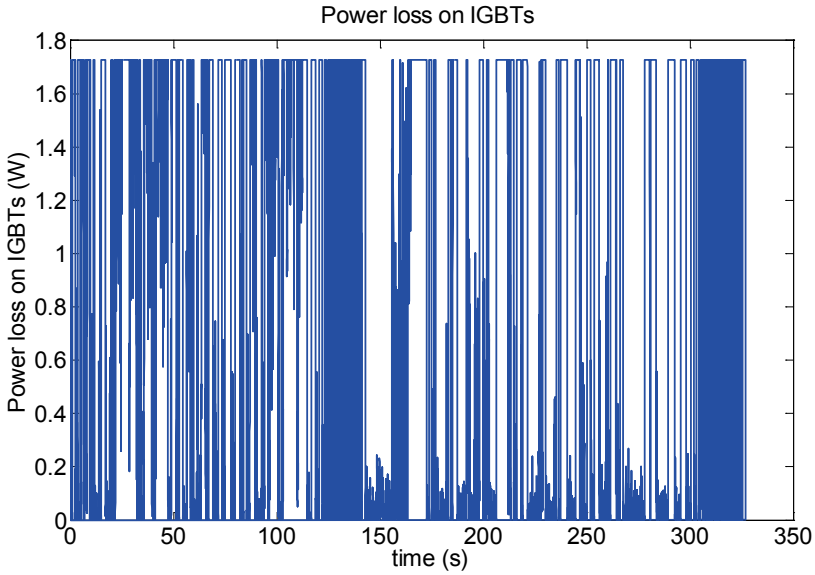

Figure 62 - Power Loss on IGBTs

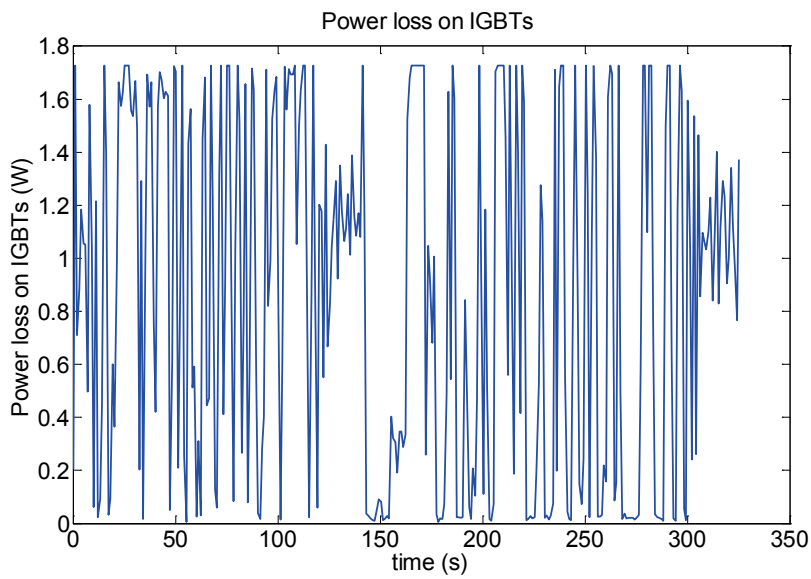

Figure 63 - Power Loss on IGBTs after Smoothing

A thermal model was developed to show the temperature profile of the control unit. There are six IGBTs under the heat spreader marked by "EP" on Figure 41. Also, the large rectangular shape object next to the heat spreader is the unloading resistor.

The model is generated in FLOTHERM in order to simulate the actual situation of different materials, changing driver unit configurations, and heat loads. In the thermal model, heat is mostly generated by the IGBTs, and the model only needs to simulate heat from the IGBTs and the unloading resistor, not from the rest of the board. Heat generated at the IGBTs is conducted to the heat sink through the heat spreader (EP). A fan provides forced air convection to remove

Approved for public release; distribution unlimited.

heat from the heat sink. In the model, the assumption is made that a Sanyo Denki 60 x 15 mm, 12 V axial fan provides forced air through the heat sink.

The heat load data for the IGBTs is provided in Figure 62. These is very high frequency data for 325 seconds (0.00282s/datum). To avoid having to use an extremely small time step for heat transfer calculations, the one-second averaged data shown in Figure 63 is used.

A thermal simulation is done using the power loss data from our model, and the temperature of the IGBTs is calculated. An initial temperature of 28°C and an ambient temperature of 26°C have been applied to the model to simulate the control unit. A comparison between the simulation and measurement of the IGBTs is shown in Figure 64. It shows that the simulation agrees well with the measured temperature on the device. The IGBTs' temperature remains approximately 2 °C higher than the ambient temperature which is sufficient to remove the heat from the IGBT package. A comparison for the unloading resistor is shown in Figure 65. In this mission profile, the unloading resistor is barely used, the capacitor is sufficient to handle the regenerative power, and very little power is dissipated on the resistor.

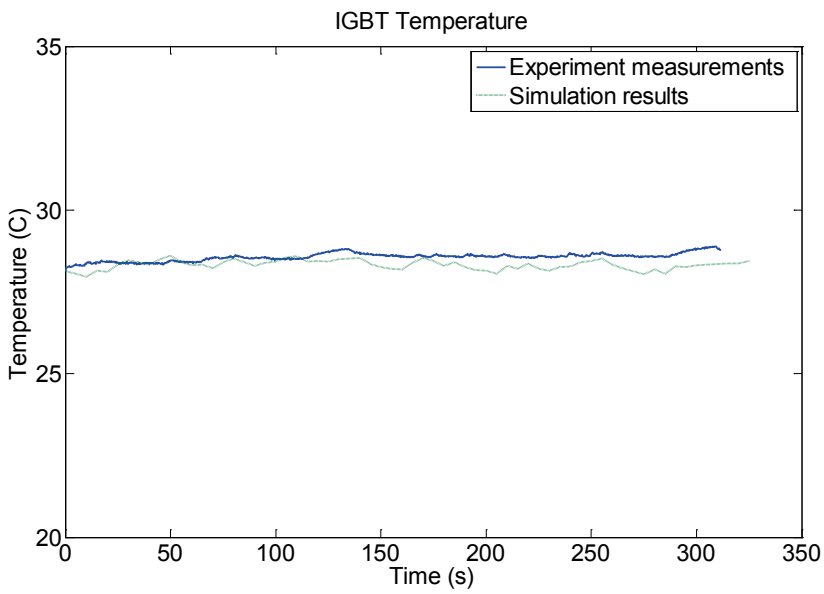

Figure 64 - Temperature on IGBTs. Hardware Test Data is compared with Simulation Data Based on the Power Loss Model

Approved for public release; distribution unlimited.

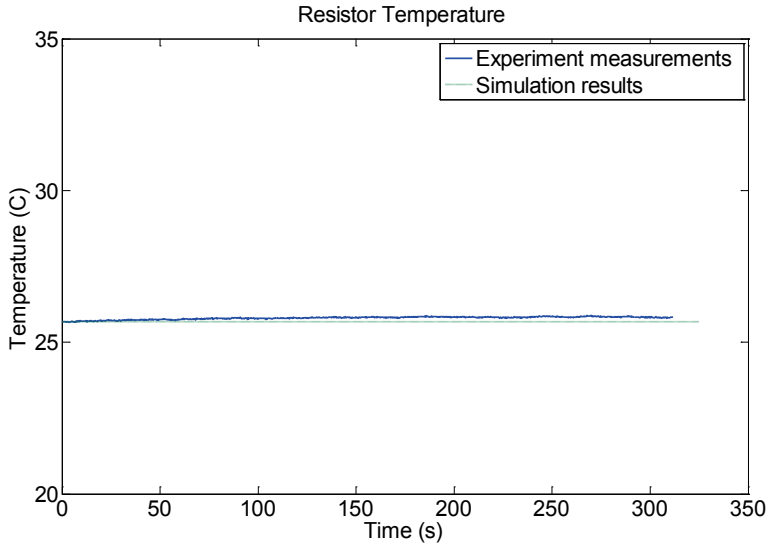

Figure 65 - Temperature on Resistors. We Pick the DC Bus Capacitor to be 0.14F, and DC Bus Voltage Limited to 340V Maximum for the Regenerative Power Loss calculation. It shows that the Unloading Resistor is barely used and the Capacitor is Fully Capable of Absorbing Regenerative Power for this Mission Profile

The power loss on the EU board is analyzed and modeled using MATLAB. Most of the power loss on the EU comes from the IGBTs in the power inverter, and the regenerative power dissipation resistor. The switching loss and on-state loss are considered for the IGBTs. Datasheets are used to obtain the input parameters of the model. A simulation is done in MATLAB, and the power loss data is plotted. Thermal analysis is done and the results are compared with the measured temperatures. The agreement validates the power loss model for the IGBTs and the unloading resistor.

Approved for public release; distribution unlimited.

5. CONCLUSION

There is a strong motivation to move towards all-electric aircraft. However, the significant issues to full realization of all-electric aircraft are the thermal management of heat loads and power management. We have successfully developed and implemented an EMA model with a control algorithm, a PWM component, an electromechanical component with nonlinear parameters, and a thermal component. The model takes a desired position profile, a load force profile, and an environmental temperature profile as inputs and predicts the thermal behavior of the motor and the transient power demands of the EMA. It was shown that the heat generation profiles are indeed highly dynamic, and control plays a powerful role in how much excess heat is generated and how much the power demand spikes.

The lumped-node thermal network is a feasible approach to simulate the EMA thermal characteristics. A thermal network is based on tuning the thermal resistance and thermal capacitance values with the FEM results. The lumped-node model has been successfully applied to step and transient heat loads with cooling by both convection and radiation. From the cases studied, it could be concluded that the major barrier to heat removal from the motor is external to the motor. Strong forced convection is needed. For situations where phase change materials may be needed to store the thermal energy to avoid the motor reaching excessively high temperature, a PCM module has been incorporated successfully into the lumped node model.

The power loss in the electronic unit (EU) of an EMA system has been simulated also. The control and drive unit (EU) processes the input data and feedback from sensors, and deliver input voltage and current to the motor through an insulated-gate bipolar transistor (IGBT) module. Most of the power loss on EU comes from the IGBTs in the power inverter, and the regenerative power dissipation resistor. The switching loss and on-state loss are considered for IGBTs.

The model was also used to compare its temperature predictions with temperature measurements of the motor and power drive provided by the Air Force Research Laboratory. Though the agreement was good, due to the low heat load associated with the test cases, the model could not be validated conclusively.

Approved for public release; distribution unlimited.

6. REFERENCES

[1] Cutts, S.J., "A collaborative approach to the More Electric Aircraft," *Power Electronics, Machines and Drives, 2002. International Conference on (Conf. Publ. No. 487)*, pp. 223-228, 4-7 June 2002.

[2] "Superconducting motors could propel all-electric aircraft," *Drives & Controls*, July 2007. http://www.drives.co.uk/fullstory.asp?id=2033

[3] Pointon, J.M., "Thermal Management of Electromechanical Actuation on an All-Electric Aircraft," MS thesis, Cranfield University, Bedfordshire, UK, 2007.

[4] McCarthy, K., Heltzel, A., Walters, E., Roach, J. et al., "A Reduced-Order Enclosure Radiation Modeling Technique for Aircraft Actuators," SAE Technical Paper 2010-01-1741, 2010.

[5] Melfi, M.J., Rogers, S.D., Evon, S., Martin, B., "Permanent-Magnet Motors for Energy Savings in Industrial Applications," *Industry Applications, IEEE Transactions*, Vol.44, No.5, pp.1360-1366, Sept. ~ Oct. 2008.

[6] Shi, K.L., Chan, T.F., Wong, Y.K., Ho, S.L. "Modeling and Simulation of the Three-phase Induction Motor Using Simulink," *Int. J. Elect. Engin. Educ.*, Vol. 36, pp. 163-172., Manchester U.P., Great Britain, 1999.

[7] Mohamed, M.A., Nagrial, M.H., "Modelling and Simulation of Vector-controlled Reluctance Motors Drive System," *International Conference on Simulation*, No. 457, pp. 380-384, ISBN: 0-85296-709-8, 1998.

[8] Sun, Fengchun, Li, Jian, Sun, Liqing, Zhai, Li, Cguo, Fen, "Modeling and Simulation of Vector Control AC Motor Used by Electric Vehicle," *Journal of Asian Electric Vehicles*, Vol. 3, No. 1, pp. 669-672, Asian Electric Vehicle Society, 2005.

[9] Soe, Nyein N., Yee, Thet T.H., Aung, S.S., "Dynamic Modeling and Simulation of Three-phase Small Power Induction Motor," *World Academy of Science, Engineering and Technology*, Vol. 42, No. 79, pp. 421-424, 2008.

[10] Lipo, Thomas A., Consoli, Alfio, "Modeling and Simulation of Induction Motors with Saturable Leakage Reactances," *IEEE Transactions on Industry Applications*, Vol. IA-20, No. 1, pp. 180-189, 1981.

[11] Dolinar, D., Weerdt, R. De, Freeman, E.M., "Calculation of Two-axis Induction Motor Model Parameters Using Finite Elements," *IEEE Transactions on Energy Conversion*, Vol. 12, No. 2, pp. 133-142, 1996.

[12] Topcu, E.E., Kamis, Z., Yuksel, I., "Simplified numerical solution of electromechanical systems by look-up tables," *Mechatronics*, Vol. 18, No. 10, pp. 559-565, Elsevier, 2008.

Approved for public release; distribution unlimited.

[13] Fitzgerald, A.H., Kingsley, C.J., Umans, S.D., *Electric Machinery*, 6th edition, NY: McGraw-Hill, 2003.

[14] Hu, Jianhui; Zou, Jibin; Liang, Weiyan; "Finite element calculation of the saturation DQ-axes inductance for a direct drive PM synchronous motor considering cross-magnetization," *Power Electronics and Drive Systems, The Fifth International Conference*, Vol.1, pp. 677- 681, 17-20 Nov. 2003.

[15] Avionics Magazine, May 1, 2001.

[16] ANSYS V12.0., ANSYS, Inc., http://www.ansys.com

[17] Mellor, P.H., Roberts, D., Turner, D. R., "Lumped parameter thermal model for electrical machines of TEFC design," IEEE Proc-B, Vol 138, No5, Sept 1991.

[18] DiGerlando, A., Vistoilo, I., "Thermal network of induction motors for steady state and transient operations analysis," Paris, ICEM 1994.

[19] Motor-CAD v3.1.7, Motor Design Ltd, http://www.motor-design.com

[20] Chin, Y.K., Staton, D.A., "Transient thermal analysis using both lumped-circuit approach and finite element method of a permanent magnet traction motor," *IEEE AFRICON* 2004.

[21] Kaliuchi, H., Yamazaki, M., Yabe, M., Chihara, S., Terunuma, Y., Sakata, Y. and Usami, T., "A Study of Erythritol as Phase Change Material," 1998.

[22] "Temperature coefficient of resistance," *All about Circuits*, 5th edition, 2006 http://www.allaboutcircuits.com/vol_1/chpt_12/6.html

[23] Blaabjerg, F.; Pedersen, J.K.; Sigurjonsson, S.; Elkjaer, A., "An extended model of power losses in hard-switched IGBT-inverters," *Industry Applications Conference*, 1996. Thirty-First IAS Annual Meeting, IAS '96, Conference Record of the 1996 IEEE, Vol.3, pp.1454-1463, Vol.3, 6-10 Oct. 1996

[24] Garcia, I., "TMS320C6412 Power Consumption Summary", *Texas Instruments Application Report*, Jan, 2005. http://www.ti.com/lit/an/spra967e/spra967e.pdf?DCMP=OTCDSP_March2005&HQS=EtechInnovations%2BNL%2Betechmar05appnc6412ai

[25] Woodburn, D., Wu, T., Chow, L., Leland, Q., Bindl, J., Hu, Y., Zhou, L., Lin, Y., Rolinski, N., Brokaw, W., Tran, B., Jordan, B., Gregory, E., Lin, S. and Iden, S., "Integrated Nonlinear Dynamic Modeling and Field Oriented Control of Permanent Magnet (PM) Motor for High Performance EMA," SAE Paper No. 2010-01-1742, *SAE Power Systems Conference*, Ft. Worth,, TX, Nov. 2-4, 2010.

Approved for public release; distribution unlimited.

APPENDIX A: HOW TO GET PARAMETERS FOR AN EMA SIMULATION

A1 WHAT PARAMETERS ARE NEEDED

A simulation model of an electromechanical actuator (EMA) requires accurate parameters in order to give accurate simulation results. The primary parameters that are required for the simulation model to run are listed here:

- Gearing ratio
- Number of poles
- Power train friction
- Shaft mass
- Moment of inertia
- Phase resistance
- PM flux linkage
- Direct inductance
- Quadrature inductance
- Thermal capacitance
- Thermal resistance

These parameters are necessary for the EMA simulation model. In addition to these parameters, it is helpful to know the limits of the motor and actuator assembly. These limits include

- No-load speed
- Stall force
- Stroke range

These three have less to do with how the EMA itself behaves and more with how it should be controlled. For example, there is no direct restriction on how much force an EMA must face before it stalls, but a force greater than a certain value would require more current than the windings of the motor could safely handle without burning out. The motor controller prevents this from happening, so we get the effect of a limit to the force we can see from the EMA.

Approved for public release; distribution unlimited.

A2 WHERE PARAMETERS CAN BE FOUND

Some of these parameters are easy to determine and others require careful analysis. There are two approaches to determining these parameters. One is to take a physical EMA and run various experiments on it measuring the parameters one-by-one. This is often a destructive process since it ultimately requires completely taking apart the machine in order to see its internal construction. The other approach is to design and model a motor that is as similar to the target motor as possible and use the parameters from the model for the full EMA simulation. This is non-destructive, but has the potential for somewhat higher uncertainties. There are some parameters, however, that can be measured without taking any components of the EMA apart.

A2.1 What Can Be Found by Measurement

The following sections explain how the various parameters of an EMA can be found experimentally.

A2.1.1 No-load speed

The no-load speed can be found by sending position commands to the actuator to move back and forth. This is done without any load attached to the EMA. Taking the minimum of the speeds in the two directions gives the no-load speed.

A2.1.2 Stall force

The stall force is measured while the actuator is connected to a hydraulic press or other active load. The load force from the hydraulic press is increased while the actuator is commanded to hold its position until the actuator begins to move. When the actuator begins to move, it is no longer able to sustain the force of the load, and this is the stall force.

A2.1.3 Stroke range

The stroke range is perhaps one of the easiest parameters to determine. It can come from either design specifications or from simply extending the actuator as far as it can reasonably go.

A2.1.4 Gearing ratio

Depending on the documentation from the manufacturer, the gearing ratio can be found either from the documentation of the actuator or by taking the gear train apart, counting the teeth on each gear and measuring the linear displacement of the actuator rod for one full revolution of the ball screw. Although this does involve some disassembly of the EMA, it is generally a non-destructive process.

A2.1.5 Number of poles

The documentation of the motor in the EMA should state the number of poles. If not, it can be found either by taking the motor apart or by scanning it with a high-intensity X-ray machine.

Approved for public release; distribution unlimited.

A2.1.6 Power train friction

One method of finding the power train friction involves using a linear load such as a hydraulic press coupled to the actuator. The EMA is driven forward and backward while the EMA is unpowered. Using the force and stroke data, the static friction can be obtained. First, the mean forces required to push or pull the EMA rod are found. Depending on the orientation of the EMA, the magnitudes of these forces will not be equal due to a bias. The bias exists because of the weight of the rod of the EMA. The difference between this bias and the push and pull forces is the friction force. As a dry (or contact) friction, it is mostly constant over a wide range of speeds.

A2.1.7 Shaft mass

The mass of the whole shaft of the EMA can be derived from the friction analysis. The bias in the force required to move the EMA rod is due to the weight of the rod.

A2.1.8 Moment of inertia

tia of the motor's rotor, the gears, and the ball screw can be found by accelerating the actuator under impulse from the hydraulic press. The curvature of the velocity curve over time is a function of the total inertia of the drive train. This inertia less the mass of the shaft is the moment of inertia.

Determining these two inertias (shaft mass and moment of inertia) separately is important in order to get an accurate force of gravity and net force in the simulations.

A2.1.9 Phase resistance

Of all the electrical parameters, the phase resistance is the easiest to obtain. It is measured by connecting leads to two of the three lines into the motor and measuring the open-circuit line-to-line resistance. This value is then divided by two if the motor is a Wye-connected motor. The resulting value is the phase resistance of the EMA. Any pair of two lines should measure the same resistance. If they do not, there is likely a short in the motor.

The remaining parameters (PM flux linkage, direct and quadrature inductances, and thermal resistances and capacitances) are very difficult to measure without destructively taking the electric motor apart.

A2.2 What Can Be Found by Modeling

The following parameters are much more readily obtained by modeling than by experimental measurement:

- PM flux linkage
- Direct inductance
- Quadrature inductance

Approved for public release; distribution unlimited.

- Thermal capacitance
- Thermal resistance

Because of the difficulty of measuring these parameters directly, developing a model and calculating these parameters from the model can be very helpful. The procedure for developing such a model is detailed in the following section.

A3 How to Model a Motor for Parameter Estimation

There are very standard designs for electric motors. A given speed and power requirement can go a long way in deciding the specific design of a motor. This fact makes it reasonable to using good design process to get a reasonable estimate of the five remaining parameters mentioned in the previous section:

- PM flux linkage
- Direct inductance
- Quadrature inductance
- Thermal capacitance
- Thermal resistance

There are four basic steps to getting these parameters from a model. The steps are

- Design an electric motor to specification
- Refine the design
- Model the motor with finite element method (FEM)
- Extract the reduced-order parameters

The following sections will detail these steps.

A3.1 Design an electric motor to specification

To design an electric motor some basic specifications are required, such as the input voltage the motor will see or the number of poles the motor should have. Included with the software package to AFRL is a script called “pmdesigner.m”. This program takes the user step-by-step through the process of designing a permanent magnet (PM) electric motor. A sample of the questions asked by pmdesigner is shown here:

```
Do you want to start a new design? [y,N]: y
Enter the name of the new design txt file: myDesign
Pout (Output power expected) bounded by 0 and Inf [W]: 300
```


Approved for public release; distribution unlimited.

```
VT (Terminal voltage) bounded by 0 and Inf [V]: 120
nm (Mechanical speed) bounded by 0 and Inf [krpm]: 1.6
DY (Connection type: D or Y) limited to one of D, Y: y
   The value given for DY does not fit the specified limits.
DY (Connection type: D or Y) limited to one of D, Y: Y
p (Number of poles) bounded by 0 and Inf: 12
sp (Fractional stator pitch) bounded by 0 and 1: 1
Ns (Target number of slots) bounded by 0 and Inf: 33
zeta_m (Mechanical skew) bounded by 0 and Inf: 0
Br (Remanence) bounded by 0 and Inf [G]: 1.4
Hc (Coercivity) bounded by 0 and Inf [Oe]: 9.31e5
eff (Efficiency (ratio, not percentage)) bounded by 0 and 1:
0.95
pf (Power factor (ratio)) bounded by 0 and 1: 1
pfSgn (Power factor sign (1 or -1)) limited to one of -1, 1:
1
osf (Overspeed factor (ratio)) bounded by 0 and 1: 0.2
emb (Magnet embrace) bounded by 0 and 1: 0.95
slotStyle (Slot style (box: 1, tight: 2, wedge: 3)) limited
to one of 1, 2, 3: 2
useLining (Use lining (1) or not (0)) limited to one of 0,
1: 1
coolingMethod (Cooling method (air: 1, water: 2)) limited
to one of 1, 2: 1
```

The details of this particular setup will be saved to a file called “myDesign,” as specified above. A design of an electric motor using several carefully chosen design equations is then output by pmdesigner. The results for this particular setup are shown here:

```
  Pout = 300        W      Output power
   Pfw = 10         W      Friction loss
  Pair = 1.0089     W      Air friction loss
 Pcore = 7.8926e-06 W      Core loss
    VT = 120        V      Rated voltage
   Vph = 69.282     V      Phase voltage
     p = 12                Poles
    Np = 2.75              Slots per pole
    Nm = 3                 Slots spanned by a coil
    Ns = 33                Slots on stator
    nm = 1600       rpm    Speed
    fm = 26.667     Hz     mechanical frequency
```


Approved for public release; distribution unlimited.

```
          fe = 160        Hz     electrical frequency
           D = 59.02      mm     Stator bore diameter
          D0 = 43426      mm     Stator core diameter
           g = 28.809     mm     Actual air gap
          ge = 29.51      mm     Effective air gap
          Dr = 1.4016     mm     Actual rotor diameter
          vr = 23.114     ft/min Actual rotor tip speed
               0.066039   %      of maximum allowable
           l = 59.02      mm     Rotor length
          Nc = 127741             Turns per coil
          Ne = 2.5513e+06         Effective turns per phase
       eff_N = 181.57     %      Turns efficiency
    lambda_s = 5.6187     mm     Slot arc spacing
          bs = 4.45       mm     Slot width
          ts = 1.1687     mm     Tooth width
         bs0 = 1.4833     mm     Mouth Width
         ds1 = 21677      mm     Slot depth (not including
wedge)
        ds0b = 1.016      mm     Trapezoidal section of
wedge depth
        ds0a = 1.016      mm     Mouth section of wedge
depth
          sw = 2.032      mm     Slot wedge depth
          sl = 0.11477    mm     Slot lining thickness
          Ss = 96468      mm^2   Total slot area
          Sc = 91486      mm^2   Total slot area minus
lining and wedge
           a = 1.0545             Slot inflation
          Sa = 0.18993    mm^2   Conductor cross-sectional
area
          Da = 0.49176    mm     Conductor diameter
         awg = 24.324            Wire gauge
         Vol = 8.7414e+10 mm^3   Total volume of motor
Malformed stator slots: ds1 is too large. Try reducing the
number of slots on the stator.
```

Notice that pmdesigner followed the request for 33 slots but indicates that this would result in a poor design. This means that another pass should be done with a value smaller than 33.
Once the design is settled upon, the rest of the output results will be helpful for modeling the motor. For the above setup, the rest of the results are shown here:

Approved for public release; distribution unlimited.

```
Converted to RMXprt variables:
Machine:
   Number of poles       12
   Frictional loss       10 W
   Windage loss      1.0089 W
   Reference speed     1600 rpm
Stator:
   Outer diameter    43426 mm
   Inner diameter    59.02 mm
   Length            59.02 mm
   Number of Slots      33
   Slot type             3
Slot:
   Hs0    1.016 mm
   Hs1    1.016 mm
   Hs2    21677 mm
   Bs0   1.4833 mm
   Bs1     4.45 mm
   Bs2     4.45 mm
   Rs         0 mm
Winding:
   Winding layers                   2
   Winding type          whole coiled
   Parallel branches                1
   Conductors per slot         255482
   Coil pitch                       3
   Number of strands                1
   Wire wrap                   0.0635 mm
   Wire size                     24.5 awg
   Slot lining                0.11477 mm
   Wedge thickness              2.032 mm
   Layer insulation          0.057384 mm
   Limited fill factor          0.999
Rotor:
   Outer diameter    1.4016 mm
   Inner diameter   0.66203 mm
   Length             59.02 mm
   Pole type              2
Pole:
```


Approved for public release; distribution unlimited.

```
    Embrace                  0.95
    Offset                      0 mm
    Magnet type           SmCo28
    Magnet thickness    0.038753 mm
  Shaft: non-magnetic
```

These specifications will then be entered into a program by Ansys called RMxprt. It is a motor designing program.

A3.2 Refine the design

RMxprt is a motor designing program that will take the rough design specifications developed above and fill in the details. It provides the bridge between the simple table of design outputs in the previous section to a full-blown finite element model. The steps to model a motor using RMxprt are detailed below in a succinct manner step-by-step.

A3.2.1 Create new motor project

A3.2.1.1 Create new project

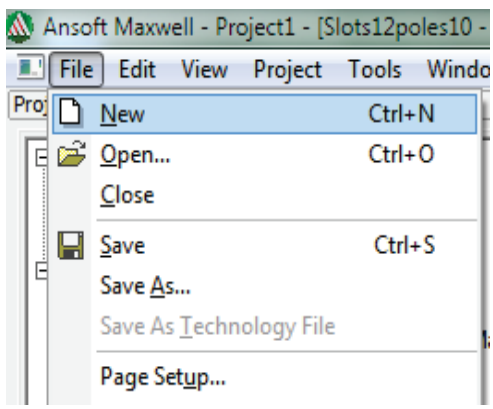

Figure A-1 - Selecting "New" from the "File" Menu

A3.2.1.2 Insert RMxprt Design

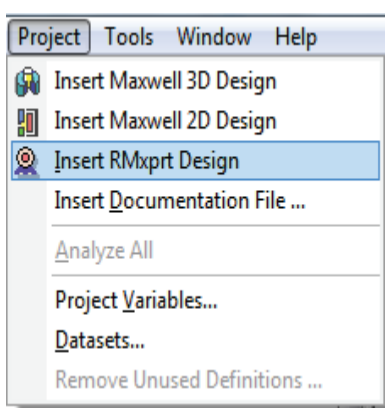

Figure A-2 - Creating a New RMxprt Design from the "Project" Menu

Approved for public release; distribution unlimited.

A3.2.1.3 Select Brushless Permanent-Magnet DC Motor

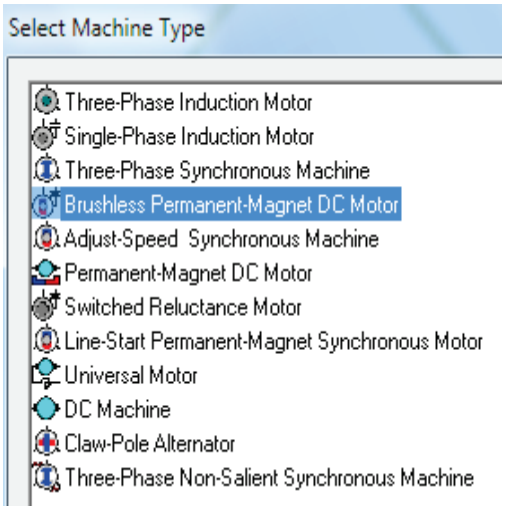

Figure A-3 - List of Machine Types

A3.2.1.4 Save the project and name it

A3.2.2 Define machine properties

Under Project Manager, select the components listed below one-by-one, each time specifying the properties shown in the Properties window.

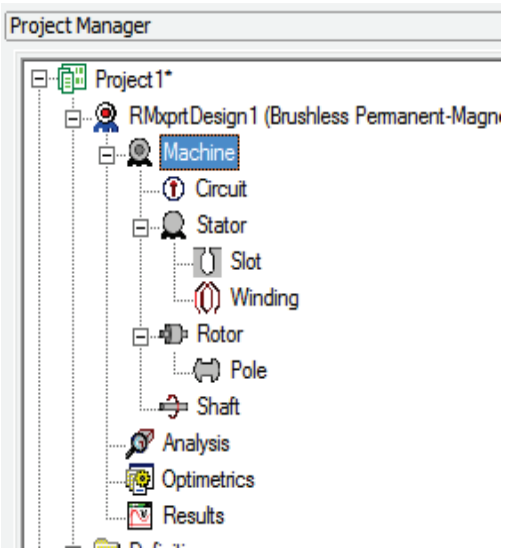

Figure A-4 - Project Manager Tree

Approved for public release; distribution unlimited.

Properties

Name	Value	Unit	Evaluated Value
Outer Diameter	77.1	mm	77.1mm
Inner Diameter	43.5	mm	43.5mm
Length	58.7	mm	58.7mm
Stacking Factor	0.95		
Steel Type	steel_1010		
Number of Slots	12		
Slot Type	3		
Skew Width	0		0

Figure A-5 - Properties List

A3.2.2.1 Machine

- Machine Type: The machine type you selected when inserting a new RMxprt design, Three Phase Synchronous Machine. It is already specified by having selected Brushless Permanent-Magnet DC Motor.

- Number of Poles: The number of poles the machine contains. This value is the total number of poles in the stator (or the number of pole pairs multiplied by two).

- Frictional Loss: the frictional power loss pfr (due to friction) measured at the reference speed nr. The frictional power loss pf at a speed n is given by pf = pfr * (n/nr).

- Windage Loss: The wind loss pwr (due to the air resistance) measured at the reference speed nr. The wind power loss pw at the real speed n is given by pw = pwr * (n/nr)^3.

- Reference Speed: The reference speed at which the frictional power loss and windage power loss are measured. It is the main speed the machine is expected to run.

- Control Type: (typical is DC)

- Circuit Type: (typical is Y3)

A3.2.2.2 Circuit

- Lead Angle of Trigger: The trigger's lead angle in electrical degrees. A positive value represents a lead angle, and a negative value represents a lag angle. An angle of 0 means that the average induced voltage in the triggered phase during the Trigger Pulse Width is at a maximum.

- Trigger Pulse Width: The period from the on-status to the off-status of a transistor, in electrical degrees.

Approved for public release; distribution unlimited.

- Transistor Drop: The voltage drop across one transistor when the transistor is turned on.

- Diode Drop: The voltage drop of one diode in the discharge loop. If you selected a star-type circuit (S3 or S4) as the Circuit Type, this is the total discharge voltage.

A3.2.2.3 Stator

- Outer Diameter: The outer diameter (or core diameter) of the stator core.

- Inner Diameter: The inner diameter (or bore diameter) of the stator core.

- Length: The length of the stator core.

- Stacking Factor: The stacking factor for the stator core. It is the ratio of metal (versus lamination) thickness to total thickness. 1 indicate no lamination. 0.95 is common.

- Steel Type: the stator core material. This must be of type Steel. Some good selections are steel-1010 or iron.

- Number of Slots: The total number of slots the stator core contains.

- Slot Type: The type of the slots in the stator core. Slot types 1 though 4 are filled with round wire. Slot types 5 and 6 are filled with rectangular wire.

- Skew Width: The slot skew width, measured in slot number. This means, as the laminations are placed one on top of the other, they might not be positioned exactly the same each time; so, from lamination to lamination, the slots skew, or twist, about the center of the center of the machine. The figure here shows a slot skew of 1.

Approved for public release; distribution unlimited.

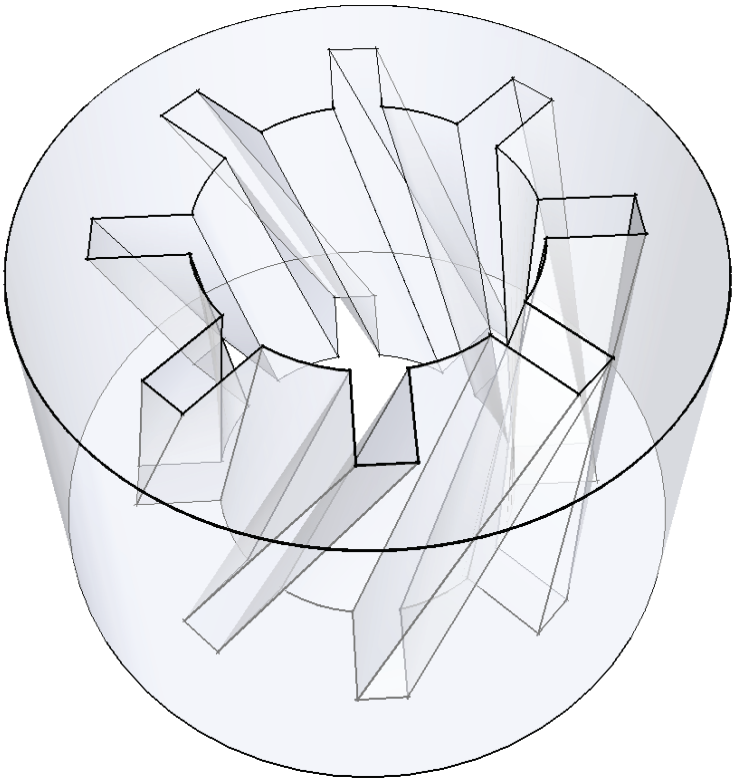

Figure A-6 - Model of Stator with Skewed Slots

A3.2.2.4 Slot

- Auto Design:
- Parallel Tooth:
- Tooth Width:
- Hs0: Slot opening height
- Hs01: Slot closed bridge height
- Hs1: Slot wedge height
- Hs2: Slot body height
- Bs0: Slot opening width
- Bs1: Slot wedge maximum width
- Bs2: Slot body bottom width, 0 for parallel teeth
- Rs: Slot body bottom fillet for slot types 3 and 4

Approved for public release; distribution unlimited.

A3.2.2.5 Winding: Winding

- Winding Layers: The number of coil layers (1 or 2) in the stator winding. This does not depend on whether the machine has lap winding or concentric winding.

- Winding Type: The type of the stator winding. To specify your own, select Editor, right click in the table to the right, and select Edit Layout... . T means top layer (closest to the mouth of the slot) and B means bottom layer. For concentric winding, just select Whole.

- Parallel Branches: The number of parallel branches in one phase of the stator winding. If all the windings of a phase are connected in series, then the number of parallel branches is 1.

- Conductors per Slot: The total number of conductors in each stator slot. This value is the number of turns per coil multiplied by the number of layers. Enter 0 to have RMxprt auto-design this value.

- Coil Pitch: (This is enabled when Winding Layers is 2.) It is the number of teeth separating two sides of one coil. For example, if a coil starts in slot 1 and ends in slot 2, it has a coil pitch of one. For concentric winding, coil pitch should be 1.

- Number of Strands: The number of wires per conductor. Enter 0 to have RMxprt auto-design this value. For simple, small motors, this is typically just 1.

- Wire Wrap: The thickness of the double-sided wire wrap (electrical insulation). Enter 0 to automatically obtain this value from the wire specification library.

- Wire Size: Wire diameter (for round wires) or width and thickness (for rectangular wires). (0 for auto-design). You can assign wire size of round wires or rectangle wires. When the slot type, under Stator, is 1 to 4, round wires are used. When the slot type you selected is 5 or 6, rectangle wires are used.

A3.2.2.6 Winding: End/Insulation

- Input Half-turn Length: Select or clear this check box to specify whether or not you want to enter the half-turn length manually.

- Half-turn Length: The half-turn length of the armature winding. It is available when Input Half-turn Length is selected.

- End Adjustment: the distance of one end of a conductor extending vertically beyond the end of the stator. It is available when Input Half-turn Length is cleared. Enter 0 for auto-design.

- Base Inner Radius: The inner radius of the base corner: how big of an arc the coil makes at the end. Enter 0 for auto-design.

Approved for public release; distribution unlimited.

- Tip Inner Diameter: The inner diameter of the coil tip, seen as Top-End Inner Diameter above.

- End Clearance: The end clearance between two adjacent stator coils.

- Slot Liner: The thickness of the slot liner insulation.

- Wedge Thickness: The thickness of the wedge insulation.

- Layer Insulation: The thickness of the insulation layer which is enabled when preformed coils (for slot types 5 or 6) are used.

- Limited Fill Factor: The limiting slot fill factor for the wire design. This value relates to how much stuff is put into the slot versus the total space available in the slot.

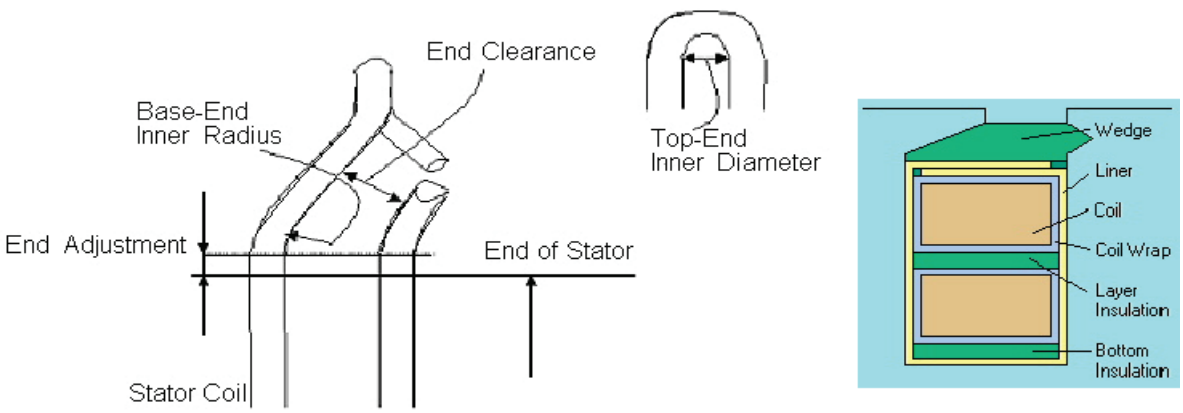

Figure A-7 - End Winding Characteristics (Left) and Slot Filling (Right)

A3.2.2.7 Rotor

- Outer Diameter: the outer diameter of the rotor core, includes the magnets.

- Inner Diameter: the inner diameter of the rotor core; diameter of axle.

- Length: The length of the rotor core.

- Steel Type: This should be a steel type, just like with the stator.

- Stacking Factor: The stacking factor for the stator core. It is the ratio of metal (versus lamination) thickness to total thickness. 1 indicates no lamination. 0.95 is common.

- Pole Type: This is the arrangement of the magnets on the rotor.

A3.2.2.8 Pole

- Embrace: This is a ratio of the arc length of a permanent magnet to the available arc length for each magnet. So, 1 means that the magnets are all touching side-to-side.

Approved for public release; distribution unlimited.

- Offset: The distance from the center of the rotor that the circle that forms the outer edge of the magnet is positioned. This is illustrated in this figure:

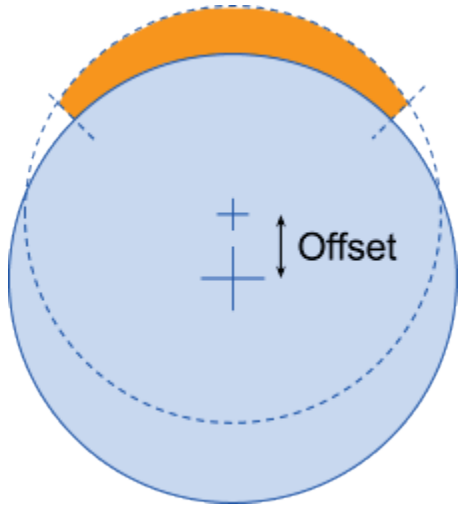

Figure A-8 - Diagram of Magnet Arc Offset from Center of Axel

- Magnet Type: The material that the magnets are made of.
- Magnet Thickness: The distance from the inner arc to the outer arc of the magnet at its thickest point.

A3.2.2.9 Shaft

Magnetic Shaft: A check box for whether the axle should be made of soft magnetic material or of non-magnetic material. In other words, should the axle have a permeability equal to air or should it be much greater than that of air.

A3.2.3 Analyze

A3.2.3.1 Select Add Solution Setup... on Analysis

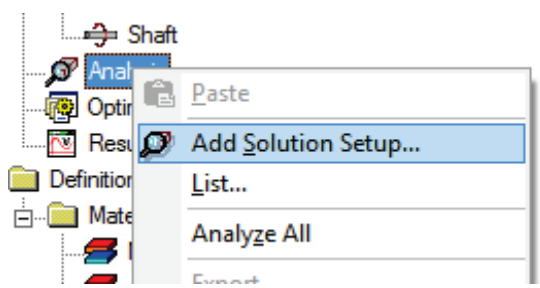

Figure A-9 - Selecting "Add Solution Setup…" from "Analysis"

Approved for public release; distribution unlimited.

A3.2.3.2 Enter the conditions under which you wish the machine to operate

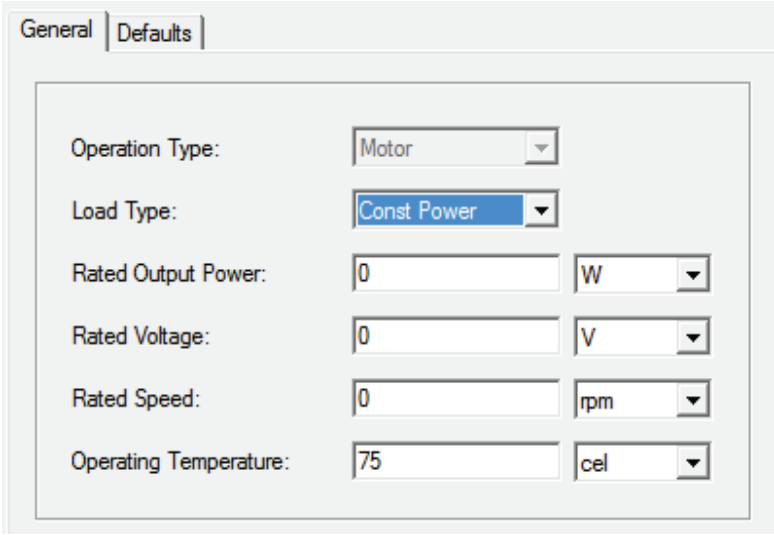

Figure A-10 - Solution Setup Ratings

- Rated Output Power: The output mechanical power developed at the shaft for the motor.
- Rated Voltage: The RMS line-to-line voltage.
- Rated Speed: The desired output speed of the motor at the load point
- Operating Temperature: The temperature at which the system functions, and select the units. The Operating Temperature will affect all winding resistances and therefore affect all ohmic losses.

A3.2.3.3 Analyze the solution setup

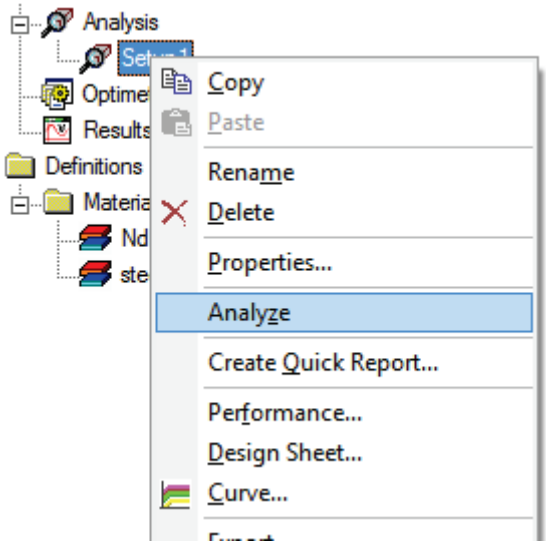

Figure A-11 - Selecting "Analyze" from "Setup1"

Approved for public release; distribution unlimited.

A3.2.3.4 Look at results. On results, select Solution Data...

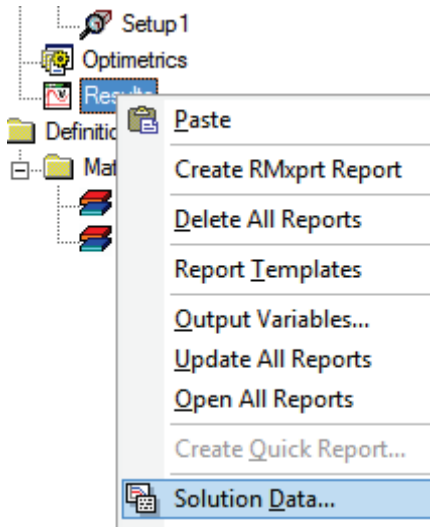

Figure A-12 - Selecting "Solution Data…" from "Results"

This will bring up a window like this:

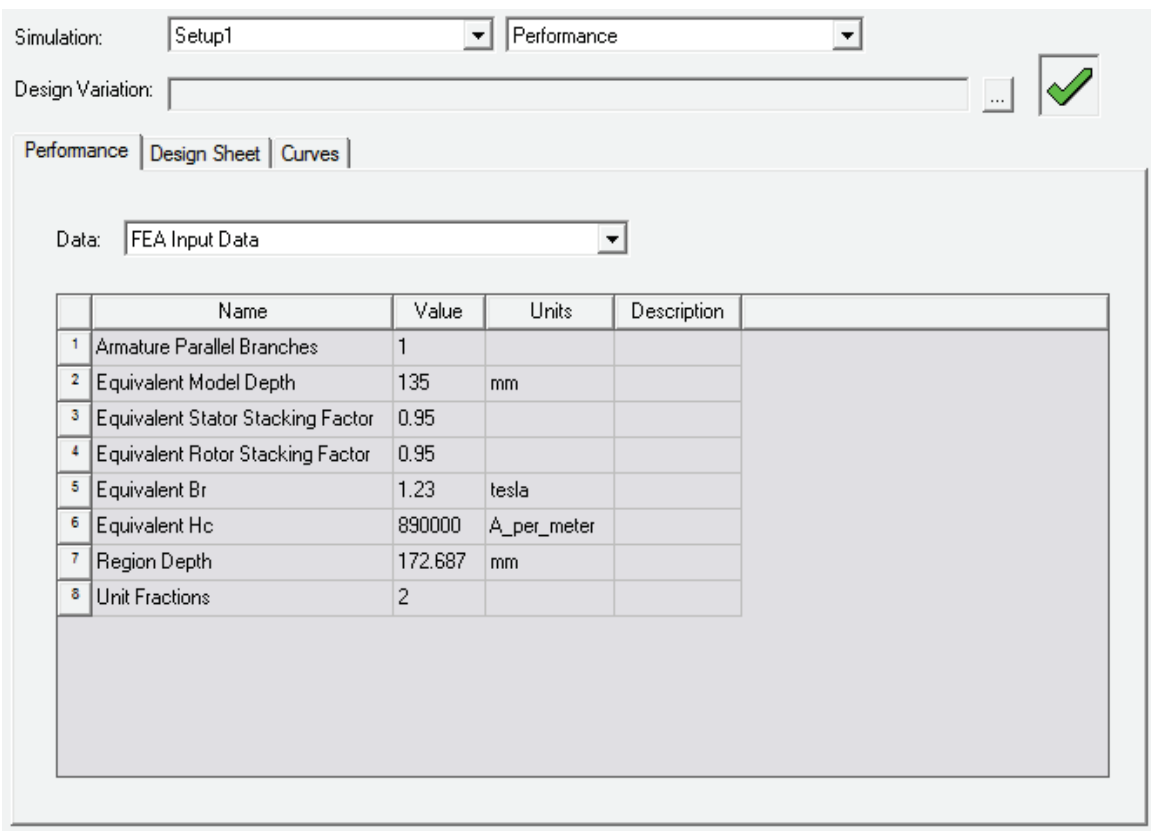

	Name	Value	Units	Description
1	Armature Parallel Branches	1		
2	Equivalent Model Depth	135	mm	
3	Equivalent Stator Stacking Factor	0.95		
4	Equivalent Rotor Stacking Factor	0.95		
5	Equivalent Br	1.23	tesla	
6	Equivalent Hc	890000	A_per_meter	
7	Region Depth	172.687	mm	
8	Unit Fractions	2		

Figure A-13 - Solution Data Sheet Showing "FEA Input Data"

The Design Sheet tab has a table of all the analysis results. The Curves tab has several plots to look at.

Approved for public release; distribution unlimited.

The D and Q inductances are listed as “D-Axis Inductance L1+Lad(H)” and “Q-Axis Inductance L1+Laq(H)”, respectively, and they are found under “STEADY STATE PARAMETERS”.

The phase resistance is listed as “Armature Phase Resistance R1 (ohm)”. It is also found under “STEADY STATE PARAMETERS”.

If the number of conductors per slot was not specified (0 was entered), RMxprt will automatically determine a number. This number can be found under “STATOR DATA” and is listed as “Number of Conductors per Slot”. So, for a double layer concentric winding arrangement, half of those conductors will belong to one winding and half to another in the same slot.

Under “STATOR DATA”, you might want to confirm that the slots were not over-filled:

```
Limited Slot Fill Factor (%):     90
Stator Slot Fill Factor (%):      38.143
```

Using RMxprt, the design can be optimized by adjusting various inputs and quickly seeing what its predicted performance would be.

Once the design of the motor has been finalized, it is ready to convert to a finite element method (FEM) model. The following section explains step-by-step how this can be done with the goal of getting three of the five parameters: PM flux linkage, direct inductance, and quadrature inductance.

A3.3 Model the motor with finite element method (FEM)

A3.3.1 Export RMxprt Model to Maxwell 2D

A3.3.1.1 After opening and selecting the RMxprt design, export it to Maxwell 2D

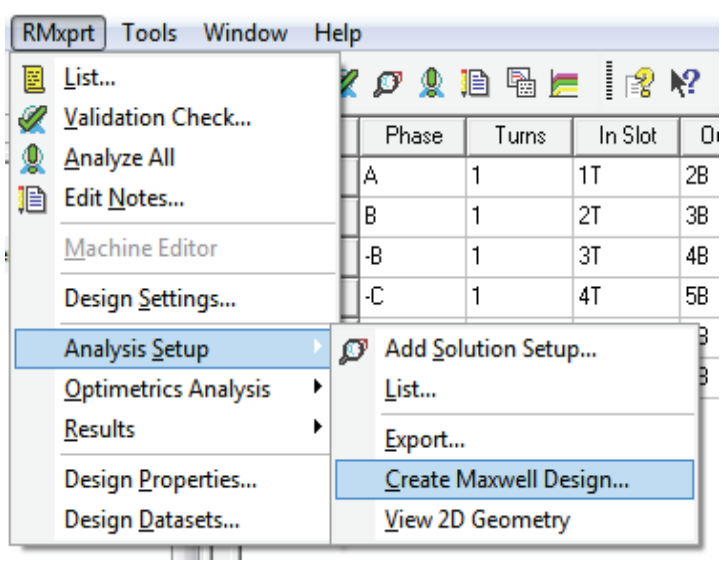

Figure A-14 - Creating a Maxwell Design from the RMxprt Model

Approved for public release; distribution unlimited.

A3.3.1.2 When the dialog opens, choose 2D

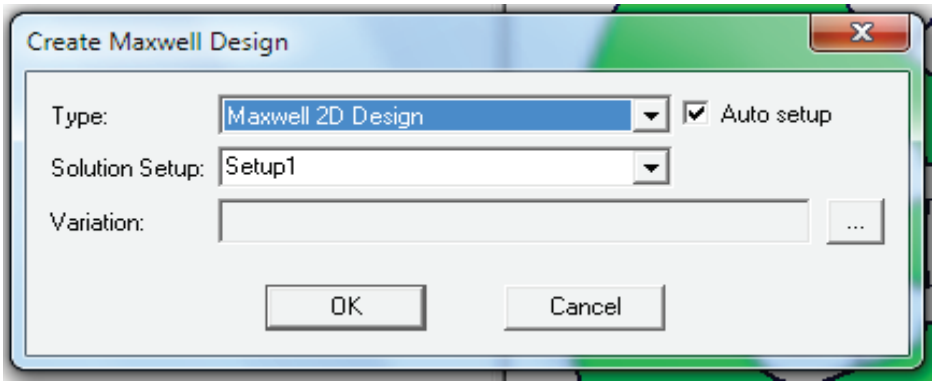

Figure A-15 - Choosing to Create a 2D Maxwell Design

A3.3.1.3 To see what the new design looks like, double click on the design name under Project Manager

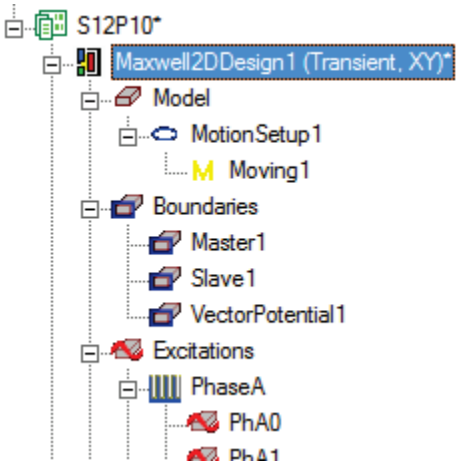

Figure A-16 - Project Manager Tree for Maxwell 2D Design

Approved for public release; distribution unlimited.

A3.3.1.4 Set solution type to Magnetostatic

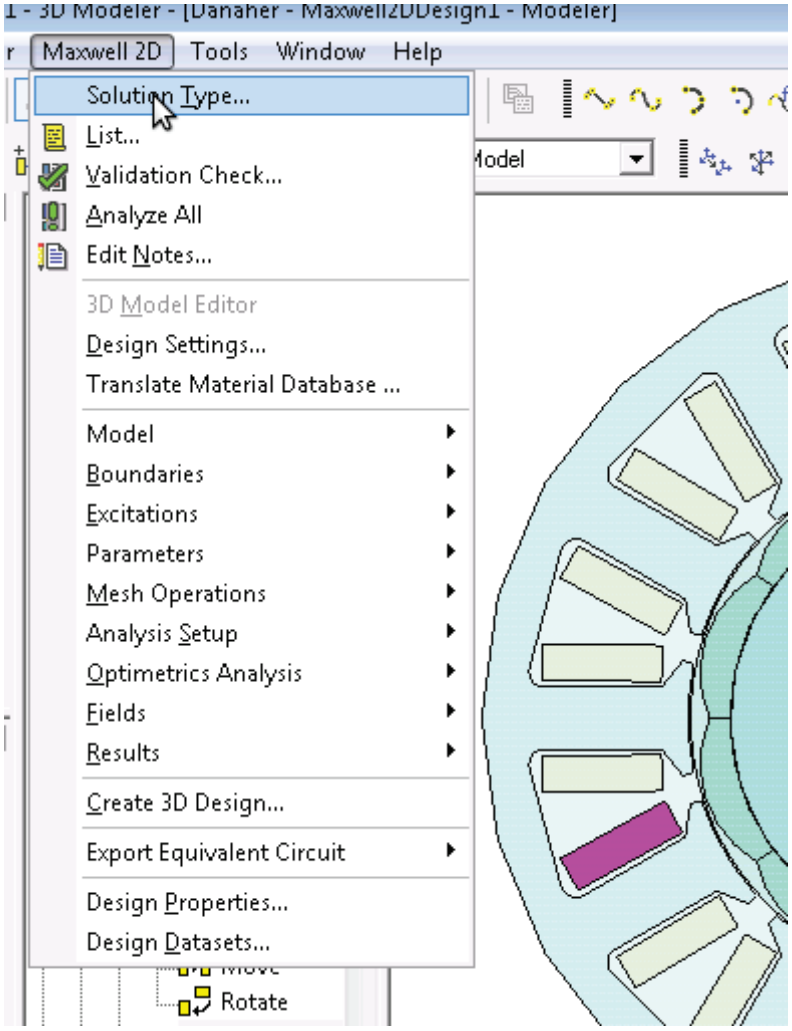

Figure A-17 - Selecting "Solution Type…" from "Maxwell 2D" Menu

Approved for public release; distribution unlimited.

A3.3.2 Make motor whole

A3.3.2.1 Select the user-defined outer vacuum. Make sure it is under OuterRegion

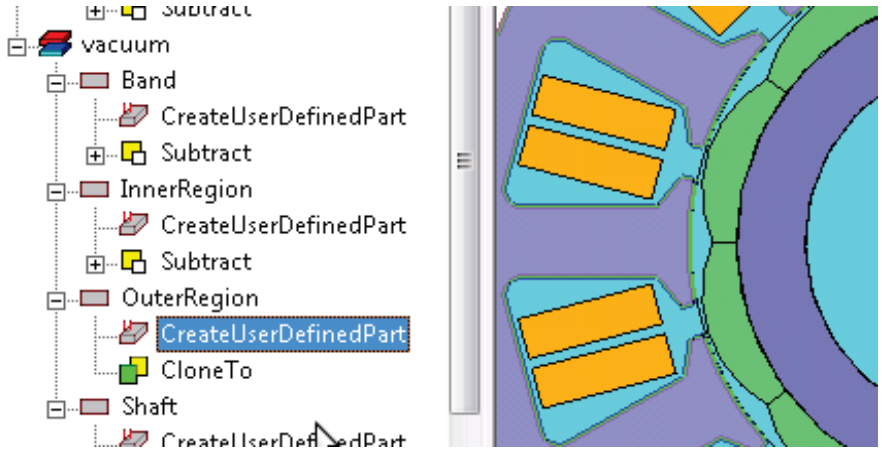

Figure A-18 - Selecting the User-Defined out Vacuum

A3.3.2.2 Change the fractions to 1. This will make the whole motor model show

Properties

Name	Value	Unit	Ev
DLL Locat...	syslib		
DLL Version	12.0		
DiaGap	43.1	mm	43.1mm
DiaYoke	77.1	mm	77.1mm
Length	0	mm	0mm
SegAngle	3	deg	3deg
Fractions	1		1
InfoCore	100		100

Figure A-19 - Model Fractions Highlighted in the Properties Box

Or you can do this by another way. Click Maxwell 2D on top of the menu and click Design Properties.

Approved for public release; distribution unlimited.

A3.3.3 Add Currents and Polarities

A3.3.3.1 Select the coils and magnets

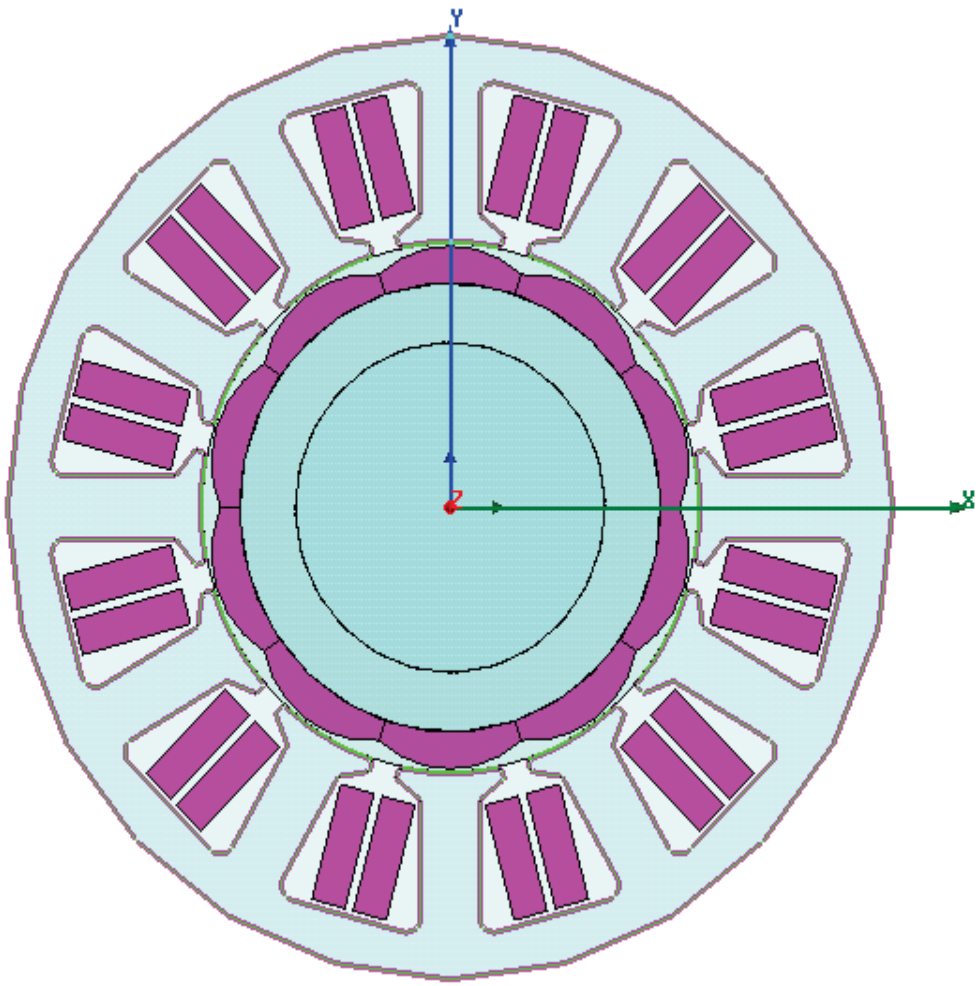

Figure A-20 - Full Model with all Windings and Magnetic Poles Selected

Approved for public release; distribution unlimited.

A3.3.3.2 Separate the bodies. This makes it so you can modify their values separately

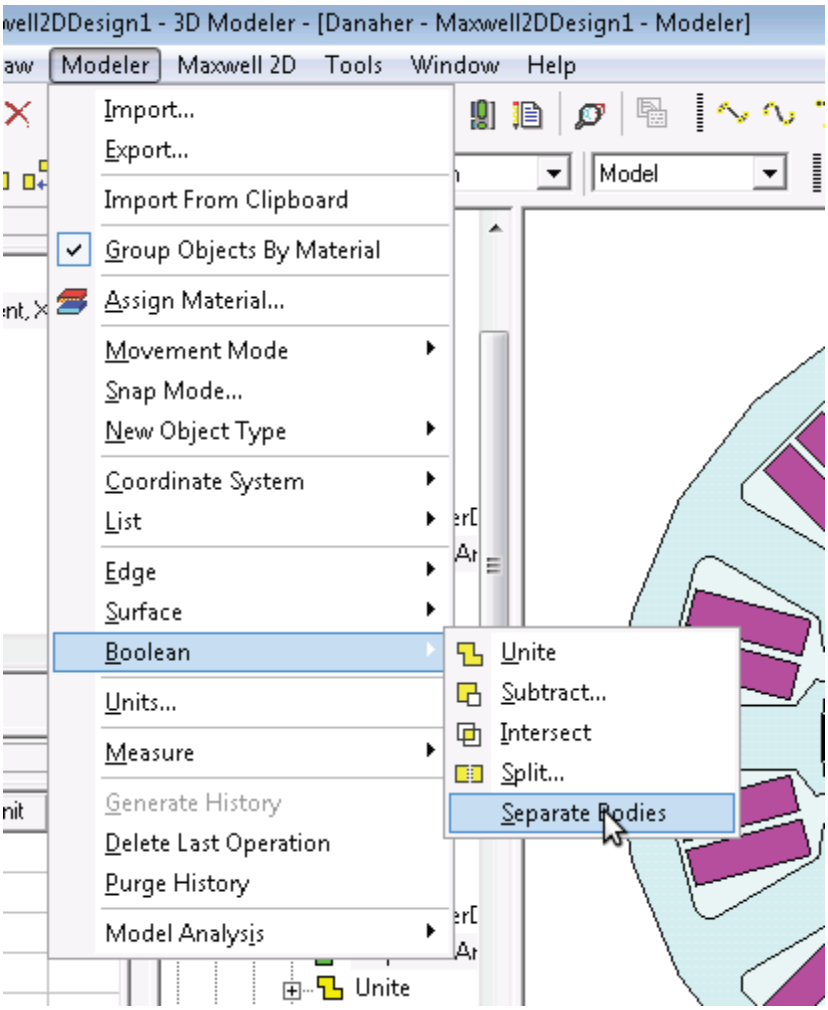

Figure A-21 - Separating the Windings and Magnets so that they are no Longer Linked

Approved for public release; distribution unlimited.

A3.3.3.3 Add variables for phase currents

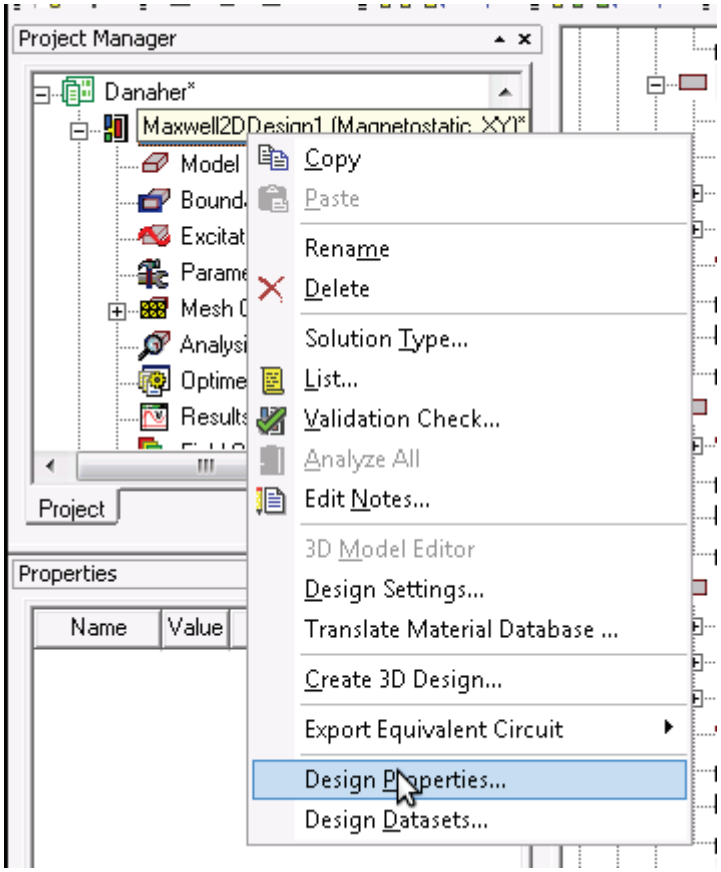

Figure A-22 - Selecting "Design Properties…" from "Maxwell2DDesign1 (Magnetostatic XY)"

A recommended set of variables is shown here:

Approved for public release; distribution unlimited.

Local Variables

Value Optimization Tuning Sensitivi

	Name	Value	Unit	
	I	1	A	1A
	th	0		0
	thRad	(th*pi/180)		0
	phiShift	0		0
	phiRad	phiShift*pi/180		0
	th120	pi*2/3		2.09439
	iaa	I*cos(thRad + phiRad)		1A
	ibb	I*cos(thRad + phiRad - th120)		-0.5A
	icc	I*cos(thRad + phiRad + th120)		-0.5A
	Nc	86		86
	iaa_Nc	iaa*Nc		86
	ibb_Nc	ibb*Nc		-43
	icc_Nc	icc*Nc		-43
	P	10		10
	thM	thRad*2/P		0

Figure A-23 - Recommended List of Design Variables

- I current amplitude
- th electrical angle of rotor [degrees]
- thRad electrical angle of rotor [rads]
- phiShift torque angle [degrees] (atan(iq/id))
- phiRad torque angle [rads]
- th120 120 degrees converted to radians. Positive for ABC winding; negative for ACB winding.
- iaa phase A current
- ibb phase B current
- icc phase C current
- Nc turns per coil
- iaa_Nc total current thru a phase A coil
- ibb_Nc total current thru a phase B coil
- icc_Nc total current thru a phase C coil
- P number of poles
- thM mechanical angle of rotor [rads]

Note that when you create these variables, only the current amplitude *I* must have a specified unit. You do this by typing the unit after its nominal value:

Approved for public release; distribution unlimited.

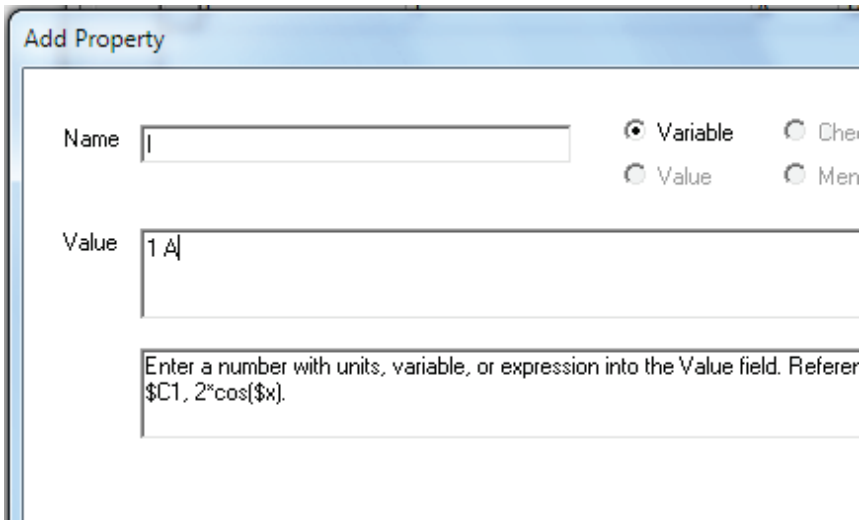

Figure A-24 - Defining the Nominal Value of *I* with the Unit A (Ampere)

A3.3.3.4 Add excitations. Consider that it might be helpful to refer to the RMxprt winding layout before creating the coil excitations. It could also be helpful to first color code your coils to guide you in assigning currents.

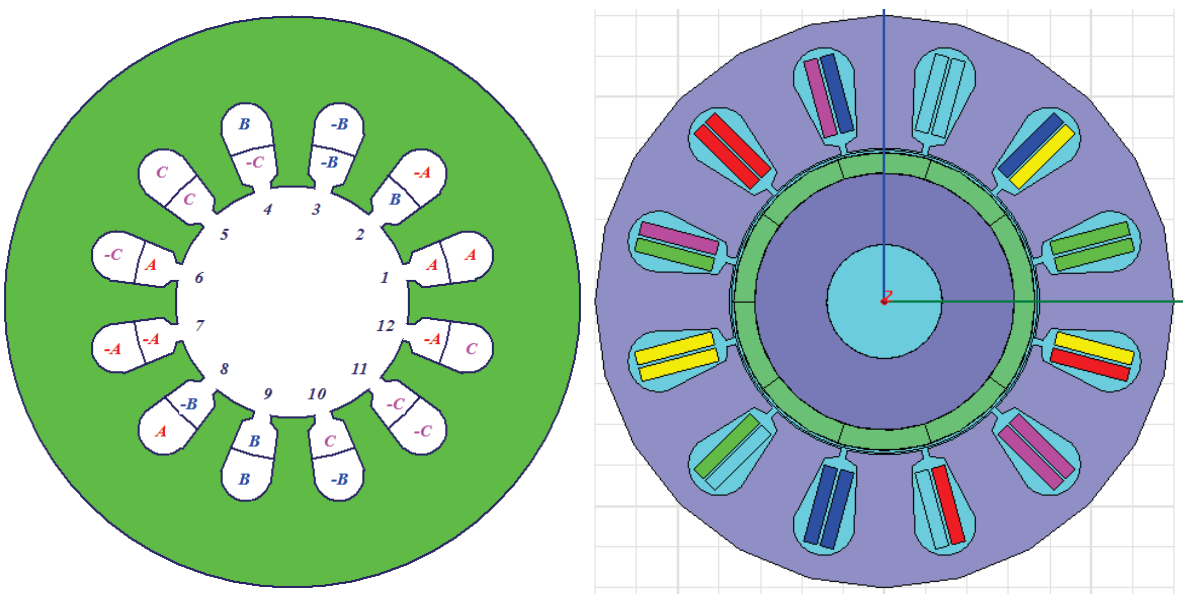

Figure A-25 - An Image from RMxprt of the Winding Layout for the Motor (Left) and an Image from Maxwell 2D of the Color-coded Winding Layout (Right). The Colors Must be added by the User

When you are ready to create excitations, select one coil at a time and assign currents. The reason for assigning current to one coil at a time is for control over naming.

Approved for public release; distribution unlimited.

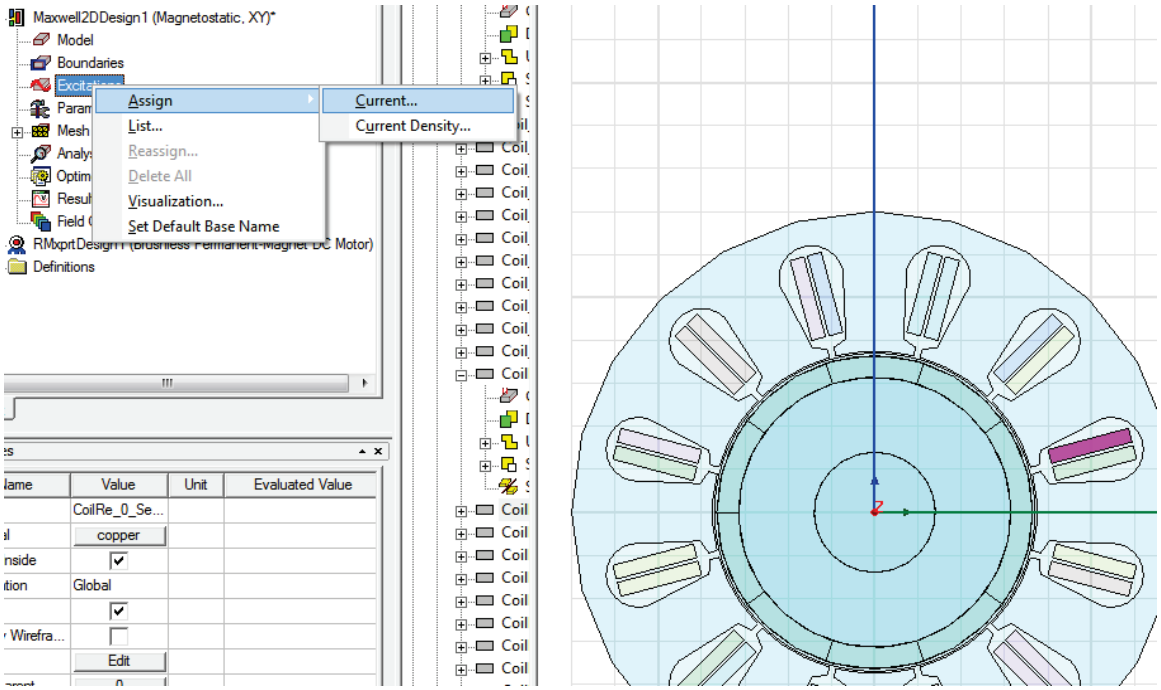

Figure A-26 - Selecting "Current…" from "Assign" from "Excitations"

Make sure the value is the phase current times the number of turns per slot, *Nc*. Note, if the coil is a return path, do not put in a negative value, but simply select *Negative* for *Ref. Direction*. Also, note that the excitations on the coils should be symmetrical.

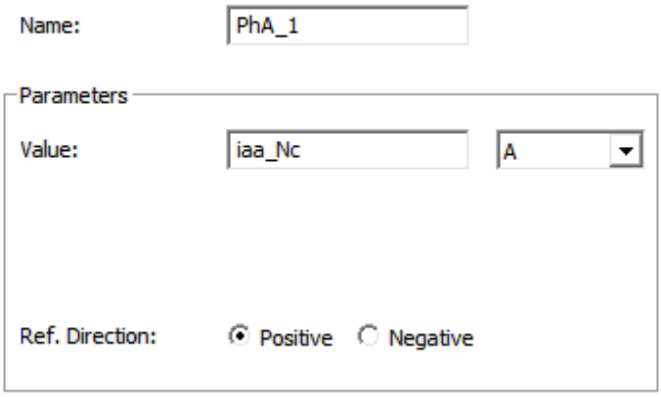

Figure A-27 - Setting the Current Excitation for a Winding

For a concentric winding, it is worth naming a coil and its return path by very similar names (e.g. PhA_1 and PhARe_1). This is why it is best to assign currents to one coil at a time.

Assigning excitations is a very delicate process. It is very important to double check your assignments. It would help to check that the phase names match the color coding and are in the right order; then check that the current values and Ref. Directions are appropriate for the excitation names; then check that each coil excitation is properly named to match its return path coil.

Approved for public release; distribution unlimited.

A3.3.4 Set magnetic polarities

Assign Magnetic material with polarity. Unfortunately, when the motor model was made whole, Ansys made the other side a mirror image, which depending on the number of poles means the magnets on the lower half will have the wrong polarity.

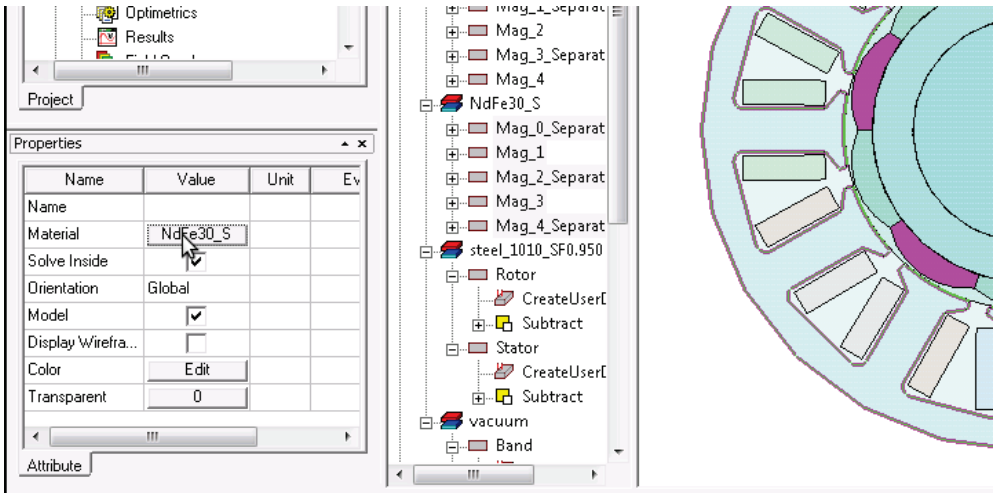

Figure A-28 - Selecting the Polarity of Magnets

A3.3.5 Assign vector potential

A3.3.5.1 Select Edges of the outer edge of motor

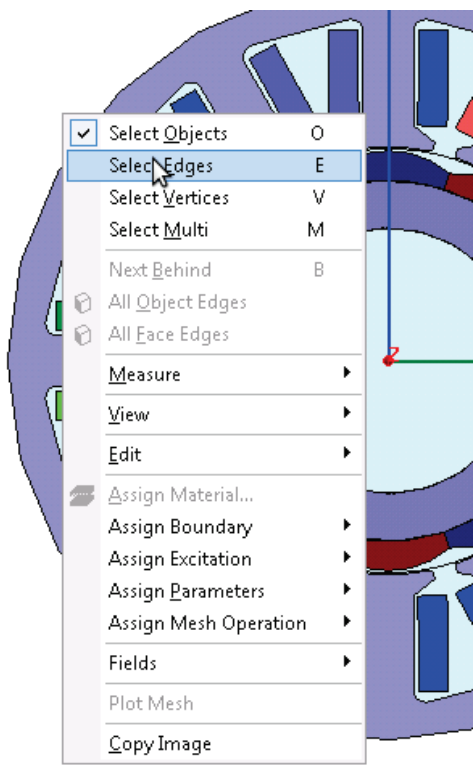

Figure A-29 - Setting the Selection Option to Edges

Approved for public release; distribution unlimited.

A3.3.5.2 Assign Vector Potential to outer edge. The value should be 0 weber/m

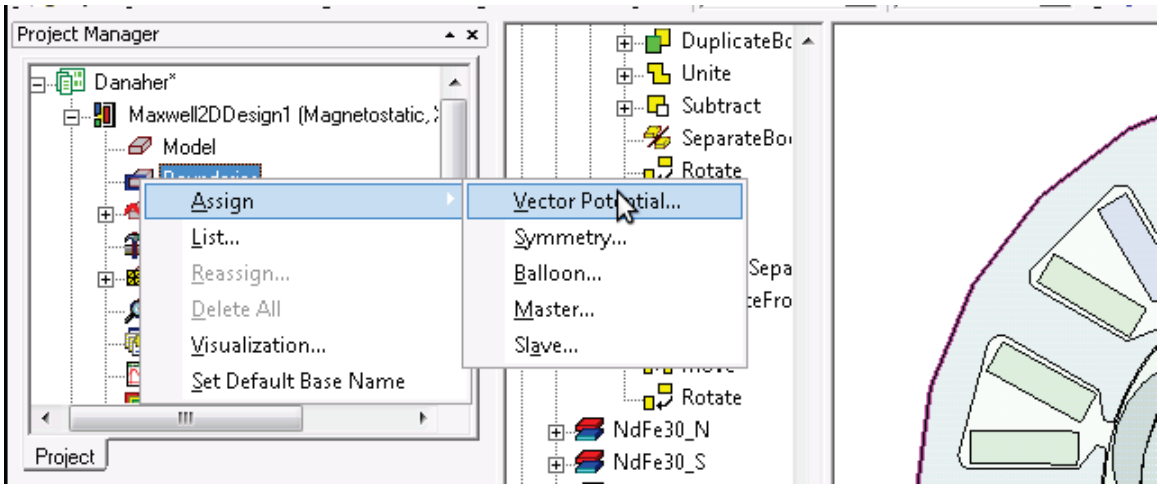

Figure A-30 - Selecting "Vector Potential…" from "Assign" from "Boundaries"

A3.3.6 Analyze

A3.3.6.1 Add solution setup. You can use all the default settings.

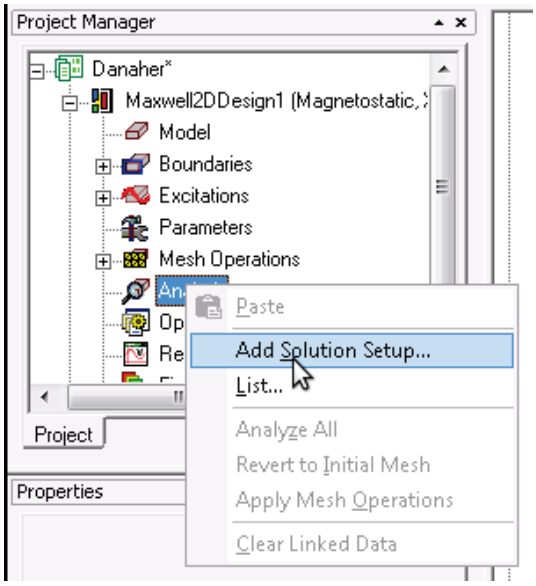

Figure A-31 - Selecting "Add Solution Setup…" from "Analysis"

Approved for public release; distribution unlimited.

A3.3.6.2 Assign Matrix. A matrix is used to define how the various coils are connected and what makes a loop.

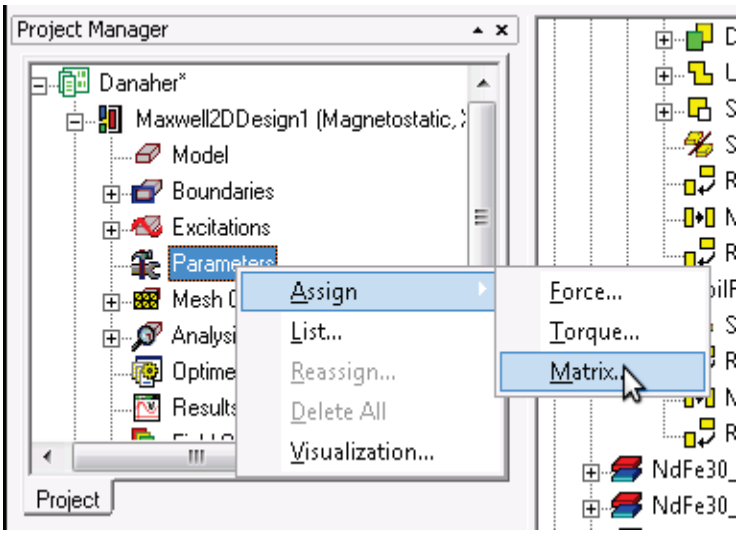

Figure A-32 - Selecting "Matrix…" from "Assign" from "Parameters"

A3.3.6.3 Include currents, but not all. In the Matrix, specify the return path for each conductor. If one conductor is selected to be the return of the other conductor, don't include it in the matrix. For example, don't include PhaseARe_1 in the matrix. Then for the return coil, make its return path be "infinite".

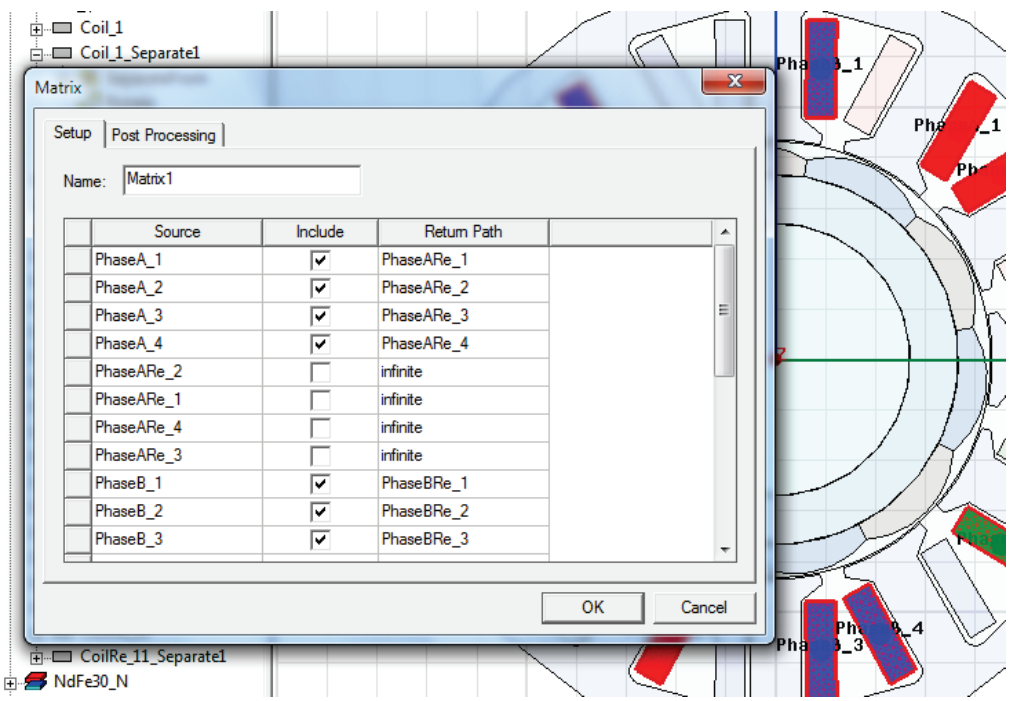

Figure A-33 - Selecting all but Return Windings

A3.3.6.4 Group currents into phases. Make sure to specify the number of turns. Also, it is a

Approved for public release; distribution unlimited.

good idea to name your groups (e.g. PhA, PhB, PhC).

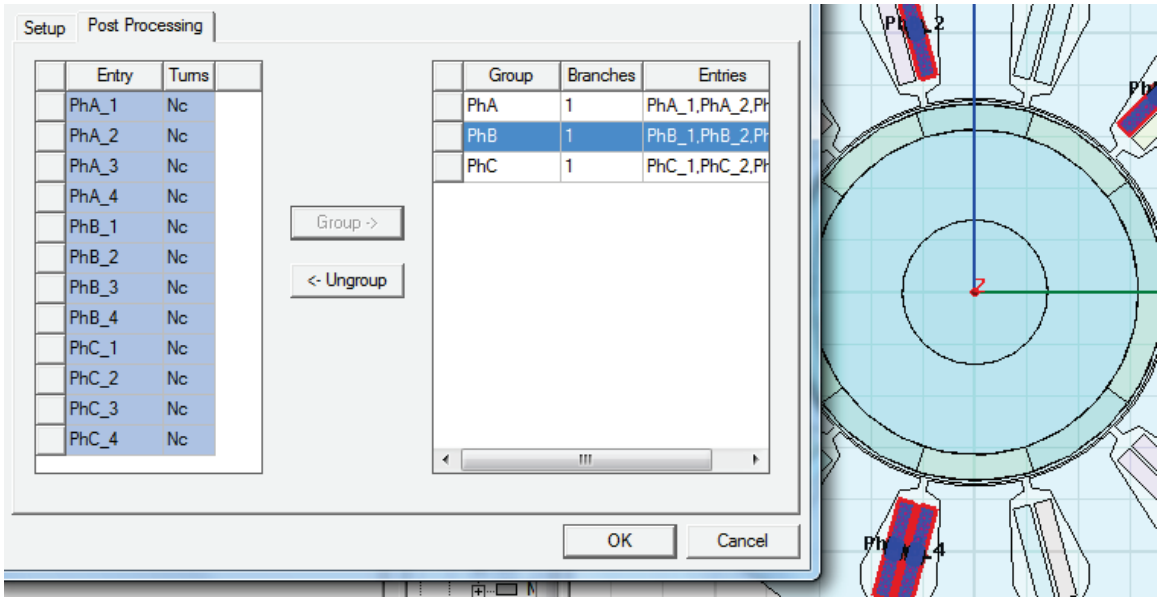

Figure A-34 - Grouping Windings into Phases

A3.3.6.5 Validate the Model

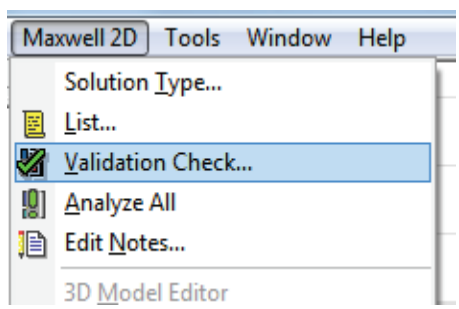

Figure A-35 - Selecting "Validation Check…" from "Maxwell 2D" Menu

A3.3.6.6 Analyze the Analysis Setup

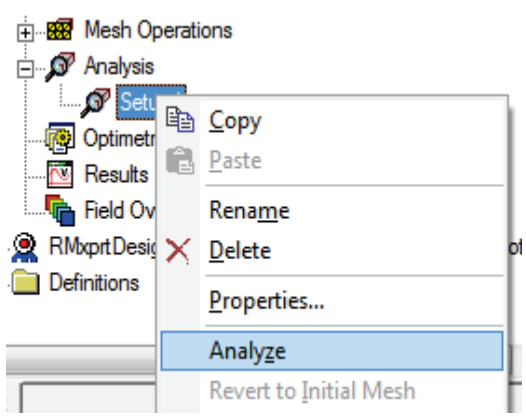

Figure A-36 - Selecting "Analyze" from "Setup1"

Approved for public release; distribution unlimited.

A3.3.6.7 Look at Solution Data

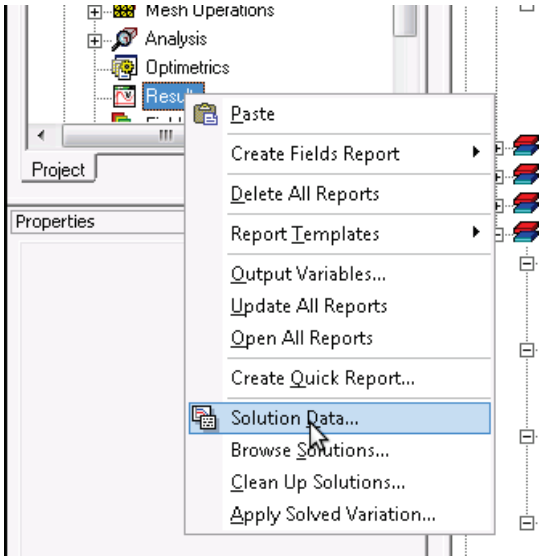

Figure A-37 - Selecting "Solution Data…" from "Results"

A3.3.6.8 Look at inductances and fluxes. Note, until you select the "PostProcessed" check box, the inductances are for each coil. Keep in mind that these inductances are actually inductances per unit meter. Therefore, these values must be multiplied by the length of the motor to get the true inductances of the motor.

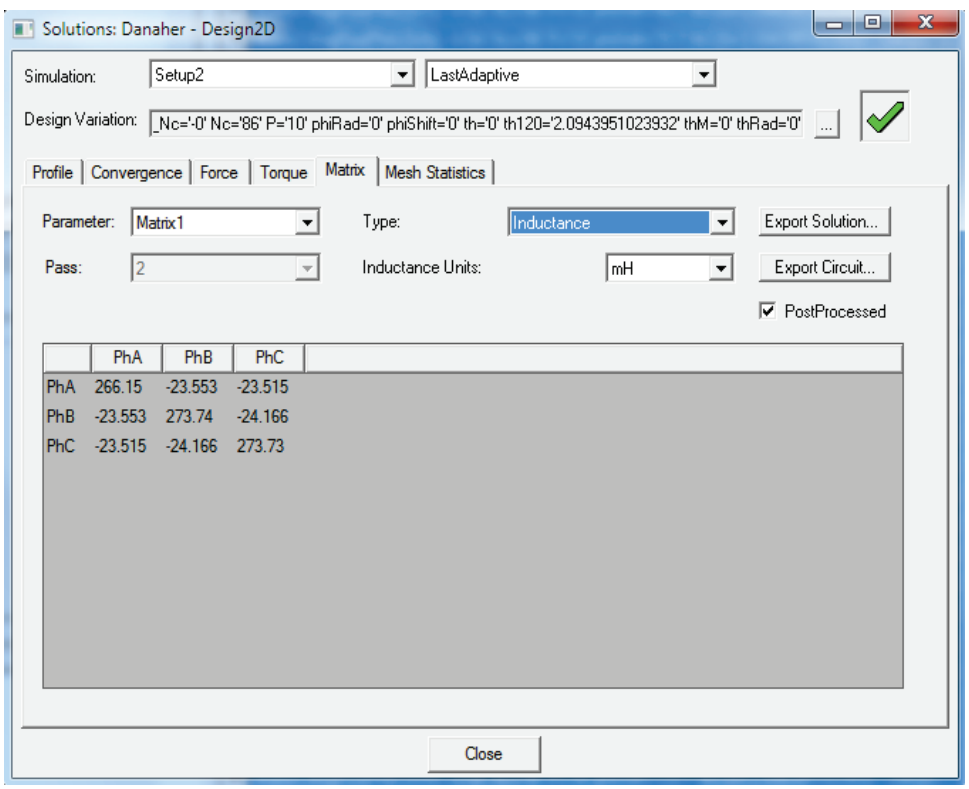

Figure A-38 - Post-processed Inductances for Phases A, B, and C

Approved for public release; distribution unlimited.

There is a Matlab function made for this analysis called “dq0.m”. It will automatically convert arrays in ABC reference frame to DQ0 reference frame. In the case of the example in the figure above, the motor length is 0.058 m. Here you can see how the first argument to dq0 is the ABC matrix of mutual and self-inductances, the second argument is the angle of the rotor converted to radians, and the third parameter is the indicator that this is an ABC wound motor (as opposed to ACB wound). Notice that the result is multiplied by 0.058 to account for the length of the motor.

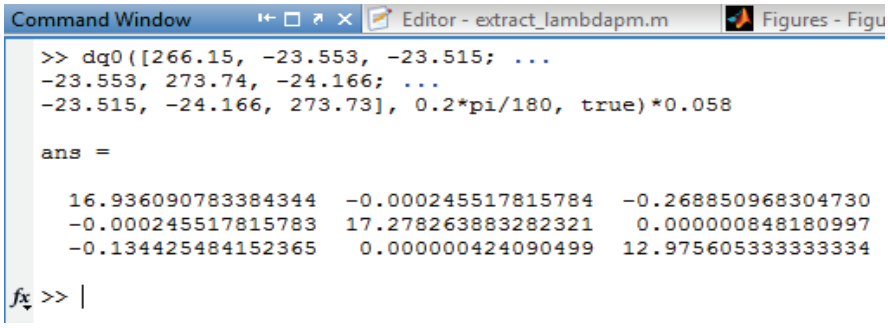

Figure A-39 - Matlab Command Window Showing the Results of Using dq0 on the ABC Phase Inductances

So, the top left value in the result is L_d, the middle value is L_q, and the bottom right value is L_0. Just because L_0 is not zero does not mean that the motor is not balanced. Also, note that the results from Maxwell 2D were in mH so the results from Matlab are also in mH. This indeed gives valid inductance values; however, inductance is a function of currents. So, a following section will discuss how to get the inductances as a function of currents.

To get the PM flux linkage, the test must be run with current set to zero the whole time. Maxwell will calculate the flux linkages into the windings. We want these values to be the result of the permanent magnets only, not from any flux set up by neighbor windings. Furthermore, the flux linkage from the permanent magnet should be independent of current.

Approved for public release; distribution unlimited.

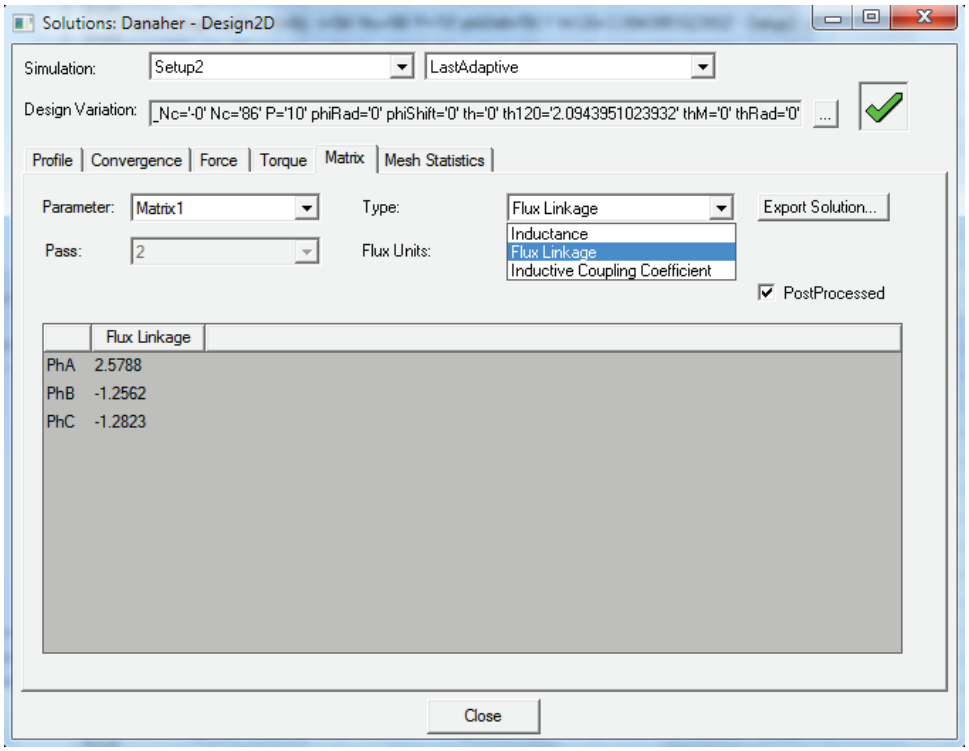

Figure A-40 - Flux Linkages for Phases A, B, and C

In much the same was as with inductances, the flux linkages can be converted to DQ0 reference frame with Matlab.

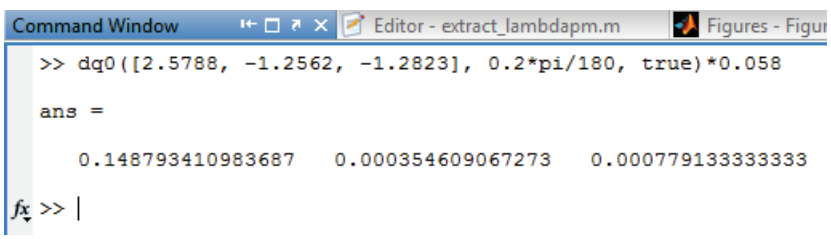

Figure A-41 - Matlab Command Window Showing the Result of Using dq0 on the ABC Phase Flux Linkages

Notice that again, the values must be multiplied by the length of the motor (in this case 0.058 m). The far left value in the result is the flux linkage in the D axis. This is the flux linkage of the permanent magnet. Now, these flux linkages are not inherently particular to the permanent magnet. Only because the currents are zero, the only flux through the stator windings is due to the permanent magnets. You will notice that the units in Maxwell 2D are probably Wb. So, the result from Matlab is also in Wb. Unfortunately, there does not seem to be any way to confirm this value with RMxprt.

The next section shows how to get the nonlinear inductances as functions of currents.

Approved for public release; distribution unlimited.

A3.4 Extract the reduced-order parameters

The purpose of using parametrics is to try many combinations of different settings such as different values of current, phase angle, rotor angle, magnet thickness, etc. The following steps show exactly how these parametrics are setup and then simulated.

A3.4.1 Simulate

A3.4.1.1 Add parametrics

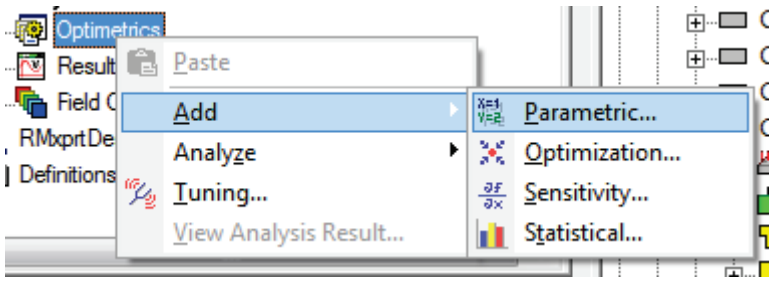

Figure A-42 - Selecting "Parametric…" from "Add" from "Optimetrics"

Approved for public release; distribution unlimited.

A3.4.1.2 Click Add..., select one of the variables from the list, specify the pattern type (e.g. Linear step), specify the Start, Stop, and Step values, and then the "Add >>" button. Make sure to press this button or else nothing will happen. To get a good sampling of the inductances, make sure to vary current magnitude from near zero to some positive number, torque angle from 0 to pi, and rotor angle from 0 to some fraction of 2*pi. The user will need to test in order to find the ranges that are best for the particular motor.

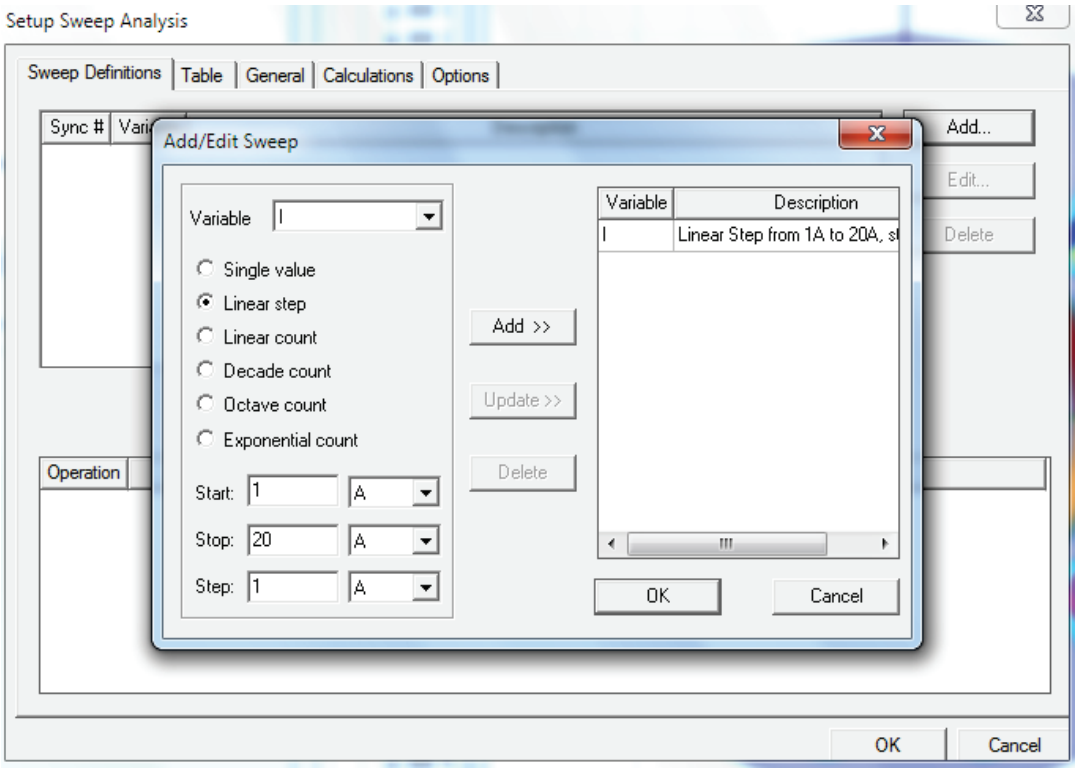

Figure A-43 - Setting up a Sweep Analysis

A3.4.1.3 Now analyze from the parametric setup. This could take quite a while depending on how many parametric combinations you set up.

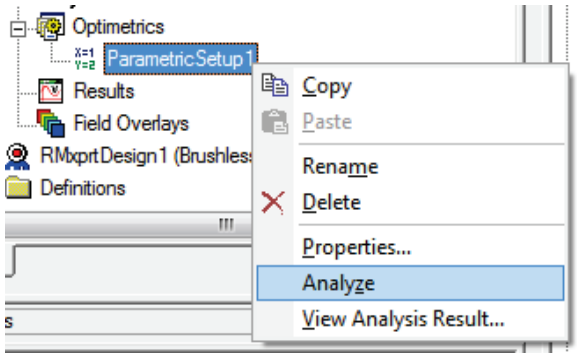

Figure A-44 - Selecting "Analyze" from "Parametric Setup 1"

Approved for public release; distribution unlimited.

A3.4.1.4 For numerical analysis on the results, create a data table.

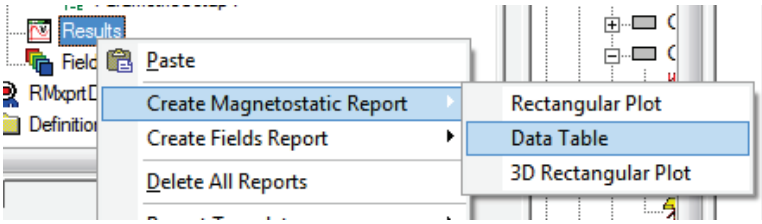

Figure A-45 - Selecting "Data Table" from "Create Magnetostatic Report" from "Results"

A3.4.1.5 For an inductance report, select all the mutual and self-inductances in the list.

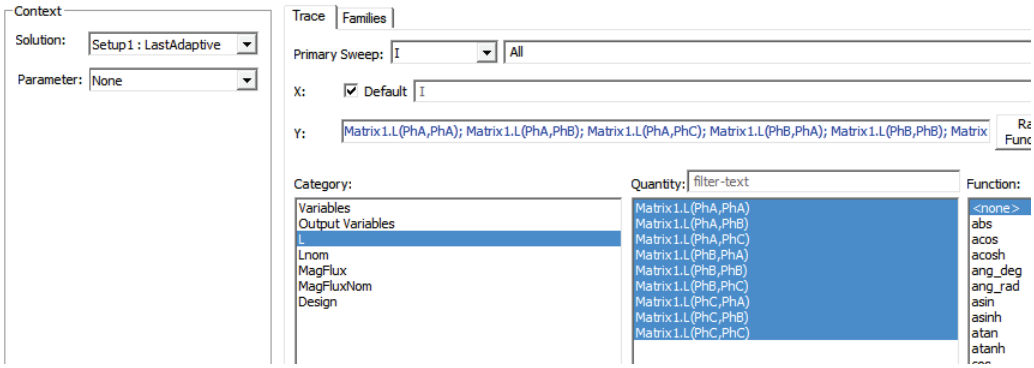

Figure A-46 - Selecting all Mutual and Self-inductances

A3.4.1.6 For a PM flux linkage report, make sure to select MagFlux and all the phases in the list.

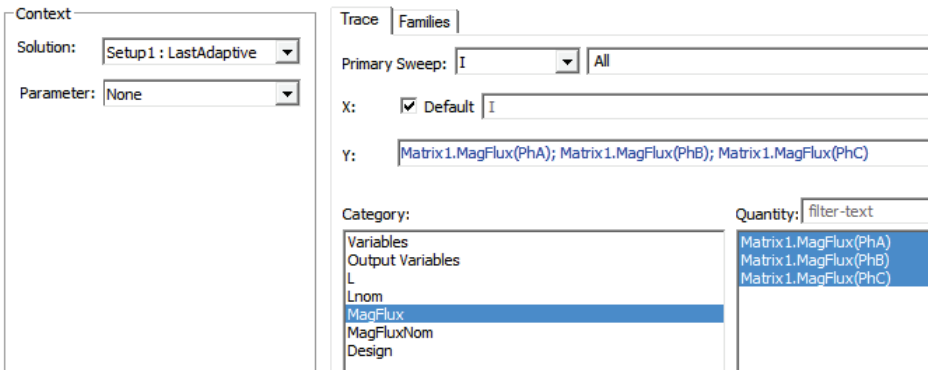

Figure A-47 - Selecting all Magnetic Flux Linkages

Approved for public release; distribution unlimited.

A3.4.1.7 Once the reports are generated, transpose the data so that the long labels are in a column on the left.

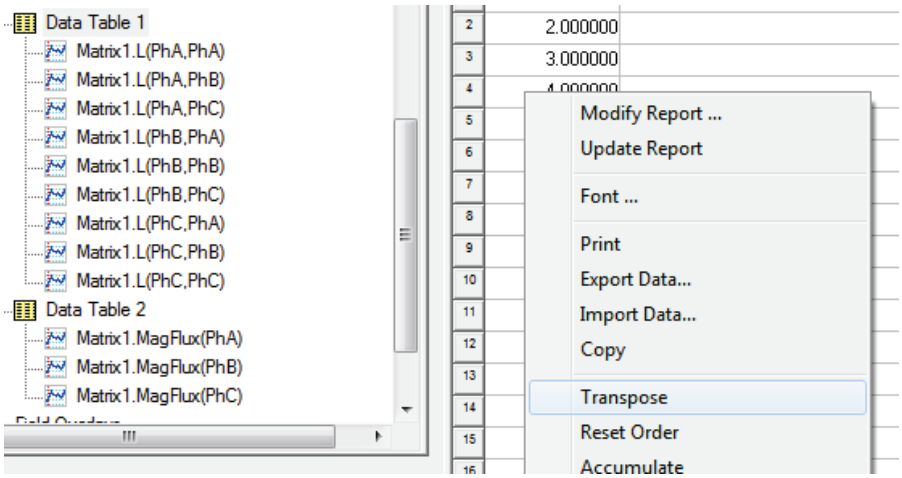

Figure A-48 - Transposing the Data Table

A3.4.1.8 Copy the data by right clicking in the table

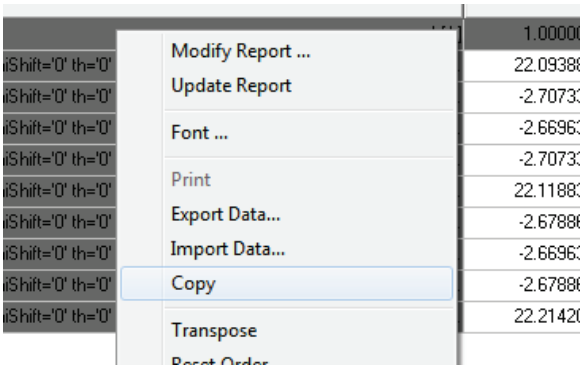

Figure A-49 - Copying the Data

Approved for public release; distribution unlimited.

A3.4.1.9 This can be then pasted into Excel. Save this as a csv file

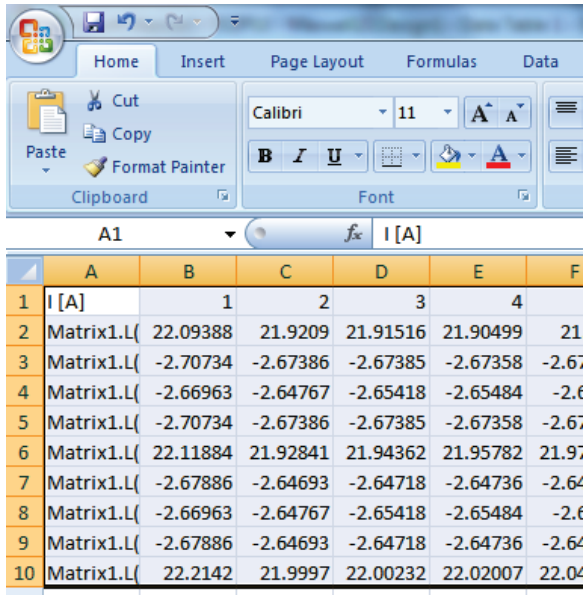

	A	B	C	D	E	F
1	I [A]	1	2	3	4	
2	Matrix1.L(	22.09388	21.9209	21.91516	21.90499	21
3	Matrix1.L(	-2.70734	-2.67386	-2.67385	-2.67358	-2.67
4	Matrix1.L(	-2.66963	-2.64767	-2.65418	-2.65484	-2.6
5	Matrix1.L(	-2.70734	-2.67386	-2.67385	-2.67358	-2.67
6	Matrix1.L(	22.11884	21.92841	21.94362	21.95782	21.97
7	Matrix1.L(	-2.67886	-2.64693	-2.64718	-2.64736	-2.64
8	Matrix1.L(	-2.66963	-2.64767	-2.65418	-2.65484	-2.6
9	Matrix1.L(	-2.67886	-2.64693	-2.64718	-2.64736	-2.64
10	Matrix1.L(	22.2142	21.9997	22.00232	22.02007	22.04

Figure A-50 - Pasting the Data into Excel

Now, the data is safely in a spreadsheet, but notice that depending on how many simultaneous parametric variables you have, the distinction of what parameters had what values is all together in one column on the left.

To extract the data into a more usable format, we need to run a Matlab script. This process is explained in the following section.

A3.4.2 Extract the data

Here are two typical lines in the first column of one of the csv files we might generate:

```
Matrix1.L(PhA,PhA) [mH] - I='64A' Nc='86' P='10'
phiShift='180.1' th120='2.0943951023932' - Setup2 :
LastAdaptive

Matrix1.L(PhA,PhA) [mH] - I='45.254833995939A' Nc='86'
P='10' phiShift='180.1' th120='2.0943951023932' - Setup2 :
LastAdaptive
```

These text strings contain the labels of the particular test that was run, but we need to parse the data into a multidimensional array that can be indexed based on each of the relevant labels (e.g. phase pair “PhA,PhA”, current value “I=’45.25’”, phase shift “phiShift=’180.1’”). This multidimensional array will be much easier to analyze than the csv file. To parse the data into such an array we need the provided Matlab script csvlabeled2num.m. This script will need to know what labels to look for. So, first we need to define the labels as cell arrays.

```
phiCell = {'phiShift=''0.1', 'phiShift=''10.1',
'phiShift=''20.1',... 'phiShift=''30.1', 'phiShift=''40.1',
```


Approved for public release; distribution unlimited.

```
'phiShift=''50.1',... 'phiShift=''60.1', 'phiShift=''70.1',
'phiShift=''80.1',...  'phiShift=''90.1',  'phiShift=''100.1',
'phiShift=''110.1',... 'phiShift=''120.1',
'phiShift=''130.1', 'phiShift=''140.1',...
'phiShift=''150.1', 'phiShift=''160.1',
'phiShift=''170.1',... 'phiShift=''180.1'};
currentCell = {'I=''1A', 'I=''1.4', 'I=''2A', 'I=''2.8',
'I=''4A', ...
   'I=''5.6', 'I=''8A', 'I=''11', 'I=''16', 'I=''22',
'I=''32', ... 'I=''45', 'I=''64'};
abcCell = {'PhA,PhA','PhA,PhB','PhA,PhC',...
   'PhB,PhA','PhB,PhB','PhB,PhC',...
   'PhC,PhA','PhC,PhB','PhC,PhC'};
```

Notice the double quotes ‘’ used to create a single quote ‘ in the actual string.

Then, these cell arrays need to be used in the csvlabeled2num.m script.

```
theArray = csvlabeled2num('LL vs phi, i, abc, theta.csv',...
   {phiCell, currentCell, abcCell})*motorLength;
```

The script takes two parameters: the name of the csv file and a cell array of the cell arrays. Notice that the cell arrays must be in the order that you want the data organized in dimensions in the array. So, in the above example, the inductance values will vary with phi along the first dimension, with current along the second dimension, and with ABC pairing along the third dimension. The last dimension is always the actual second dimension in the csv file. So, in the above example, each column in the csv file was for a different value of theta. Thus, the fourth dimension varies theta in the array.

This analysis can quickly become rather complicated. So, to simplify the problem, use the Inductances package. To extract the inductances, run extract.m. The inputs are set in the section labeled "Get the array of inductances from the csv file." There are two output files: L(phi,i).mat and L(phi,i,theta).mat. The inductances from a typical motor would look something like these:

Approved for public release; distribution unlimited.

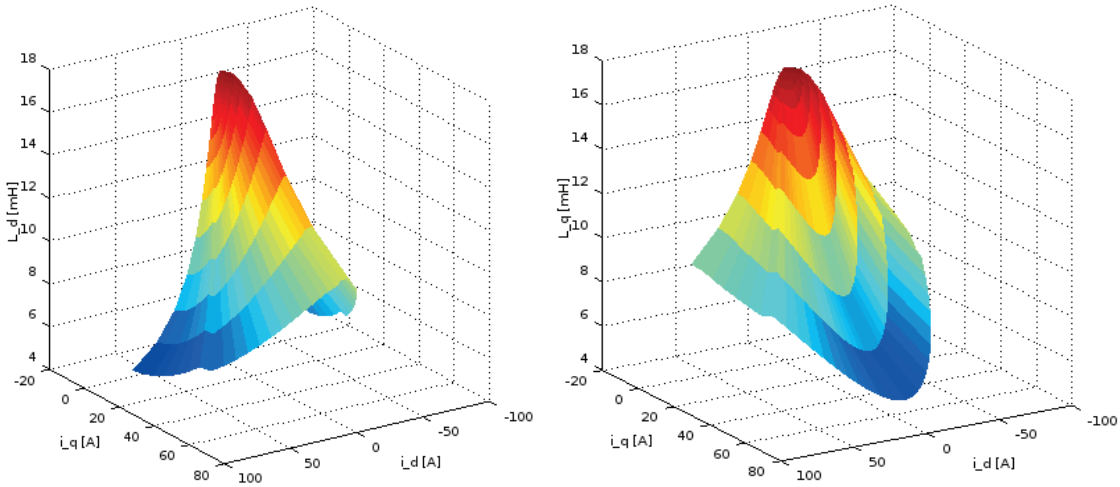

Figure A-51 - Direct inductance (left) and quadrature inductance (right), both as functions of direct and quadrature currents

To smooth the inductances and calculate their derivatives with respect to id and iq, run smooth2d.m. Its input is L(phi,i).mat. It smooths the inductances and calculates the derivatives with respect to id and iq. Its output file is L(phi,i), DL(id,iq) smooth.mat. After smoothing, the inductances would look more like these:

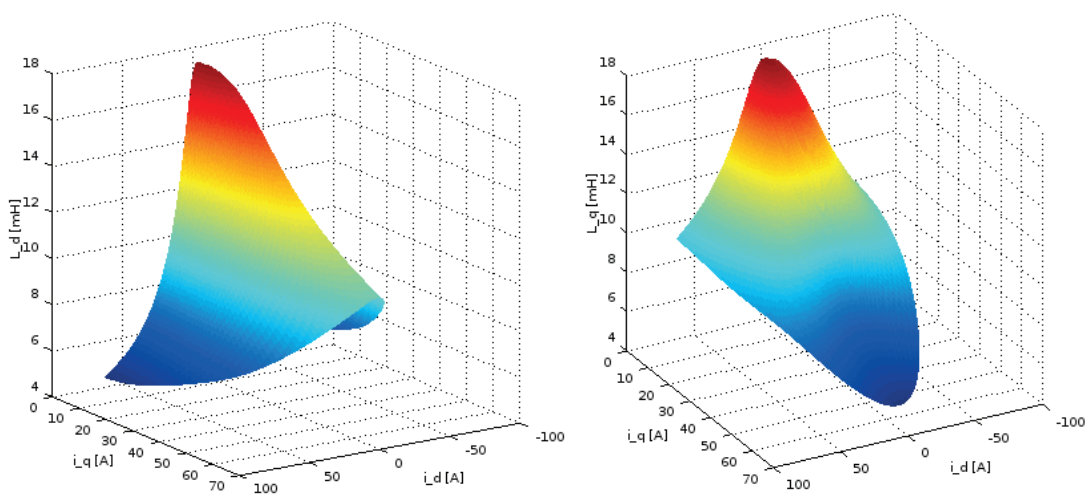

Figure A-52 - Direct (Left) and Quadrature (Right) Currents Smoothed

These tables of inductances then need to be placed into the motor module in the EMA package, in the Modules folder.

In addition to developing the inductances, the FEM model that was built for Maxwell 2D can also be ported into other ANSYS software to do thermal analysis. Here short FEM simulations of thermal response can be run to collect data for developing lumped element parameters of thermal resistance and thermal capacitance.

Approved for public release; distribution unlimited.

A4 CONCLUSION

While many of the necessary parameters for EMA simulation can be found through non-destructive experiments, some parameters are best determined by using a closely matched model. The main parameters that need to be found by modeling are

- PM flux linkage
- Direct inductance
- Quadrature inductance
- Thermal capacitance
- Thermal resistance

The process to find these requires great care and precision, but they can be found without destroying the EMA.

Approved for public release; distribution unlimited.

LIST OF ACRONYMS, ABBREVIATIONS, AND SYMBOLS

ACRONYM	DESCRIPTION
AFRL	Air Force Research Laboratory
EMA	Electromechanical Actuator
EU	Electronic Unit
FEM	Finite Element Method
FOC	Field-oriented Control
HPEAS	High Performance Electric Actuation Systems
IGBT	Insulated-gate Bipolar Transistor
INVENT	Integrated Vehicle and Energy Technology
NL-LEM	Nonlinear Lumped-element Model
PCM	Phase Change Materials
PM	Permanent Magnet
PMSM	Permanent Magnet Synchronous Machine
PWM	Pulse-width Modulation
UCF	University of Central Florida

Approved for public release; distribution unlimited.